JOURNAL OF APPLIED PHYSICS

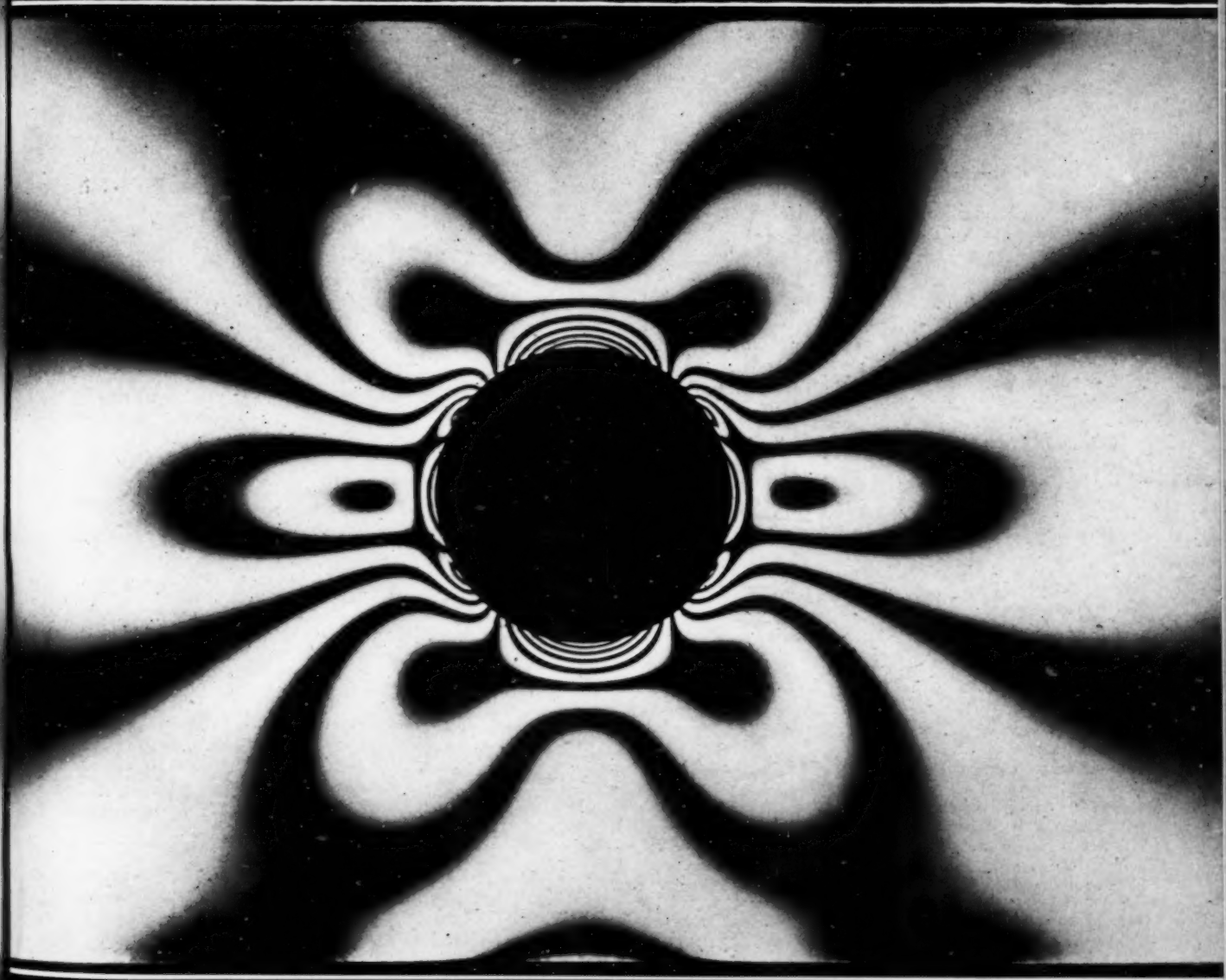

JOURNAL
OF
APPLIED PHYSICS

AUGUST, 1941 Vol. 12, No. 8

In This Issue

		Page
"Physics of Air Raids"		583
Influence of Certain Variables on the Stresses in Gear Teeth	Thomas J. Dolan	584
On Similarities Between Stress and Flow Patterns	Miklós Hetényi	592
Rational Approach to the Numerical Solution of Laplace's Equation. (The Four-Point Influence Method)	M. M. Frocht and M. M. Leven	596
Classification of Isotropic Points as Defined by $\sigma_1-\sigma_2=0$ within a Regular Region	Michael A. Sadowsky	605
Three-Dimensional Photoelasticity Using Scattered Light	R. Weller	610
Photoelastic Study in Vibrations	W. M. Murray	617
Abstracts from Eleventh Photoelasticity Conference		623
Frictional Phenomena. II. A. Gases	Andrew Gemant	626
Velocity Measurement of Transient Mechanical Motions	S. Keilien	634
Simple and Rigorous Method for the Determination of the Heat Requirements of Simple Intermittently Heated Exterior Walls	Elmer G. Smith	638
Heat Requirements of Simple Intermittently Heated Interior Walls and Furniture	Elmer G. Smith	642
Effects of Heat Treatment on Field Emission from Metals	J. H. Daniel	645

Letter to the Editor

Deterioration of Photographic Films before Development	Wayne T. Sproull	654

In Every Issue

Here and There	652
Index to Advertisers	viii

BOARD OF EDITORS

Elmer Hutchisson,
Editor

Associate Editors

Francis Bitter
W. F. Busse
Robley D. Evans
Morris Muskat
B. E. Warren
J. B. Whitehead

Publication of the American Institute of Physics

ADMINISTRATIVE STAFF

Henry A. Barton,
Director

Madeline M. Mitchell,
Publications Manager

John T. Tate,
Adviser on Publications

GOVERNING BOARD

Paul E. Klopsteg,
Chairman
George B. Pegram,
Secretary
Karl T. Compton
Wheeler P. Davey
Floyd A. Firestone
Harvey Fletcher
R. C. Gibbs
Arthur C. Hardy
George R. Harrison
A. Stuart Hunter
H. R. Lillie
A. G. Worthing
W. B. Rayton
John T. Tate
Wallace Waterfall

The Journal of Applied Physics, published monthly at Prince and Lemon Sts., Lancaster, Pa., is devoted to physics in its role as the science basic to other natural sciences and to the arts and industries. Previous to 1937 this publication was known as Physics. It aims to be of service not only in physical laboratories, but also in the laboratories of industrial, chemical, geological, geophysical, meteorological, radio, and similar concerns. The Journal of Applied Physics publishes editorials, news of physicists and reviews, as well as technical papers of applied physics.

Manuscripts should be submitted to Elmer Hutchisson, Editor, American Institute of Physics, 175 Fifth Avenue, New York, New York.

Subscriptions and orders for back numbers should be addressed to Prince and Lemon Streets, Lancaster, Pa. or to the American Institute of Physics, 175 Fifth Avenue, New York, N. Y.

SUBSCRIPTION PRICE

	U. S. AND CANADA	ELSEWHERE
To members of scientific societies	$5.00	$5.70
To all others	7.00	7.70

Single copies are $.70 each.

Changes of address and proofs should be addressed to the Publications Manager.

Advertising rates supplied on request. Orders, advertising copy and cuts should be sent to the American Institute of Physics.

Entered as second class matter at the Post Office at Lancaster, Pennsylvania, under the Act of March 3, 1897. Accepted for mailing at the special rate of postage provided for in the Act of February 28, 1925, authorized May 2, 1932.

Copyright 1941, by the American Institute of Physics.

Journal
of
Applied Physics

Volume 12 August, 1941 Number 8

"The Physics of Air Raids"

A TIMELY and interesting report of an afternoon lecture delivered by Professor J. D. Bernal appeared recently in "Nature."* This lecture delivered at the Royal Institution was entitled "The Physics of Air Raids" and has as its purpose the quieting of fears by a rational explanation of what can and what does occur in bomb explosions. Unknowns are always much more fearful than knowns. For instance, a little understanding of electric discharges goes a long way in quieting one's nerves in a thunderstorm; particularly if one happens to be in a closed automobile. Another very important point is that rational means of minimizing the effects of air raids require first of all an understanding of the physics involved.

Professor Bernal has the faculty of eliminating from his discussion many of the unnecessary details and thus making the general principles stand out clearly. He opens his article with an explanation of the fact that as a bomb explodes a single wave pulse or sound of very high intensity is generated. If sounds of all frequencies and intensities traveled at the same speed, this high intensity pulse would retain its shape as it is propagated outwards. However, since the elasticity of the medium increases considerably under the enormous compression involved in explosions the high pressure phase breaks away from the center of the pulse just as the tops of water waves break ahead near the shore. Thus the sharp wave of the explosion is smoothed out at relatively short distances from the source.

Many seemingly freakish effects occur during air raids which are in reality fine examples of the application of the most elementary laws of physics. In a narrow street with tall buildings on either side, an air compression rises to the top of the buildings where free expansion can take place. A suction wave then travels back toward the street. The suction wave may pull windows and doors out of place in a violent and seemingly impossible way. Another freakish effect is the sharpness of the shadows produced by the high frequency components of the intense wave pulse. For example, a person behind a garden wall close to an explosion is uninjured while some one else at a considerable distance is badly hurt.

Since much of the damage from air raids is produced by splinters and earth shock, Professor Bernal has analyzed in a broad way the mechanism of the explosions. When the bombs burst, the expanding gases are held in a more or less spherical compression chamber. Failure takes place along a conical surface and fragments varying from 40 lb. lumps to dust particles are projected with speeds up to 4000 ft. per sec. By studying the penetration of these particles, more efficient ways of stopping them can be developed and the bomb shelters improved.

There is need for more discussions of the type that Professor Bernal has written. Naturally the requirement of secrecy in connection with war work limits the range of topics which can be discussed. However, a statement of general principles without giving the details of the research valuable to the enemy serves the very useful purpose of quieting the nerves of the general public and giving the people more confidence in their leaders.

* J. D. Bernal, "The Physics of Air Raids," Nature **147**, 594 (May 17, 1941).

Influence of Certain Variables on the Stresses in Gear Teeth*

BY THOMAS J. DOLAN

University of Illinois, Urbana, Illinois

A photoelastic study was made to obtain a more accurate picture of the localized stresses in gear tooth fillets than can be obtained from the commonly used Lewis equation. A set of approximate stress concentration factors are presented for fillets in gear teeth based upon a set of variables such as the radius r of the fillets, thickness t of tooth, height h of load position on the tooth, etc. The problem was attacked by making a series of tests of "conventionalized gear teeth" in the form of short cantilever beams in which one factor at a time could be varied. The values of stress concentration factor were computed as the ratio of the maximum stress in the fillet to the calculated stress at the "assumed weakest section," as defined by Lewis' equation. In general, it was noted that as the height of load position (h/t) was increased, the maximum stress increased, but the stress concentration factor decreased. An approximate equation for the tensile stress concentration factors, k, for the conventionalized models with sides of the tooth parallel is: $k=1.25(t'/r)^{0.2}(t/h)^{0.3}$. *A definite decrease in the tensile stress concentration factor was observed as the tooth model was gradually tapered inward to approach Lewis' ideal shape of the parabola of uniform strength, whereas no change in the compressive stress concentration factor occurred as the angle was varied over a 25° range. Tests now in progress on generated gear teeth having a 14½-degree pressure angle and a diametral pitch of 2 indicate that the stress concentration factor for the tensile fillet is given fairly accurately by the formula:* $K=0.22(t/r)^{0.2}(t/h)^{0.4}$.

Introduction

LOCALIZED stresses of large magnitude are always present in a loaded gear tooth at the point of load application and at the fillets. In order to facilitate and improve present methods of gear design there is a definite need for more exact information as to the magnitudes of these stress concentrations. The present paper will be limited to a discussion of some of the factors that affect the stress concentrations occurring at the fillets of a gear tooth, as determined by a series of photoelastic tests on models designed to simulate the structural action of spur gear teeth. Investigations have been carried out along somewhat similar lines by Timoshenko,[1] Baud and Peterson,[2,3] Black,[4] and others; it was hoped that the present investigation might cover a wider range of variables and yield a clearer understanding of the relative effect of some of the variables affecting the localized stresses at gear tooth fillets than the results thus far available. It is realized, of course, that the photoelastic method yields only theoretical values of stress based on elastic action in the members; no attempt has been made to determine the extent to which these theoretical stresses are of significance in causing damage to actual metal gears in which the relative "notch sensitivity," localized plastic readjustments in the material, and distribution of the loads among several

* Paper presented at the Eleventh Semi-Annual Eastern Photoelasticity Conference, May 24–25, 1940, at the Carnegie Institute of Technology, Pittsburgh, Pennsylvania.

[1] S. Timoshenko and R. V. Baud, "Strength of gear teeth," Mech. Eng. **48**, 1105 (1926).

[2] R. V. Baud and E. Hall, "Stress cycles in gear teeth," Mech. Eng. **53**, 207 (1931).

[3] R. V. Baud and R. E. Peterson, "Load and stress cycles in gear teeth," Mech. Eng. **51**, 653 (1929).

[4] P. H. Black, "An investigation of relative stresses in solid spur gears by the photoelastic method," Bull. 228, Eng. Exp. Sta., University of Illinois (1936).

teeth may greatly influence the damaging value of stress.

At present most designers use the Lewis equation,[5] in designing spur gear teeth, or employ modifications of this equation in the design of bevel gear, helical gear, and other special forms of gear teeth. The basic assumptions as made by Lewis in the equation for the maximum stress developed at the fillet in a gear tooth were: (a) the load is carried by one tooth and acts along the face of the gear at the tip of the tooth in a direction normal to the tooth surface; (b) this force can be resolved into two components at the intersection of the line of force with the radial center line of the tooth, one component acting radially and the other tangentially; the radial component was disregarded in his analysis because it was small and served as (an unreliable) source of strength to materials weak in tension. The Lewis equation treats the gear tooth as a cantilever beam and determines the value of a nominal flexural stress at an "assumed weakest section" of the tooth. This "weakest section" is located between the two points of tangency of the tooth profile with a parabola inscribing in the tooth outline (referred to as the parabola of uniform strength) with its apex at the intersection of the action line of the applied force and the radial center line of the tooth. For example, in Fig. 1, the parabola ACB locates the "weakest section" between the points of tangency A and B. Since it is based on erroneous assumptions, this equation does not give the true stress values developed, but has served remarkably well for a period of years without change (probably due largely to the accommodating properties of the materials used and to the low working stresses employed in actual design).

Object and Scope of the Tests

A photoelastic study was made in an attempt to obtain a more accurate picture of the localized stresses in gear tooth fillets than can be obtained from the Lewis equation. The main purpose of the tests was to determine a set of approximate stress concentration factors for fillets in gear teeth based upon a set of variables such as the radius r of the fillets, thickness t of tooth, height h of load position on the tooth, and the angles at which the flank and bottom land of the tooth meet; these variables were selected as being the ones that were significant in determining the effect of the shape of the tooth on the localized stresses developed.

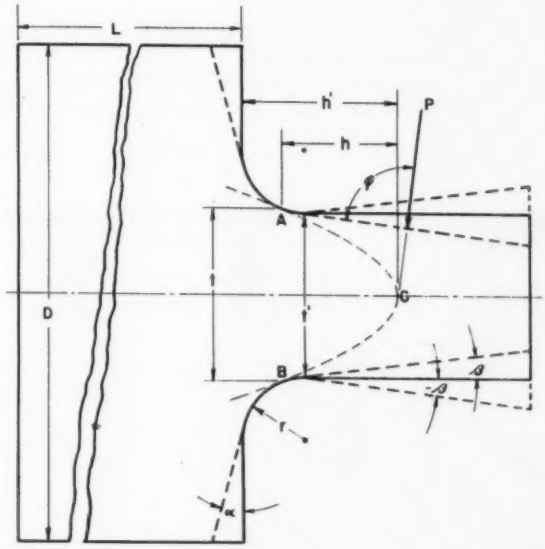

FIG. 1. Gear tooth notation and model dimensions. A and B are points of tangency of parabola ACB with the tooth profile.

In order to present the results in a form most familiar to the gear designer, it was found advisable to express the localized stresses in the gear teeth (or the equivalent test specimens) in terms of the Lewis equation but modified by the introduction of a stress concentration factor.

Before proceeding with an analysis of the stresses in generated gear teeth, it was deemed advisable to study the effect of the shape factors that are altered in producing the various contours of generated gear teeth to determine their relative importance in influencing the magnitude of the stress concentration factor. This phase of the problem was attacked by making a series of tests of "conventionalized gear teeth" in the form of short cantilever beams in which one factor at a time could be varied.

The series of alterations of shape that were chosen to represent the most important variables for this series of tests of "equivalent" models

[5] O. A. Leutwiler, *Elements of Machine Design* (McGraw-Hill Book Company, Inc., New York, 1917), Chapter XII.

are illustrated diagrammatically in Fig. 1. These may be briefly summarized as follows:

(1) The radius r of the fillet between the flank of the tooth and the root circle.
(2) The nominal thickness t', and the thickness t, at the "assumed weakest section" of the tooth.
(3) The height of load position h above the "assumed weakest section."
(4) The angle β between the side of the tooth and the radial centerline.
(5) The angle α between the bottom land of tooth space and the thickness chord.
(6) The angle φ that the action line of the load makes with the tooth face. (This angle was maintained constant at 90° in the tests.)

A series of models was made with the dimensions shown in Fig. 1 having nominal values of $L=3''$, $D=3''$, and $t'=1''$, and values of h were varied from $\frac{1}{4}''$ to $1\frac{1}{2}''$. All models were made from $\frac{1}{4}''$ thick polished plates of BT61893 Bakelite and were annealed after roughly sawing them slightly oversize from the plate. Immediately after annealing, they were machined to finished size with light cuts, and the tests completed within a few hours after machining. No appreciable residual stresses or edge effects were present in the models tested. Calibration beams used for determination of the fringe stress values were cut from the rear portion of the model after the tests on the model were completed.

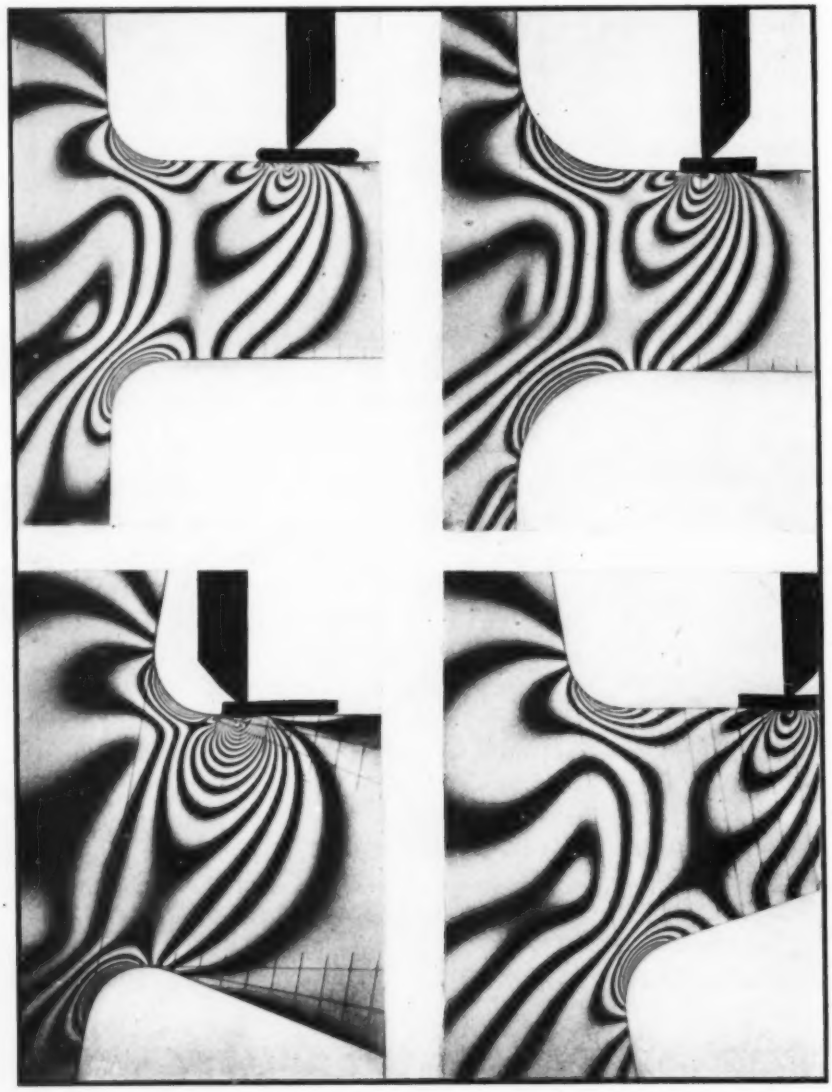

FIG. 2. Typical fringe photographs of several models.

Each model was supported by lightly clamping (the lower edge of length "L" in Fig. 1) to a rigid bar, and was loaded with a line load across the face of the tooth; successive fringe photographs were made in monochromatic (mercury green line) light with a series of different load positions h. The model was then altered by varying the fillet radius r (or the angle β of the tooth sides, etc.,) in a series of successive increments, and a complete new set of fringe photographs were made with loads at the same positions for each new alteration of the model. Eight of these "equivalent" models were tested, and approximately 170 negatives of fringe photographs were obtained and analyzed.

Test Data and Discussion of Results

In Fig. 2 are shown photographs of typical

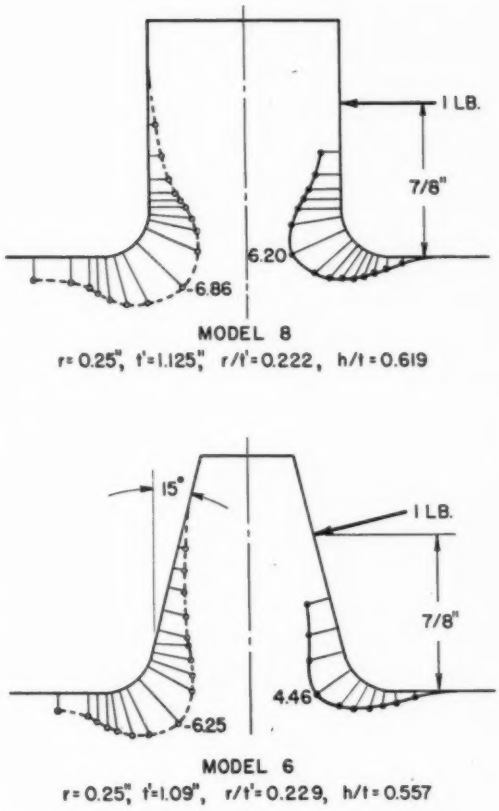

FIG. 3. Stress distribution curves. Stress scale: 1″=10 p.s.i. Approximate enlargement=0.9/1. Curves based on 1-inch face.

fringe patterns for several of the models tested, and in Fig. 3 and Fig. 4 are shown typical distributions of stress around the fillets for several of the test loadings. In analyzing the results, the stresses were converted to values of stress for a "unit" model (1″ thick) loaded with a unit load (one pound), and the nominal values for this same "unit" model were computed from the Lewis equation. It is a relatively simple matter to obtain the value of this calculated stress for any load position by the use of a graphical method of locating the assumed weakest section, and a direct application of the flexure formula. One set of results showing changes produced in the fillet stresses by a variation of the load position and fillet radius is plotted in Fig. 5, in which all other variables of shape were maintained constant.

It will be observed that the stresses increased rapidly as the fillet radius was reduced, and that the stresses also increased (but not in direct proportion) as the height of load position above the bottom of the tooth was increased. Furthermore, the maximum stress on the fillet in compression was, in general, often larger than that at the fillet in tension. From the viewpoint of design, the maximum tensile stress is perhaps the most important consideration, but the stress concentration factors for both fillets of each tooth were computed and these values are shown in Fig. 6 for the above data.

The values of the stress concentration factors were computed as the *ratio of the actual maximum stress in the fillet, as obtained from the photoelastic fringe pattern, to the calculated stress at the "assumed weakest section," as defined by Lewis, using his original assumption that the radial component of load can be neglected.*

In general, it will be noted that as the height of load position (h/t) was increased, the maximum *stress increased*, but the stress concentration *factor decreased*. It is also evident that a generous radius on the fillet was very effective in decreasing the stress concentration factor.

By scaling off the ordinates to the curves in

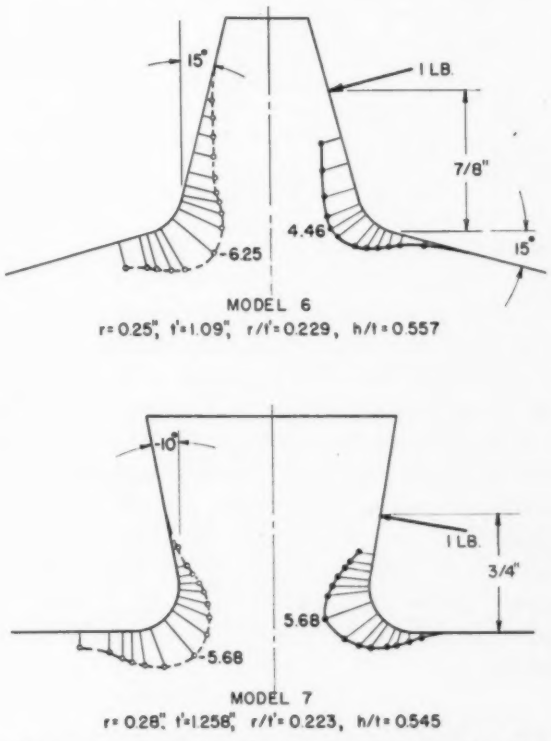

FIG. 4. Stress distribution curves. Stress scale: 1″=10 p.s.i. Curves based on 1-inch face. Approximate enlargement=0.78/1.

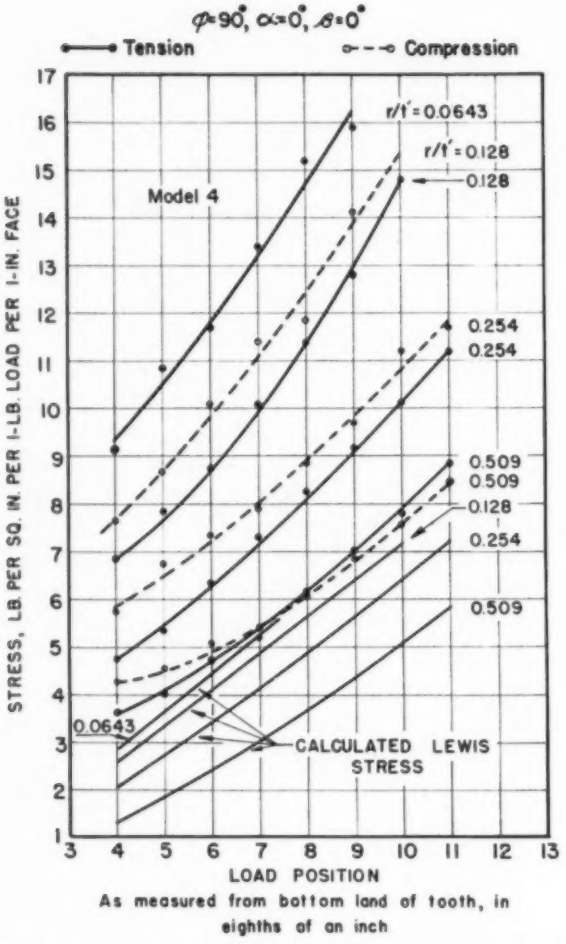

FIG. 5. Variation of the fillet stresses with the tooth fillet radius and the load position.

Fig. 6 at various ratios of h/t, the data may be replotted as shown in Fig. 7; for comparison with these results, curves determined by Frocht[6] and by Weibel[7] have been added showing stress concentration factors for a beam with fillets and subjected to pure bending. This type of loading would approach the condition for $h/t=\infty$ and it will be noted that the localized stresses were much more severe in the short stubby cantilever beams that approximated the proportions of gear teeth. An approximate equation for the tensile stress concentration factors k for the conventionalized models with sides of the tooth parallel is:

$$k=1.25(t'/r)^{0.2}(t/h)^{0.3}.$$

[6] N. C. Riggs and M. M. Frocht, *Strength of Materials* (Ronold Press Company, New York, 1938), p. 389.

[7] E. E. Weibel, "Studies in photoelastic stress determination," Trans. A. S. M. E. **56**, 637 (1934).

This relationship fits the data within an accuracy of about 5 percent for the range of values covered in the tests.

The curves in Figs. 8 to 10 show the variations obtained for the stress concentration factor when the fillet radius was kept constant but the angle β of the side of the tooth varied. A definite decrease in the *tensile* stress concentration factor was observed as the tooth model was gradually tapered inward to approach Lewis' ideal shape of the parabola of uniform strength, whereas no change in the *compressive* stress concentration factor occurred as the angle was varied over a 25° range.

Tests of models in which the angle α, between the bottom land of tooth space and the thickness chord, was varied, showed no measurable change in stress concentration at either the tensile or the compressive fillet for angles α up to 15 degrees. This was perhaps to be expected since the material removed from the model by increasing the angle α was usually in regions of relatively low stress and consequently did not

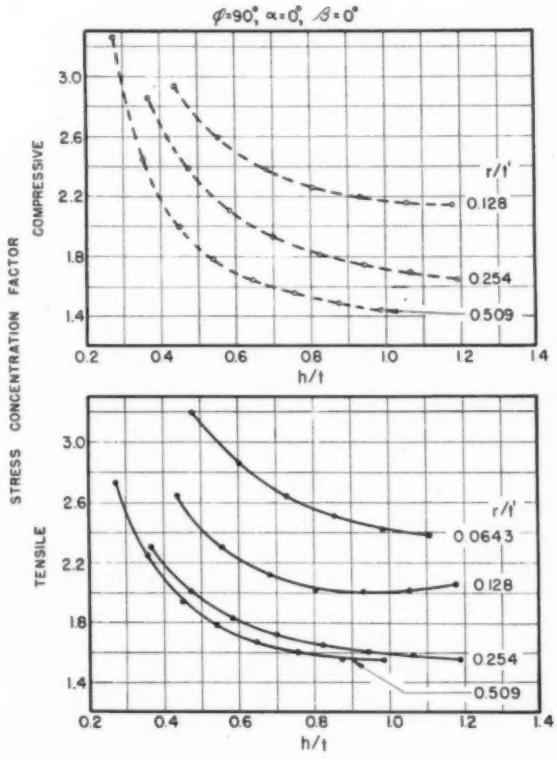

FIG. 6. Variation of the stress concentration factors with the tooth fillet radius and the load position.

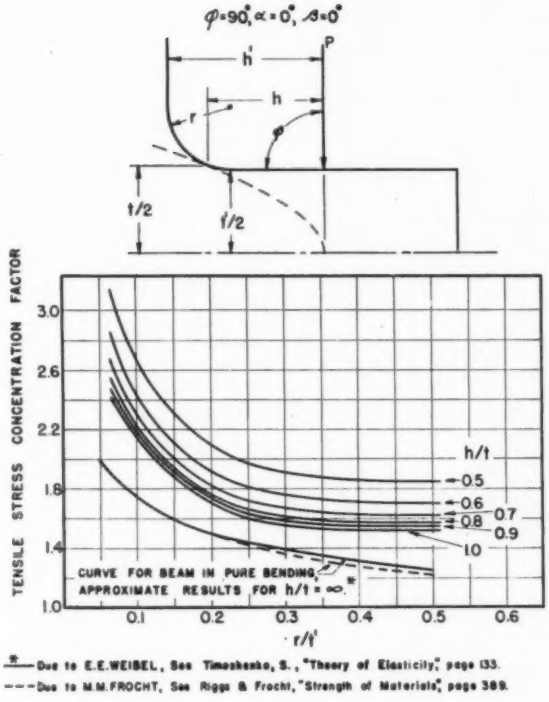

FIG. 7(a). Variation of the tensile stress concentration factor with the load position and the tooth fillet radius.

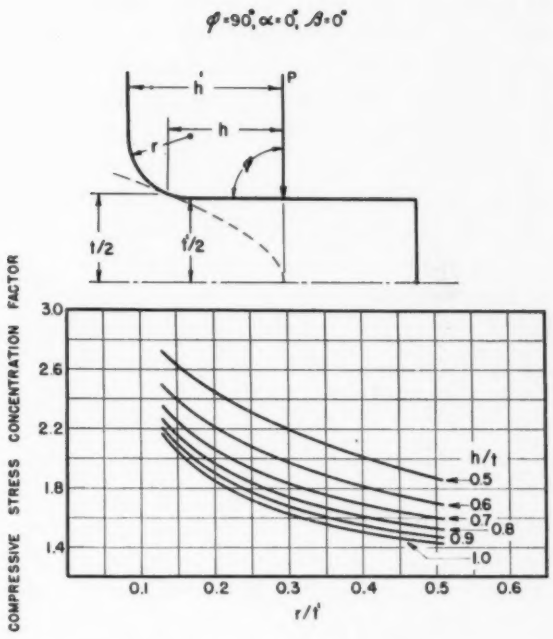

FIG. 7(b). Variation of the compressive stress concentration factor with the load position and the tooth fillet radius.

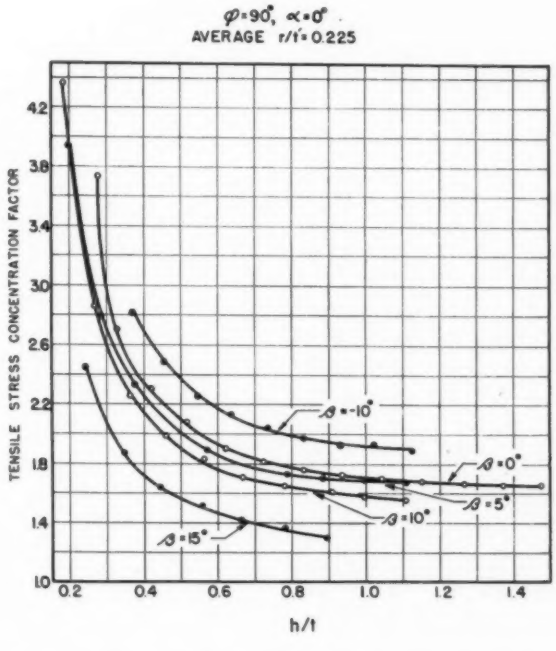

FIG. 8. Variation of the tensile stress concentration factor with the angle β and the load position.

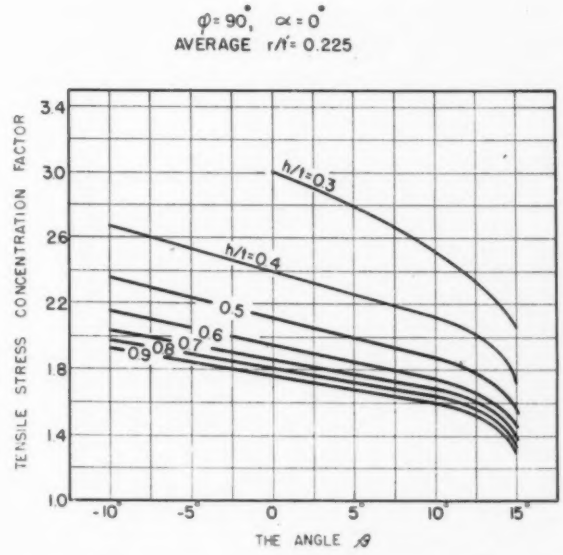

FIG. 9. Variation of the tensile stress concentration factor with the load position and the angle β.

necessitate much readjustment of stresses in the regions of high stress.

A companion series of tests is now in progress in which models of actual generated gear tooth shapes are being studied. However, the variations

in shape of the models in this latter series of tests are being controlled by the process of generation of the tooth to conform to standard gear practice. For instance, in Fig. 11 the tooth is generated by a rack tool rolling on the pitch circle, and hence the shape depends upon the pitch, edge radius of the cutting tool, addendum and dedendum lengths, and the pressure angle.

In comparing the preliminary results of tests on actual tooth forms with the data shown in Fig. 7, one important variation between the two sets of tests has been noted, namely: the *tensile* stress concentration factors (shown in Fig. 7(a)), were from 12 to 25 percent higher than those obtained for models of true gear tooth contours having the same minimum fillet radius and relative proportions, whereas the *compressive* stress concentration factors (shown in Fig. 7(b)) ranged from zero to ten percent higher than those obtained from models of actual gear teeth. The greatest differences between the two sets of data occurred with the fillets of sharpest curvature (small r/t' values).

One reason the stress concentration factor for the tensile fillet in the actual gear tooth was much smaller than the values shown in Fig. 7(a) is that the generated gear tooth models were

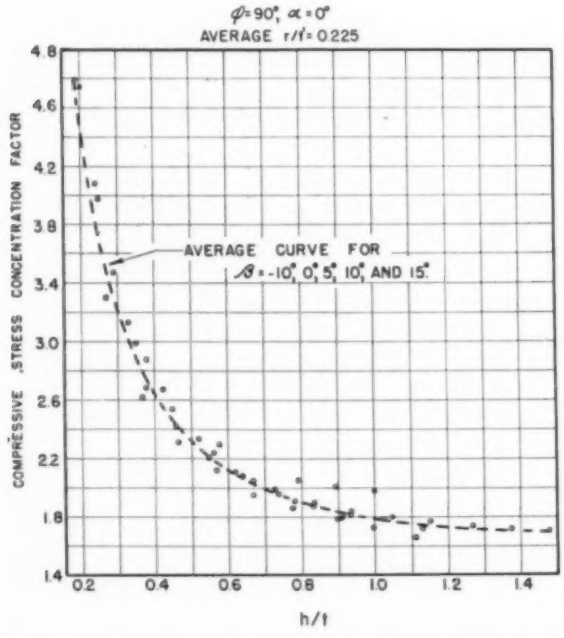

FIG. 10. Variation of the compressive stress concentration factor with the angle β and the load position.

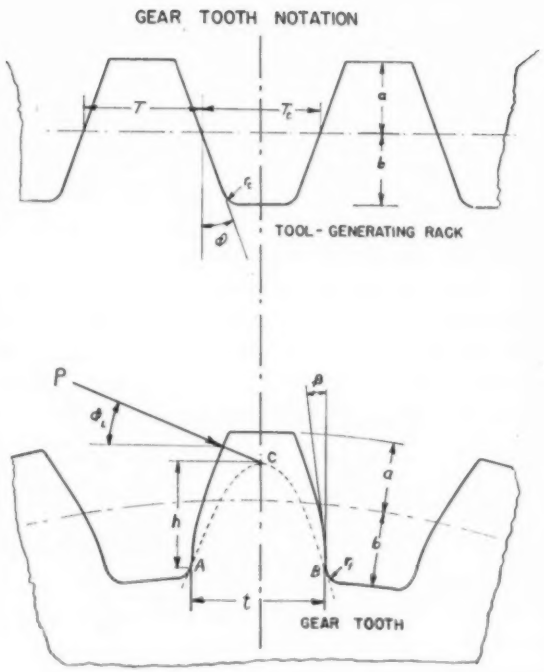

FIG. 11. Gear tooth notation. Angle $\varphi = 14\frac{1}{2}°$.

loaded in a direction normal to the tooth face, and the radial (compressive) component of load was neglected in the analysis by using as the theoretical stress only the value of Lewis' flexural stress. This small radial component of load would produce a slight lowering of the observed stress at the fillet in tension, and hence result in a smaller stress concentration factor. Similarly, the radial component of load would produce a higher observed stress at the fillet in compression, and should result in a higher stress concentration factor being obtained. However, a rough check on the radial components of load indicated that their magnitudes were small and they produced only a very small increment of stress as compared with the flexural stress developed by the transverse component of the applied load.

The main reason that the generated gear teeth exhibited somewhat lower stress concentration factors than did the conventionalized models probably lies in the fact that the conventionalized tooth models had *circular* fillets, whereas the fillets on the true gear tooth were somewhat spiralled by the process of generation with the minimum radius at the root being the assumed value of the fillet radius. Consequently, it is evident that the equivalent circular radius of the

fillet on a generated gear tooth that is effective as a stress raiser is not the minimum radius of curvature of the fillet contour; if the values of stress concentration factor shown in this paper were used for design purposes they would probably be on the safe side and yield values of stress that were slightly too high.

Further tests are now in progress on the stresses in models of actual generated gear teeth, covering a wide range of standard shapes. It is hoped that, by a careful analysis of the results, the above variations can be accounted for and a set of stress concentration factors, based on the shape factors of the teeth, can be devised which will be an aid to more efficient gear design. The tentative results of the tests thus far on generated gear teeth having a $14\frac{1}{2}$-degree pressure angle, and a diametral pitch of 2, indicate that the stress concentration factor for the tensile fillet as obtained by dividing the observed stress by the computed combined (flexural plus direct) stress is given fairly accurately by the formula:

$$K = 0.22(t/r)^{0.2}(t/h)^{0.4}.$$

In closing, it should again be emphasized that the significance of photoelastically determined localized stresses for purposes of design of actual metal members is greatly influenced by the properties of the materials of which the members are made; the exact importance of these theoretical stresses in measuring the nearness to structural damage of the member can only be determined by correlation with carefully conducted laboratory fatigue tests and by comparison with service records.

Acknowledgment

This investigation is being conducted as a part of the work of the Engineering Experiment Station of the University of Illinois, of which Dean M. L. Enger is the director, and of the Department of Theoretical and Applied Mechanics, of which Professor F. B. Seely is the head. Much credit for this work is due to Mr. D. G. Richards, graduate assistant, who conducted the tests of the conventionalized models, and to Mr. E. L. Broghamer, instructor in Mechanical Engineering, who is conducting the tests on generated gear teeth. This study has grown out of suggestions and correspondence with Mr. A. H. Candee of the Gleason Works, and the author is indebted to Mr. Candee for many valuable suggestions and criticisms during the progress of the tests.

On Similarities Between Stress and Flow Patterns*

BY MIKLÓS HETÉNYI

Westinghouse Research Laboratories, East Pittsburgh, Pennsylvania

(Received March 29, 1941)

The purpose of this paper is to review established relationships between stress and flow problems. Two-dimensional plane stress systems were found to have features analogous to non-viscous potential flow fields on one hand, and to viscous flow on the other hand. Accordingly, this discussion is divided into two parts. In each case the fluid is assumed to be continuous, homogeneous, and incompressible.

I. Similarities Between Plane Stress and Potential Flow Fields

1. In a plane stress system there exist the following relations between the stress components σ_x, σ_y, τ_{xy}, the strain components ϵ_x, ϵ_y, γ_{xy} and the displacement components u and v:

$$\epsilon_x=\frac{\partial u}{\partial x}=\frac{1}{E}(\sigma_x-\mu\sigma_y),$$

$$\epsilon_y=\frac{\partial v}{\partial y}=\frac{1}{E}(\sigma_y-\mu\sigma_x),$$

$$\gamma_{xy}=\frac{\partial u}{\partial y}+\frac{\partial v}{\partial x}=\frac{2(1+\mu)}{E}\tau_{xy},$$

where E denotes the modulus of elasticity and μ the Poisson's ratio of the material. Substituting these values into the equilibrium equations:

$$\partial\sigma_x/\partial x+\partial\tau_{xy}/\partial y=0,$$
$$\partial\sigma_y/\partial y+\partial\tau_{xy}/\partial x=0,$$

we have:

$$\left.\begin{aligned}\frac{2}{1-\mu}\frac{\partial}{\partial x}\left(\frac{\partial u}{\partial x}+\frac{\partial v}{\partial y}\right)-\frac{\partial}{\partial y}\left(\frac{\partial v}{\partial x}-\frac{\partial u}{\partial y}\right)=0\\ \frac{2}{1-\mu}\frac{\partial}{\partial y}\left(\frac{\partial u}{\partial x}+\frac{\partial v}{\partial y}\right)+\frac{\partial}{\partial x}\left(\frac{\partial v}{\partial x}-\frac{\partial u}{\partial y}\right)=0\end{aligned}\right\}. \quad (A)$$

Putting

$$\partial u/\partial x+\partial v/\partial y=(1-\mu)\lambda/\mu,$$
$$\partial v/\partial x-\partial u/\partial y=2\omega,$$

where λ denotes the lateral contraction and ω the rotation at any point of the stress field, it is seen that

$$\left.\begin{aligned}&\frac{\partial^2\lambda}{\partial x^2}+\frac{\partial^2\lambda}{\partial y^2}=0; \quad \frac{\partial^2\omega}{\partial x^2}+\frac{\partial^2\omega}{\partial y^2}=0\\ \text{while}\quad &\frac{\partial}{\partial x}\frac{\lambda}{\mu}=\frac{\partial}{\partial y}\omega; \quad \frac{\partial}{\partial y}\frac{\lambda}{\mu}=-\frac{\partial}{\partial x}\omega\end{aligned}\right\}. \quad (1)$$

Comparing these results with a two-dimensional flow problem where the velocities $v_x=\partial\phi/\partial x$ and $v_y=\partial\phi/\partial y$ can be considered as derivatives of a velocity potential ϕ, the conditions of a source-free and irrotational flow can be written as $\partial v_x/\partial x+\partial v_y/\partial y=0$ and $\partial v_y/\partial x-\partial v_x/\partial y=0$, respectively. Since the relations between the stream function ψ and the velocity potential ϕ are

$$\left.\begin{aligned}&\partial\phi/\partial x=\partial\psi/\partial y; \quad \partial\phi/\partial y=-\partial\psi/\partial x\\ &\text{in addition to } \partial^2\phi/\partial x^2+\partial^2\phi/\partial y^2=0\\ &\text{we also have } \partial^2\psi/\partial x^2+\partial^2\psi/\partial y^2=0\end{aligned}\right\}. \quad (2)$$

Comparing Eq. (2) with Eq. (1) it is seen that the relationship between ϕ and ψ is the same as that found between λ/μ and ω. Hence the conclusion that:

The equipotential and stream lines of a flow pattern can always be considered as lines of equal lateral contractions (isopachics) and lines of equal rotations in a corresponding plane stress system.

Possibilities of using this analogy in solving stress problems were discussed by R. Doerfel.[1]

2. Another analogy has been established by relating elastic displacements to flow velocities. Using the above-introduced notations and taking the displacement components u and v propor-

* Paper presented at the Eleventh Semi-Annual Eastern Photoelasticity Conference, May 24–25, 1940, at the Carnegie Institute of Technology, Pittsburgh, Pennsylvania.

tional to the velocity components v_x and v_y

$$u=kv_x=k\partial\psi/\partial y \quad \text{and} \quad v=kv_y=-k\partial\psi/\partial x,$$

we find by substitution that these expressions will satisfy Eq. (A). Hence:

The velocities of a potential flow can be considered as displacements in a plane stress system.

It is to be noted that the opposite is not true. From the fact that in every stress system equivalent to a flow pattern the displacements will have to be simple harmonic functions, it follows that such stress systems where the displacement components are not simple harmonic functions will have no equivalents in potential flow.

This displacement-velocity analogy is discussed in a paper by J. Barta[2] with reference to aeronautical problems.

3. The conditions under which the orthogonal system of the equipotential and stream lines in a flow problem is equivalent to a system of stress trajectories were investigated by P. Neményi[3] and U. Wegner.[4] Their findings can be summarized as follows:

A. *It is always possible to establish a system of stress trajectories equivalent to the stream and potential lines of a given flow problem.*

Denoting by $\omega(z)$ the known complex velocity function ($z=x+iy$) which is the derivative of a complex potential $\omega(z)=S'(z)$ the equivalent stress system can be found as

$$\sigma_x=\eta Re[\omega^2(z)]-2Re\left[\int_{z_0}^{z}(at+\alpha)\omega^2(t)dt+p\right],$$

$$\sigma_y=-\eta Re[\omega^2(z)]-2Re\left[\int_{z_0}^{z}(at+\alpha)\omega^2(t)dt+p\right],$$

$$\tau_{xy}=-\eta Im[\omega^2(z)].$$

Here *Re* and *Im* denote the real and the imaginary part of the complex function in question and $\eta=a(x^2+y^2)+2bx+2cy+d$; $\alpha=b+ic$. There are five real parameters in the above formulas: a, b, c, d and p. Consequently there is a variety of stress systems whose trajectories are equivalent to those of the given flow problem. The physical interpretation of the parameters is as follows: a, b and c are geometric constants; a determines the scale, b and c determine the origin of the coordinates. The parameter d shows the possibility of superposing a harmonic stress field which does not change the system of stress trajectories while p gives a superposed uniform tension or compression.

B. *The solution for finding a flow problem whose stream and potential lines are equivalent to the trajectories of a given stress system is possible only if one of the following conditions is satisfied:*

(1) $$N(z)=\frac{z(\bar{\alpha}z+d)}{az+\alpha}F(z),$$

(2) $$\left(\frac{\partial^2}{\partial x^2}+\frac{\partial^2}{\partial y^2}\right)\log|\sigma_1-\sigma_2|=\frac{4(ad-b^2-c^2)}{[a(x^2+y^2)+2bx+2cy+d]^2}.$$

(3) $$|\sigma_1-\sigma_2|=|F(z)|[a(x^2+y^2)+2bx+2cy+d],$$

(4) $$\sigma_x=-Re[N(z)],\quad \sigma_y=+Re[N(z)],\quad \tau_{xy}=Im[N(z)].$$

Here $\bar{\alpha}=b-ic$ and $N(z)$ and $F(z)$ are two analytical functions of the complex variable z, whose imaginary parts have to satisfy the equation

$$\tau_{xy}=(x^2+y^2)Im[F(z)]+Im[N(z)].$$

Otherwise the notations are the same as above. Wegner[4] suggested using condition (2) in connections with photoelastic test results. The procedure would then be to determine photoelastically at every point of the stress field the value $|\sigma_1-\sigma_2|$ then carry out the assigned operations on the left side of Eq. (2), and finally to try out if, by a proper choice of the parameters a, b, c and d on the right side, the equality could be satisfied. This semi-experimental method seems to be so involved that its final result could hardly be accepted for an accurate proof.

In both of the above cases, A and B, the question of boundary conditions was still left open. In general, we will find that the boundaries of the equivalent stress field will have to be subjected to distributed loadings of varying intensity. Of greater interest are the cases where an equivalent stress system with unloaded boundaries can be found. This phase of the

problem was investigated by H. Neuber[5] who also disclosed some new and interesting properties of the stress trajectories. He has shown that, if the orthogonal trajectories of the principal stresses σ_1 and σ_2 are given as two sets of curves, $p=$const. and $q=$const., where $p=p(x, y)$ and $q=q(x, y)$ are functions of the Cartesian coordinates x and y, then the equilibrium equations can be written as

$$\left.\begin{aligned} h_p\partial\sigma_1/\partial q+(\sigma_1-\sigma_2)\partial h_p/\partial q=0 \\ h_q\partial\sigma_2/\partial p-(\sigma_1-\sigma_2)\partial h_q/\partial p=0 \end{aligned}\right\}. \qquad \text{(a)}$$

Here h_p and h_q denote the spacing of the curves p and q, respectively. Assuming that a curve $p=$const. represents an unloaded boundary we put $\sigma_2=0$ and find that, in this case, the first of the above equations reduces to

$$h_p\partial\sigma_1/\partial q+\sigma_1\partial h_p/\partial q=\partial/\partial q(\sigma_1 h_p)=0,$$

the solution of which is

$$\sigma_1=C/h_p.$$

According to this result, which is of general validity and is not limited to analogous stress and flow fields: *In any plane stress system the variable distance h_p between the unloaded boundary and the principal stress trajectory p is inversely proportional to the boundary stress value σ_1.*

It is seen that on the basis of this fundamental relationship alone a new optical method of stress analysis could be developed, which would make use only of the isoclinic lines, deriving from those the stress trajectories and obtaining thus the principal stress values and stress concentration factors at any point along the unloaded boundary.

Many of the problems related to stress and flow fields can be analyzed most conveniently in the curvilinear coordinate system p and q. We find, for instance, that if the principal stress trajectories p and q are to be considered as stream and potential functions of an analogous flow problem, then they have to satisfy the Cauchy-Riemann equations

$$\partial q/\partial x=\partial p/\partial y;\quad \partial q/\partial y=-\partial p/\partial x$$

and also

$$\partial x/\partial q=\partial y/\partial p;\quad \partial x/\partial p=-\partial y/\partial q.$$

A substitution of these expressions into the formulas

$$h_q^2=(\partial x/\partial q)^2+(\partial y/\partial q)^2$$

and

$$h_p^2=(\partial x/\partial p)^2+(\partial y/\partial p)^2$$

leads to

$$h_p=h_q=h.$$

An orthogonal system of trajectories which has the above property is called *isometric*. Hence we have the general rule that:

Only an isometric set of stress trajectories can be considered as a set of potential and stream lines of a flow problem.

From the conditions of equilibrium Eq. (a) and the compatibility equation

$$\Delta(\sigma_1+\sigma_2)=0$$

follows by integration that

$$\sigma_1-\sigma_2=(1/h^2)[a(x^2+y^2)+bx+cy+d],$$

which, along the unloaded boundary where $\sigma_2=0$, through the substitution $\sigma_1=C/h$ gives the formula

$$\sigma_1=C^2/[a(x^2+y^2)+bx+cy+d].$$

Thus, in an isometric case, when the stress trajectories can be considered as potential and stream lines of a flow pattern, the principal stress along the unloaded boundary must be expressible in the above form. This formula can be used for deciding whether a given stress problem with known boundary stress values has an equivalent flow field.

From the above formula we also find that the principal stress along the unloaded boundary will vanish if $C=0$, and then it can be shown that also

$$a(x^2+y^2)+bx+cy+d=0.$$

Since the above equation is the general equation of a circle, the conclusion is that:

In an isometric case the stress along the unloaded boundary will vanish only if the boundary is a circular segment or, in the limiting case, a straight line.

Neuber has shown a variety of stress problems which are isometric and thus have an equivalent flow pattern. The boundary lines in these problems are composed of circles, which are first assumed to intersect giving various crescent-shaped figures, and secondly are assumed not to

intersect and result in plates having circular holes. As a special case of the first class of these problems we have the diametrically compressed circular roller, where both of the principal stresses vanish along the boundary and which has been recognized for long as a case which has an equivalent flow pattern.

4. A number of analogies were established by Lord Kelvin, Boussinesq and others[6] between flow problems of various types and the stress distribution in a prismatical bar subjected to torsion. Though problems of torsion do not belong to the class of plane stress, they may be mentioned here on account of their two-dimensional character. On the basis of the Kelvin analogy, experiments were carried out by Den Hartog and McGivern.[7]

II. Similarities Between Plane Stress and Viscous Flow Problems

The stream function of flow ψ, whose derivatives give the velocity components $v_x=-\partial\psi/\partial y$ and $v_y=\partial\psi/\partial x$, satisfies the equation $\Delta\Delta\psi=0$ where $\Delta=\partial^2/\partial x^2+\partial^2/\partial y^2$ is the Laplacian operator. The flow of the viscous fluid is assumed infinitely slow. The same biharmonic equation is satisfied by the transverse deflection of an elastic plate, and also by the Airy stress function of any plane stress system. The first of these analogies was established by Lord Rayleigh[8] while the second one, which will be discussed here, has been applied by J. N. Goodier.[9]

Since the second derivatives of the stress function F give the stress components

$$\sigma_x=\partial^2F/\partial y^2, \qquad \sigma_y=\partial^2F/\partial x^2, \qquad \tau_{xy}=-\partial^2F/\partial x\partial y,$$

we have

$$\Delta F=\sigma_x+\sigma_y,$$

which is proportional to the lateral contraction in a plane stress problem. In case of viscous flow

$$\Delta\psi=\partial v_y/\partial x-\partial v_x/\partial y$$

represents the vorticity of the flow. Hence we have the general correlations that: lines of constant thicknesses (isopachics) in the stress problem will correspond to lines of constant vorticity in the flow field and the lines of constant rotations, being orthogonal trajectories of the isopachics, will be equivalent to the lines of constant fluid pressure in the flow problem. It also follows that the stress trajectories and isochromatics will represent in the field of flow the orientation of maximum distortion and the lines of constant maximum distortion, respectively.

In this analogy the equivalent boundary conditions have also simple physical interpretation. If the rigid boundaries in the flow problem are at rest or in uniform motion the corresponding stress system will have the same boundaries stress free or subjected only to uniform normal stress. The tangential drag and normal pressure along the boundaries of the flow field can be determined from the isochromatic and isopachic lines of a corresponding photoelastic model. Several interesting applications of this analogy have been suggested by Goodier in his abovementioned paper.

Bibliography

1. R. Doerfel, "Die Lösung der Fragen der Zahnflankenberührung," Zeits. V. D. I. **69**, 149–154 (1925).
2. J. Barta, "Die Darstellung ebener Potential-Strömungen mittels einer elastischen Scheibe," Ing. Arch. **6**, 396–402 (1935).
3. P. Neményi, "Über Spannungsfelder, die mit bekannten Strömungsfeldern isomorph sind," Proceedings of the *Third International Congress for Applied Mechanics* (Stockholm, 1930), Vol. II, pp. 155–166. "Stromlinien und Hauptspannungs-Trajectorien," Zeits. f. angew. Math. u. Mech. **13**, 364–366 (1933).
4. Udo Wegner, "Über den Zusammenhang von Strömungs und Spannungsproblemen," Ing. Arch. **5**, 449–469 (1934).
5. H. Neuber, "Der ebene Stromlinienspannungszustand mit lastfreiem Rand," Ing. Arch. **6**, 325–334 (1935). "Die Randbedingungen der Hauptspannungs-Stromlinien," Zeits. f. angew. Math. u. Mech. **15**, 374–375 (1935).
6. S. Timoshenko, *Theory of Elasticity* (McGraw-Hill Book Company, New York, 1934), pp. 263.
7. J. P. Den Hartog and J. G. McGivern, "On the hydrodynamic analogy of torsion," J. App. Mech., Trans. A. S. M. E. **57**, Paper A-47 (1935).
8. Lord Rayleigh, Phil. Mag. [5] **36**, 354 (1893). Also: *Papers* IV, p. 78.
9. J. N. Goodier, "An analogy between the slow motions of a viscous fluid in two dimensions, and systems of plane stress," Phil. Mag. [7] **17** (1934), 554–576. Additional note in same volume, pp. 800–803.

A Rational Approach to the Numerical Solution of Laplace's Equation*

(The Four-Point Influence Method)

BY M. M. FROCHT** AND M. M. LEVEN†

Carnegie Institute of Technology, Pittsburgh, Pennsylvania

THE solution of many physical problems depends upon the numerical solution of Laplace's equation for given boundary values. Methods have been perfected which materially reduce the time and labor involved in the iterative process. In this process arbitrary values are assumed at the points of intersection of a square network, and these values are systematically and repeatedly adjusted in accordance with the well-known requirement that the value of a harmonic function at every point must equal the mean of the values at four equidistant nearby points. Notable improvements in the process of iteration were made by Shortley and Weller.[1] They introduced the use of the nine-block unit, the preliminary coarse network and the general rectangular network.

In this paper a method is suggested which further improves the iterative process by providing a *rational* set of initial values in the place of the *arbitrary* numbers with which the iteration process generally begins. Another object of this paper is to provide a method for a first approximation to the value of a harmonic function at an isolated interior point from given boundary values. Such a method is of value in problems of elasticity and may be likened in its purpose to a lateral extensometer. A simplified method is also given for the transitions in a mixed network. Two examples illustrating the method are included.

The Four-Point Influence Equation

Let ψ_a, ψ_b, ψ_c, and ψ_d represent the known values of a harmonic function $\psi(x, y)$ at four points A, B, C, and D, of coordinates $(a, 0)$, $(0, b)$, $(-c, 0)$, and $(0, -d)$, respectively, as shown in Fig. 1. It can be shown that the values of the function $\psi(x, y)$ at four such given points determine a first approximation to the value of the function at the point of intersection of the two lines on which the points are located, point O, Fig. 1, and that this approximation is given by[2]

$$\left(\frac{1}{ac}+\frac{1}{bd}\right)\psi_o=\frac{1}{a(a+c)}\psi_a+\frac{1}{b(b+d)}\psi_b+\frac{1}{c(c+a)}\psi_c+\frac{1}{d(d+b)}\psi_d. \quad (1)$$

We observe that the denominators on the right side of the equation represent simple areas. Thus $a(a+c)$, $c(c+a)$ represent, respectively,

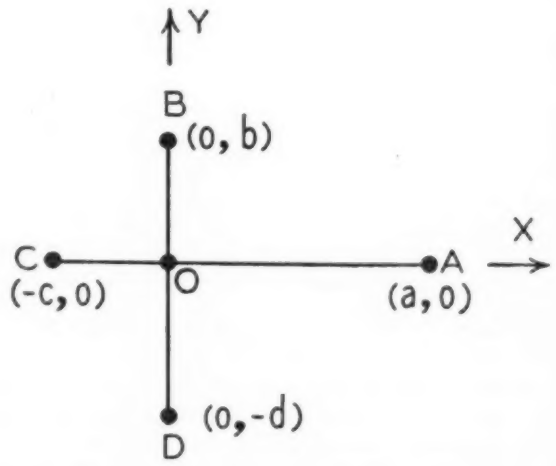

FIG. 1. Representation of the known values of a harmonic function at four points.

---

* Paper presented at the Eleventh Semi-Annual Eastern Photoelasticity Conference, May 24–25, 1940, at the Carnegie Institute of Technology, Pittsburgh, Pennsylvania.

** Associate Professor of Mechanics, Carnegie Institute of Technology.

† Mechanician and part-time instructor, Mechanics Department, Carnegie Institute of Technology.

[1] See G. H. Shortley and R. Weller, "The numerical solution of Laplace's equation," J. App. Phys. **9**, 334 (1938).

[2] See reference 1, Eq. (23).

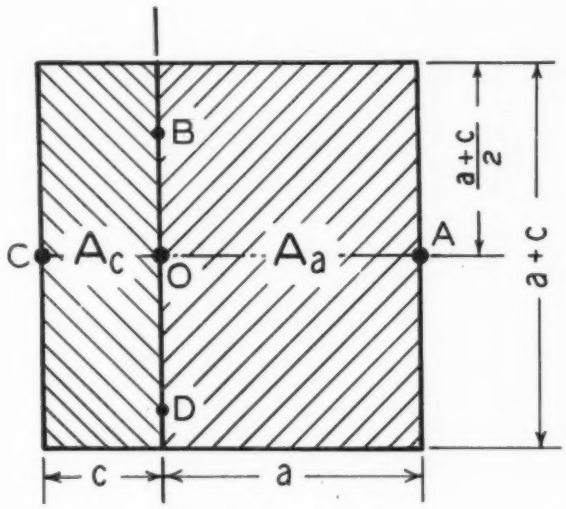

FIG. 2. Areas of diffusion.

areas A_a and A_c shown in Fig. 2. These areas we term *areas of diffusion*. Each of the four boundary points may thus be associated with an area of diffusion. The ratio of boundary value at a point by the corresponding area of diffusion we define as the *diffused boundary value* and denote by w_i. Thus

$$w_a=\psi_a/A_a, \quad \text{etc.}$$

In terms of this notation Eq. (1) becomes

$$\psi_o=\beta(w_a+w_b+w_c+w_d), \tag{2}$$

in which

$$\beta=\frac{1}{(1/ac+1/bd)}. \tag{3}$$

The coefficient β will be spoken of as the four-point coefficient and the value of ψ_o given by Eq. (2) as the *four-point influence*. We thus have the following proposition: *the four-point influence at a point is given by the product of the four-point coefficient and the sum of the four diffused boundary values*. We note that the diffused boundary value diminishes as the distance from the origin increases.

The Four-Point Influence Curve

The four-point influence given by Eq. (1) represents a close approximation to the true value of ψ_o at the origin O when the variation in the boundary stresses about the point are negligible. This is, of course, always the case when the distances from the point to the boundaries are infinitesimally small. When these distances are not small the four-point influence may differ radically from the true local value of $\psi(x, y)$. If, however, the influences of several four-point sets from different directions be determined, and a curve plotted with these influences as ordinates and angular displacements as abscissae as shown in Fig. 6, it is reasonable to assume that the mean value of these four-point influences will be a better approximation to the true value of the harmonic function $\psi(x, y)$ at the given point than any one of the separate values. The curve determined from the four-point influences will be referred to as the *four-point influence curve*, or as the *influence curve*.

The influence curve repeats itself when the coordinate axes rotate through an angular region of $\pi/2$. In the special case when a point lies on a line of symmetry the influence curve for that point becomes symmetrical at $\theta=\pi/4$ where θ is measured from the line of symmetry. The mean ordinate of the influence curve furnishes the first approximation to the value of a harmonic function at an interior point from given boundary values.

Example 1.—Consider the bar with the circular hole shown in Fig. 3, and let it be required to

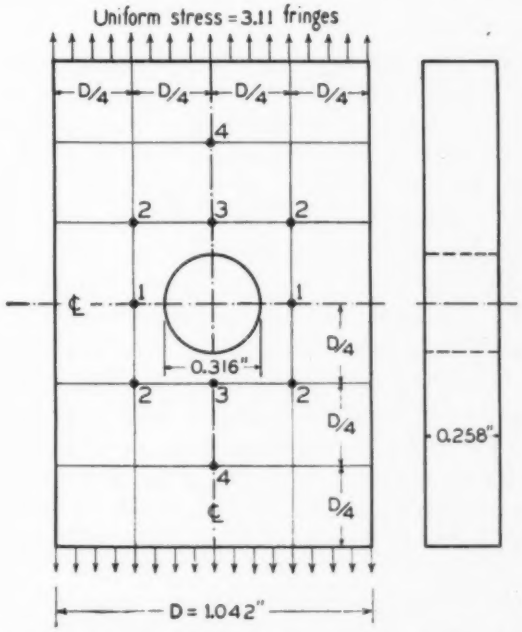

FIG. 3. Sketch showing dimensions of a bar with an axial circular hole in tension and key points.

TABLE I. *Bar with central circular hole subjected to pure tension data for key-point calculations.*

Point	Angular Position	a	c	b	d	$p+q$ a	c	b	d	i	Mean $(p+q)_i$	From Harmonization
1	0°	0.392	1	3	3	9815	2890	3110	3110	7665	5850	5510
	14°	0.405	1	3	3	9280	2940	3110	3110	7265		
	28.5°	0.455	1	3	1.8	7400	3190	3110	3750	5880		
	37°	0.64	1	3	1.31	800	3400	3110	4100	2090		
	37°	3	1	3	1.31	3270	3400	3110	4100	3550		
	45°	3	1	3	1	3110	3750	3110	3750	3590		
2	0°	1	3	2	4	3750	3750	3110	3110	3575	3300	3175
	20°	1	3	2	2.75	4120	2900	3110	3750	3665		
	20°	1	1.21	2	2.75	4120	−2120	3110	3750	1670		
	22°	1	1.00	2	2.48	4140	−4000	3110	4150	660		
	45°	1	0.57	2	1	3500	2860	3110	2890	3064		
	68.5°	2	1.06	3	1	3110	9815	3300	3280	5750		
	70.5°	2	1.22	3	1	3110	8100	3420	3310	4920		
	70.5°	2	4	3	1	3110	3110	3420	3310	3280		
	90°									3575		

determine the sum of the principal stresses at the points 1, 2, 3 and 4. It is well known that in a plane stress system the sum of the principal stresses p and q satisfies Laplace's equation,[3] i.e.,

$$\partial^2(p+q)/\partial x^2+\partial^2(p+q)/\partial y^2=0.$$

We also observe that the edges of the bar are free boundaries, so that at every point one principal stress vanishes and the remaining stresses are parallel to the edges. Furthermore, the photoelastic stress pattern, Fig. 4, furnishes the values of $(p-q)$ at every point, and at free boundaries it gives also directly the sum of these stresses.

We then proceed as follows: through point (1) we draw several pairs of coordinate axes, each pair in different directions. In the case under consideration these directions were chosen at 0°, 14°, 28°, 30°, 37° and 45° with the horizontal, Fig. 5. The coordinate axes are produced to the free boundaries and the distances from the origin, point (1), to the points of intersection with the boundaries measured for each set of axes. These distances represent the coordinates a, b, c and d entering into Eq. (1) and they, as well as the boundary values of $(p+q)$, are shown in Table I. From these data the four-point influence for each set of axes is calculated by means of Eq. (1) and an influence curve plotted, Fig. 6. The area under this curve is then measured with a planimeter and the mean ordinate calculated. The abrupt drops or changes in the curve correspond to positions of the axes at which there are two different boundary values. This happens where $\theta=37°$. One axis is then tangent to the circle representing the hole and

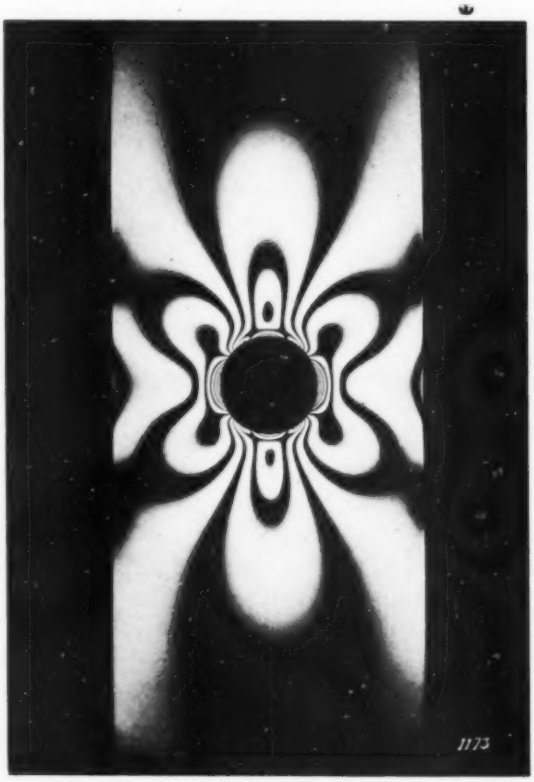

FIG. 4. Photoelastic stress pattern for the bar shown in Fig. 3. Model fringe value = 340 psi tension or compression.

[3] For a proof see Max M. Frocht, "Isopachic stress patterns," J. App. Phys. **10**, 248 (1939) or *Theory of Elasticity* by S. Timoshenko (McGraw-Hill Book Company, New York, 1934).

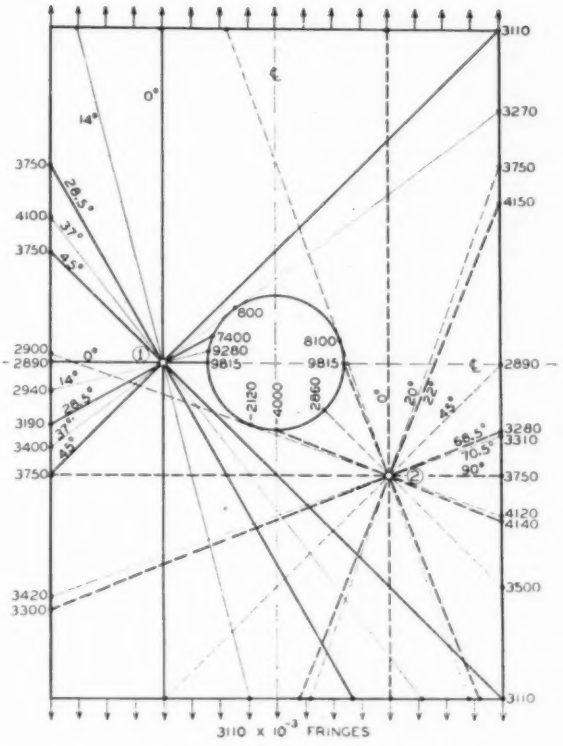

FIG. 5. Drawing showing coordinates and their directions for key points (1) and (2).

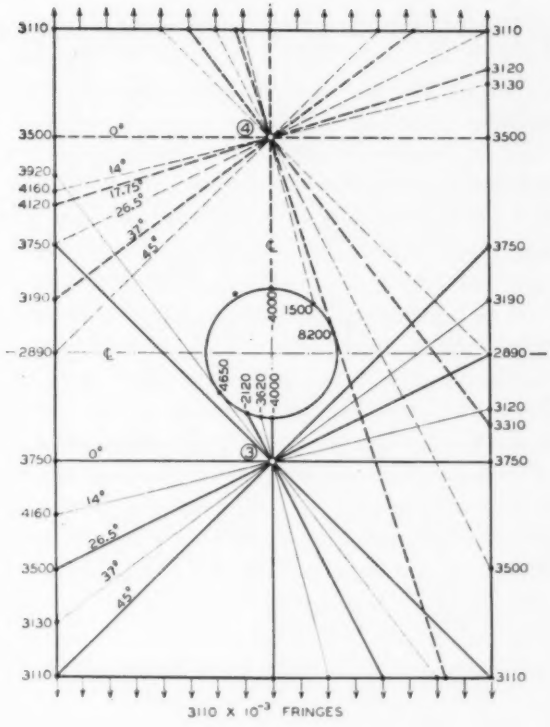

FIG. 7. Drawing showing coordinates and their directions for key points (3) and (4).

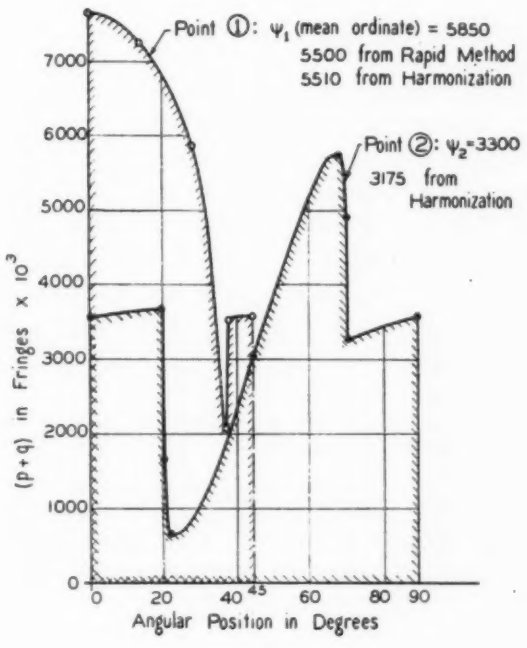
Point ①: ψ1 (mean ordinate) = 5850
5500 from Rapid Method
5510 from Harmonization
Point ②: ψ2=3300
3175 from Harmonization
(p+q) in Fringes x 10³
Angular Position in Degrees

FIG. 6. Influence curves for key points (1) and (2).

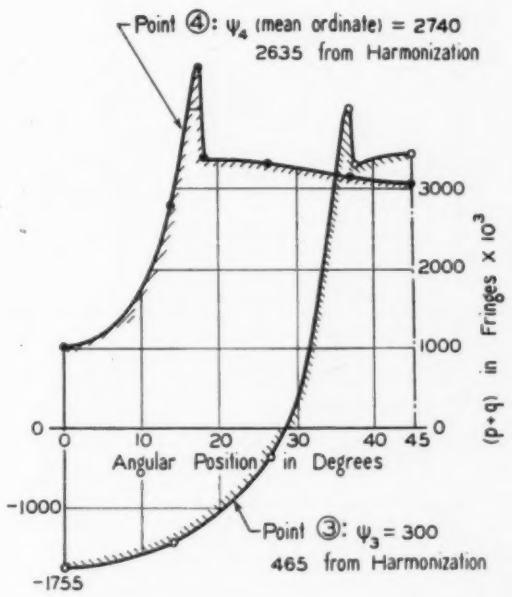
Point ④: ψ4 (mean ordinate) = 2740
2635 from Harmonization
Point ③: ψ3 = 300
465 from Harmonization
(p+q) in Fringes x 10³
Angular Position in Degrees

FIG. 8. Influence curves for key points (3) and (4).

$(p+q)$ equals 800 at the point of tangency or 3270 at the right edge. At point (1) the mean value of $(p+q)$ obtained from the four-point influence method is 5850 psi.

In a similar manner the mean four-point influence value was determined for points 2, 3 and 4 which were found to be 3300, 300 and 2740 psi, respectively. The coordinate axes and the resulting curves are shown in Figs. 5, 6, 7 and 8.

It is interesting to compare the values so obtained with what may be called theoretical values for the same problem which are 5510, 3175, 465 and 2635 psi for points 1, 2, 3, and 4, respectively. These have been obtained by a process of iteration and may be looked upon as values at convergence. It is seen that the differences between the two sets of values are small. Moreover, the results from this problem seem to be typical. A fairly large number of other problems have been solved and the differences were approximately the same. There is, of course, no certainty that such will always be the case, and no claim is made that the errors will never be greater. But nearly the same situation exists in other approximate methods, such as the Ritz method, which is widely used in problems of vibrations. For practical purposes the suggested procedure may be viewed as giving a good first approximation to the value of $(p+q)$ at an isolated point.

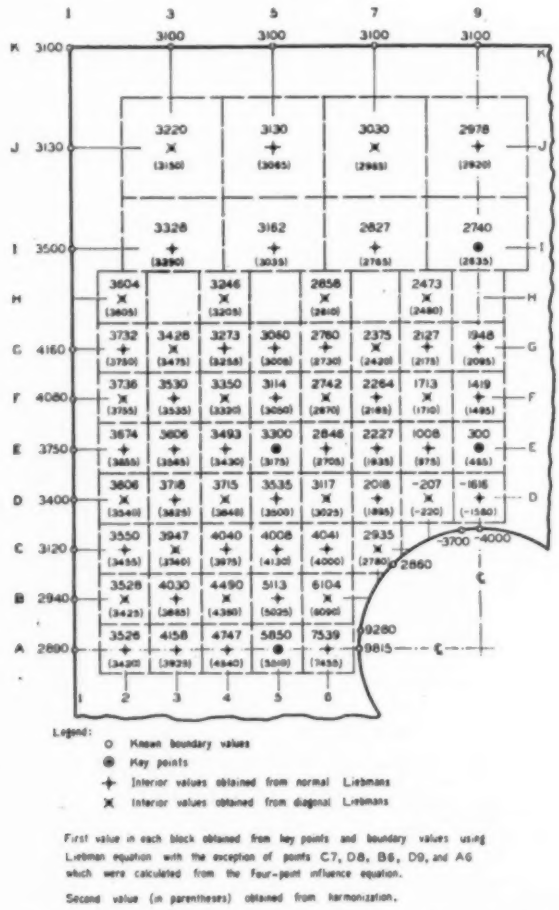
Legend:
Known boundary values
Key points
Interior values obtained from normal Liebmans
Interior values obtained from diagonal Liebmans
First value in each block obtained from key points and boundary values using Liebman equation with the exception of points C7, D8, B6, D9, and A6 which were calculated from the four-point influence equation.
Second value (in parentheses) obtained from harmonization.

FIG. 9. Values of $(p+q)$ obtained by breaking down the key points. Final values from harmonization are shown in parentheses for comparison.

The above application of the mean four-point influence value is, however, incidental. Its main value lies in providing a rational approach to the problem of determining a complete solution for the values of $(p+q)$ for the whole bar by the process of iteration or harmonization. To illustrate this we again refer to Fig. 3 and observe that points 1, 2, 3, and 4 have been chosen in such a manner that they furnish key points for the direct transition to the finer mixed network shown in Fig. 9, this transition to be effected by means of the simple Liebman equation,

$$(p+q)_o=\sum_o=\tfrac{1}{4}(\sum_a+\sum_b+\sum_c+\sum_d),$$

used either normally or diagonally at all points except those on the curved boundary. The final broken-down values of $(p+q)$ are shown in Fig. 9.

Improvement in the Transition from a Coarser to a Finer Network in a Mixed System

At a curved boundary, where the values of the function change abruptly, it is desirable to have a much finer network than at straight portions where the changes in function are much smaller. To facilitate the work of iteration or harmonization Shortley and Weller[1] give the following improvement formulas:

$$\psi_d=\tfrac{1}{4}(\psi_a+\psi_c+\psi_j+\psi_e),$$
$$\psi_n=\tfrac{1}{4}(\psi_j+\psi_n+\psi_g+\psi_o),$$
$$\psi_g=\tfrac{1}{6}(2\psi_b+\psi_f+\psi_m+2\psi_i),$$
$$\psi_j=\tfrac{1}{9}(2\psi_d+3\psi_i+\psi_n+3\psi_k),$$
$$\psi_i=\tfrac{1}{16}(4\psi_c+5\psi_g+\psi_m+\psi_n+5\psi_j),$$

the notation being as shown in Fig. 10.

However, the introduction of a few auxiliary points (S), in the manner shown in Fig. 10,

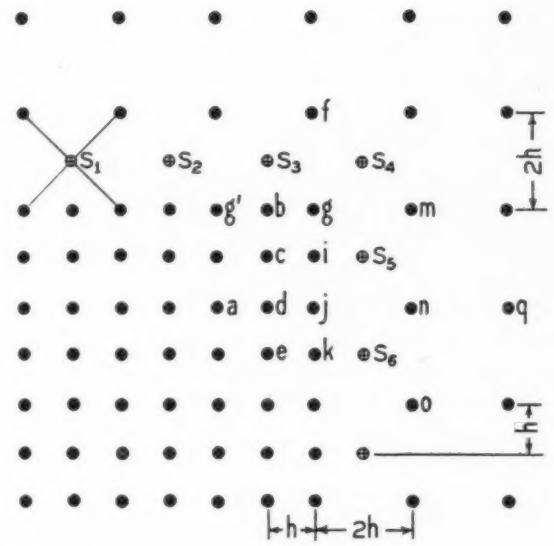

FIG. 10. Sketch showing transition from coarse to finer network in a mixed system.

eliminates the need for special equations and makes it possible to pass from one network to another twice or half the size of the first by the direct and simple use of the Liebman equation, employed either normally or diagonally. The values at the auxiliary points marked S can obviously be calculated by the Liebman equation used diagonally. Thus

$$\psi_{S_5}=\tfrac{1}{4}(\psi_g+\psi_m+\psi_n+\psi_j).$$

Points g', b, g, i, j, k, etc., on the rows of the fine network adjacent to the coarse one can now be improved using the auxiliary points S as follows:

$$\psi_g=\tfrac{1}{4}(\psi_{S_3}+\psi_{S_4}+\psi_{S_5}+\psi_c),$$
$$\psi_b=\tfrac{1}{4}(\psi_{g'}+\psi_{S_3}+\psi_g+\psi_c), \quad \text{etc.}$$

The final values of $(p+q)$ shown in Fig. 9 have been obtained from the values at the key points by the above method.

The Use of Conformal Transformations

In problems of elasticity it often happens that the boundaries contain circular holes, grooves, or other discontinuities. In such problems, Cartesian coordinates necessitate correction factors at the curved boundaries. Furthermore, since such discontinuities are generally sources of stress concentration, it is also necessary to use a much finer network near these sources, which results in measurable increase in the amount of work.

Considerable labor can be saved in such cases by combining the four-point influence method with polar coordinates. The use of such coordinates eliminates the need for correction factors, and gives from the start as large a number of points on the curved boundaries as conditions require. This automatically results in a finer network in the regions surrounding the sources of stress concentrations, and a progressively coarser network in the regions removed from the origin.

The theoretical justification for this procedure rests on the possibility for a conformal transformation of rectangles into circles and vice versa, Fig. 11, by means of the equations

$$u=\log r \quad (a); \quad v=\theta \quad (b). \qquad (4)$$

It can be shown that, for analytic functions, all the essential relations between points in Cartesian coordinates, such as the nine-block procedure suggested by Shortley and Weller, are also valid at the corresponding points of the polar coordinate system.

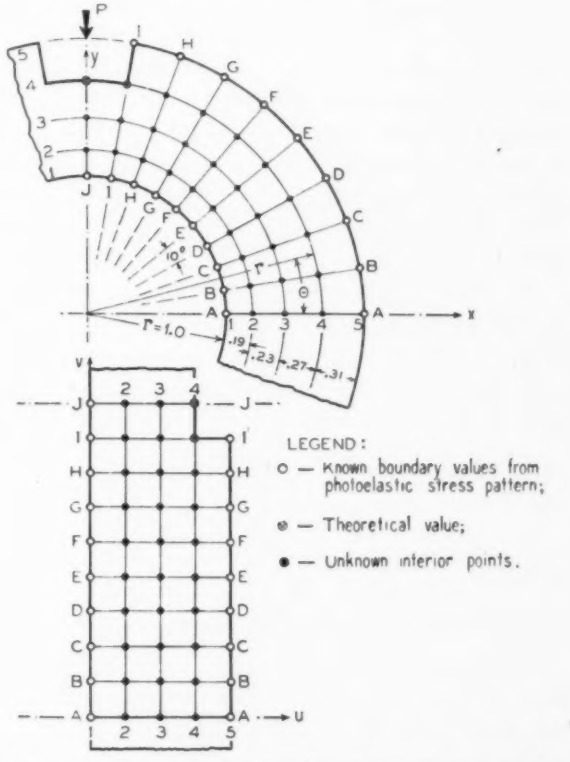

FIG. 11. Drawing showing conformal transformation of a quadrant of a circle into squares.

FIG. 12. Photoelastic stress pattern of a ring subjected to diametral compression. Loads and dimensions as shown in Fig. 13. Model fringe value = 500 psi tension or compression; thickness = 0.1795 in.

Example 2.—An ideal example illustrating the combined use of the four-point influence method and polar coordinates is the circular ring under diametral loads. Figure 12 shows the photoelastic stress pattern of such a ring. The dimensions of the polar coordinates which are necessary in order to transform the ring into an approximately square network are shown in Fig. 13. These dimensions Δu and Δv are calculated from Eqs. (4a and b).

In order to have a square network it is obviously necessary to divide the interval $A-A$, Fig. 13, into an integral number of equal intervals, say four. The value of Δu representing one side of the transformed squares is given by

$$\Delta u = (\log 2 - \log 1)/4 = 0.1735.$$

But for a square network

$$\Delta v = \Delta u.$$

Hence

$$\Delta\theta = \Delta v = 0.1735 = 10°, \text{ approximately.}$$

It is obvious that in cases such as rings it may not be possible to find a polar network which will transform into perfect squares. These errors can, however, be made small enough to be negligible.

Furthermore, in the immediate vicinity of the load, it is convenient to replace the concentrated load P by a radial stress system[4]

$$\sigma_r = -2P\cos\theta/\pi rt, \tag{5}$$

in which P is the applied load, r and θ the polar coordinates, and t the thickness of the ring.

Figure 14 shows a typical repeating section of the ring after transformation. It also shows the three key points as well as systems of coordinates in different directions for each key point, and the corresponding values of $(p+q)$ obtained from the stress pattern of Fig. 12.

Figure 15 shows the three resulting influence curves and the mean influence values of $(p+q)_1$, $(p+q)_2$, and $(p+q)_3$. These were broken down and transferred to the finer network shown in Fig. 16 by means of the Liebman equations used normally or diagonally. The results from the first breaking down of the key points are given by the upper and heavier number in each block. For purposes of comparison the values at convergence are shown in parenthesis in both Figs. 9 and 16.

The suggested procedure is therefore as follows: We determine several key values by the four-point influence method for a coarse network, break these down by use of the Liebman equation

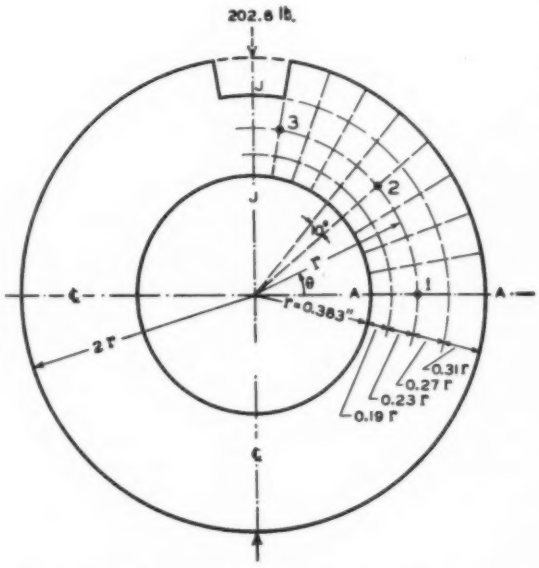

FIG. 13. Sketch showing key points in a quadrant of a ring.

[4] See S. Timoshenko, reference 3, p. 104.

to a finer network in the manner shown in Figs. 9 and 16, and then test the solution by traversing. In the problems which we solved, one—or at most two—traverses were all that was needed. However, no general rule need be laid down for the number of traverses required as this is automatically indicated by the changes produced by the iteration.

Discussion of Results

Inspection of Fig. 9 shows some rather interesting results. The upper value in each block is obtained from the key points calculated from the mean four-point influence, whereas the lower values have been obtained from repeated traversing or iteration and may be taken as the values at convergence. The closeness of the results is indeed striking. Thus, at point *G*5, the corresponding values are 3060 and 3005, and at *D*5 they are 3535 and 3500.

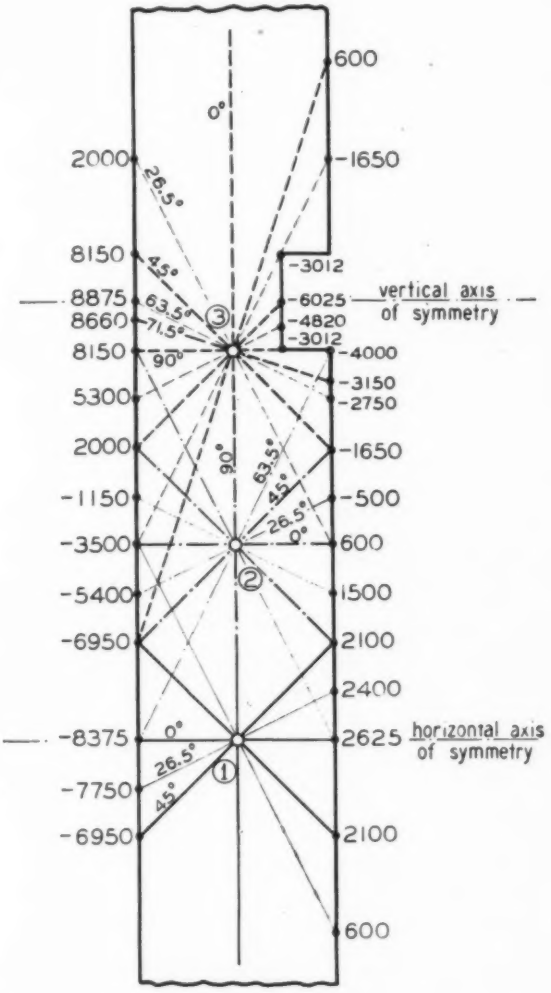

FIG. 14. Drawing showing coordinates and their directions for the key points in a repeating section of the conformally transformed ring.

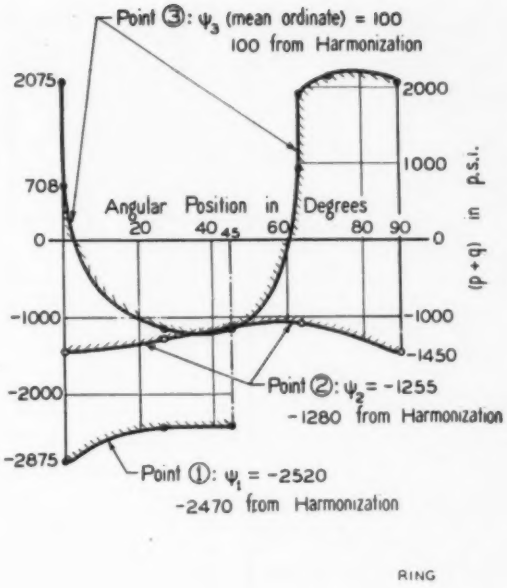

FIG. 15. Influence curves for the key points in the ring.

Inspection of Fig. 16 shows an even greater degree of agreement between the unimproved values obtained from the key points and those at convergence obtained after many traverses. At the key points themselves these values are −2520, −1255, and 100, compared with −2420, −1280, and 100 at points (1), (2), and (3), respectively.[5]

Limitation of space does not permit further illustrations. Other problems involving bipolar coordinates and the rational approach have, however, been worked out. In general, where the boundaries are curved, the mean unimproved influence values after a conformal transformation represent a closer approximation to the true values than those from the original boundaries.

The original paper presented before the conference also contained a discussion of a funda-

[5] Contours or isopachic curves for the ring under consideration, based on the values from the numerical solution, and a composite photograph of the theoretical isopachic curves and those obtained by means of interference fringes from the surface of a steel model can be found in the paper given in footnote 3.

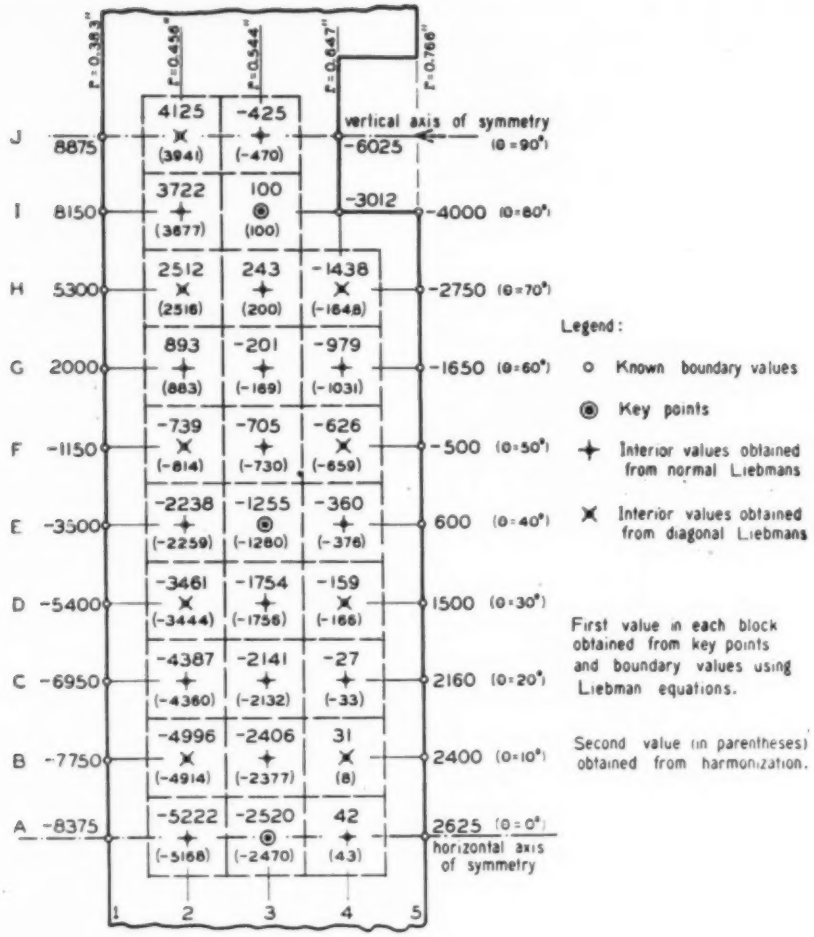

FIG. 16. Values of $(p+q)$ obtained by breaking down the key point values. Final values from harmonization are shown in parentheses for comparison.

mental theorem on stress trajectories. This theorem and its applications have since been published, and will therefore be omitted from this paper.[6]

[6] See Max M. Frocht, *Photoelasticity*, Vol. I, pp. 205–213 (John Wiley and Sons, Inc., New York, 1941).

Acknowledgment

The authors take this opportunity to express their appreciation to Dr. Robert E. Doherty, President of the Carnegie Institute of Technology, and to Dr. Webster N. Jones, Director of the College of Engineering, for their support of this work.

Classification of Isotropic Points as Defined by $\sigma_1-\sigma_2=0$ within a Regular Region*

BY MICHAEL A. SADOWSKY

Illinois Institute of Technology, Chicago, Illinois

(Received February 19, 1941)

1. *Limitations of the Proposed Problem*

AS seen by the title of the present paper we are not going to consider isotropic points located on the boundary of the elastic body, nor shall we deal with singular points which correspond to applied external efforts, such as a force or a moment, concentrated at the point of application. However, the methods as developed in the present paper may be readily extended to cover the excluded cases. For the present, we assume that the stress components σ_x, σ_y, τ_{xy} and the displacements u and v are one-valued finite regular functions of the coordinates x and y.

2. *One-Valued Determination of Principal Stresses*

Having two principal stresses and two letters σ_1 and σ_2 to denote them by, let us establish a one-to-one correspondence by means of the condition

$$\sigma_1 \geqslant \sigma_2. \tag{2.1}$$

If the principal stresses are different in value, the question as to which one is σ_1 and which one is σ_2 is now answered in a unique sense by (2.1). If, however, the principal stresses are equal in value, the above question becomes vacuous. Hence, (2.1) leads to a one-valued determination of σ_1 and σ_2 in any case.

Considering the difference of the principal stresses $\sigma_1-\sigma_2$, we derive from (2.1)

$$\sigma_1-\sigma_2 \geqslant 0. \tag{2.2}$$

To compute that difference, we may use

$$(\sigma_1-\sigma_2)^2=(\sigma_x-\sigma_y)^2+4\tau_{xy}^2 \tag{2.3}$$

in Cartesian coordinates, or

$$(\sigma_1-\sigma_2)^2=(\sigma_r-\sigma_\theta)^2+4\tau_{r\theta}^2 \tag{2.4}$$

in polar coordinates. In either case, a consideration of (2.2) will lead to a one-valued determination of the difference of the principal stresses.

3. *Isotropic Points*

Points at which the difference of principal stresses is equal to zero play an exceptional rôle relative to stress trajectories, isoclinic and isochromatic curves, etc. All those curves show characteristic irregularities at such points, namely angular points, knots, multiple points, isolated points, etc. For this reason a special terminology is introduced and points at which

$$\sigma_1-\sigma_2=0 \tag{3.1}$$

are called *isotropic*. Considering the stresses, isotropic points do not display any irregular features, since the stresses are finite and can be represented by Taylor's expansions. The influence of isotropic points is structural: they determine the topological structure of the systems of stress trajectories, isoclinic and isochromatic curves, etc.

An isotropic point, P, is called *isolated* if a circle of radius $\rho>0$ may be drawn around it such that P (the center) be the *only* isotropic point within that circle.

4. *Indefiniteness of ϕ at Isotropic Points*

The direction angle ϕ of a principal stress is given by

$$\tan 2\phi=2\tau_{xy}/(\sigma_x-\sigma_y) \tag{4.1}$$

in Cartesian coordinates, and by

$$\tan 2(\phi-\theta)=2\tau_{r\theta}/(\sigma_r-\sigma_\theta) \tag{4.2}$$

in polar coordinates. The above formulas become indefinite if, and only if, both numerator and

* Paper presented at the Eleventh Semi-Annual Eastern Photoelasticity Conference, May 24–25, 1940, at the Carnegie Institute of Technology, Pittsburgh, Pennsylvania.

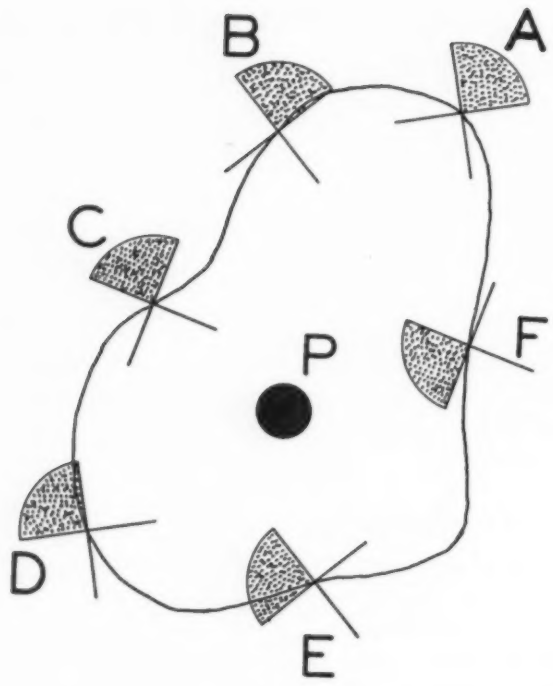

FIG. 1.

denominator of either fraction vanish. In such a case (2.3) and (2.4) give $\sigma_1-\sigma_2=0$, which means an isotropic point. Hence, at regular (non-isotropic) points the value of ϕ is definite and can be found from (4.1) or (4.2), while at isotropic points neither (4.1) nor (4.2) gives a definite answer for ϕ on account of the indeterminate form 0/0.

The reason for the above failure of ϕ at isotropic points is that ϕ is *discontinuous* at such points, and thus no value at all is being assigned to ϕ at isotropic points.

5. *Index of an Isotropic Point*

Let P be an isolated isotropic point within a regular region. Let $ABCDEFA$ be a circuit about P such that P is the only isotropic point within that circuit and no isotropic point is on the path of the circuit, either. Let us now consider the variation of ϕ as corresponding to a motion from A to A along the closed circuit $ABCDEFA$ (Fig. 1). The variation of ϕ will be continuous since there is no isotropic point *on* the circuit. Back at A, the ultimate orientation of principal directions has to be congruent with the initial orientation at A. Moreover, the first and the second principal directions, separately, have to arrive at A in positions congruent to their respective positions at start, because the principal directions cannot exchange their rôles of being "first" and "second" during the circuit: such an exchange between σ_1 and σ_2, which are *continuous*, would be possible only at a place where $\sigma_1=\sigma_2$. But there is no place of this kind on the circuit—it would be an isotropic point, which we have excluded.

Hence, *the principal directions* (σ_1, σ_2) *have rotated through an integer multiple of* 180° *during the circuit.* This can be written as

$$\oint d\phi = j\pi, \tag{5.1}$$

in which j is an *integer* (positive, negative, or zero, as depending on the intrinsic nature of the isotropic point P and independent of the shape of the circuit). The number j may be called the *index* of the isotropic point P:

$$j=\frac{1}{\pi}\oint d\phi. \tag{5.2}$$

For a regular (non-isotropic) point, $\oint d\phi=0$ and thus $j=0$. The converse is not true, since there exists an isotropic point (No. 8) for which $j=0$. As will be shown later, unit is an upper bound to j, hence all possible values of j are given by

$$j=1,\ 0,\ -1,\ -2,\ -3,\ \cdots. \tag{5.3}$$

6. *Airy's Stress Function in the Vicinity of an Inner Point*

Airy's stress function, F, is given by

$$F=\frac{T}{2}r^2+\frac{S}{2}r^2\cos 2(\theta-\theta_0)+\sum_{m=1}^{\infty}\frac{r^{m+2}}{m+1}\left[\frac{L_m}{m}\cos(m\theta-\lambda_m)+\frac{M_m}{m+2}\cos((m+2)\theta-\mu_m)\right]. \tag{6.1}$$

In the above, T, S, θ_0, L_m, M_m, λ_m, μ_m are arbitrary constants, and $L_m\gtrless 0$, $M_m\gtrless 0$ for all values of m.

Absent from F are terms with negative or fractional exponents of r as well as the following terms:

$$x \log r, \quad y \log r, \quad x\theta, \quad y\theta, \quad \log r, \quad \theta, \quad r^2 \log r, \quad r^2\theta, \quad \sin 2\theta, \quad \cos 2\theta, \qquad (6.2)$$

because such terms would give rise to either infinite or many-valued displacements and stresses, which is excluded by the condition that the point P be an inner point of a regular region.

7. *Order of an Isotropic Point*

Using Airy's stress function to compute the stresses in polar coordinates, we find that $S=0$ for an isotropic point while the term with T has no influence whatsoever upon the formation of stress trajectories, isoclinic and isochromatic curves, etc., because the direction angle ϕ of the principal stresses does not depend on the term with T. Hence, we may confine our consideration to that part of F which is given by the infinite series in (6.1). The value of m corresponding to the initial term in that series (first term *actually present*) is called the order of the isotropic point and is denoted by n. We may write formally,

$$\text{Order} = n = \text{minimum of } m \text{ for } (L_m, M_m) \neq (0, 0). \qquad (7.1)$$

As the summation in the series (6.1) starts with $m=1$, the order, n, cannot be less than one, hence, the possible values are

$$n = 1, 2, 3, 4, \cdots. \qquad (7.2)$$

8. *Isotropic Points without Complications*

An isotropic point of order n for which

$$L_n \neq M_n \qquad (8.1)$$

will be referred to as isotropic point without complications. If, to the contrary, $L_n = M_n$, the point will be called isotropic with complications. It will be shown that isotropic points without complications necessarily are *isolated* points. Hence, isotropic lines are made up of isotropic points with complications.

9. *The Index-Order Equation*

For an isotropic point without complications, the initial term of Airy's stress function determines completely and exhaustively the structure of stress trajectories, etc., at the isotropic point. To simplify the analysis, let us consider a one-term stress function and drop the superfluous subscript n:

$$F = \frac{r^{n+2}}{n+1}\left[\frac{L}{n}\cos(n\theta-\lambda) + \frac{M}{n+2}\cos((n+2)\theta-\mu)\right], \qquad (9.1)$$

in which

$$L \geqslant 0, \quad M \geqslant 0, \quad L \neq M. \qquad (9.2)$$

Computing stresses from (9.1) and using them to determine ϕ by (4.2), we obtain by a subsequent differentiation after rather lengthy identical trigonometrical transformations,

$$2\frac{d\phi}{d\theta} = -(n-1) + \frac{L^2-M^2}{L^2+M^2+2LM\cos(2\theta-\mu+\lambda)}. \qquad (9.3)$$

Using (9.3) in combination with (5.2) to compute the index j, we obtain the index-order equation:

$$j = -(n-1) + \operatorname{sgn}(L-M), \qquad (9.4)$$

in which Kronecker's sign function, $\operatorname{sgn} x$, is

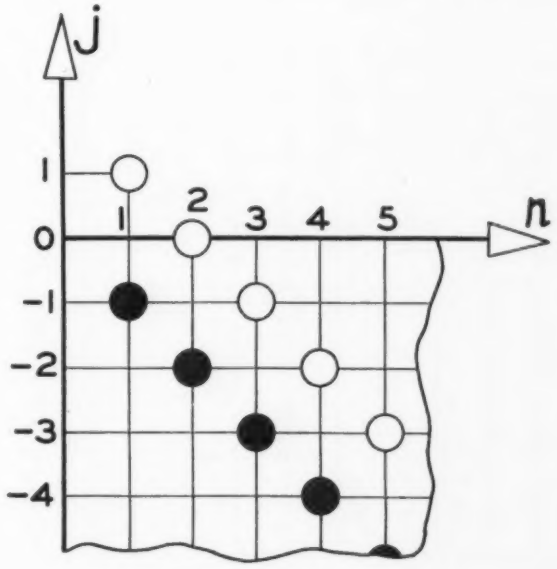

FIG. 2.

equal to one, zero, or minus one, according as its argument x is positive, zero or negative. Hence, considering (9.2), we note

$$\text{sgn } (L-M)=\begin{cases}1 \text{ if} & L>M,\\ -1 \text{ if} & L<M.\end{cases} \tag{9.5}$$

Figure 2 shows a graphical representation of the index-order equation, ring-shaped marks having been used for $L>M$, disks for $L<M$. The limitation $n\geqslant 1$ (7.2) now immediately gives rise to the limitation (5.3) of the index.

10. The Isotropic Point of Index Zero

Figure 2 shows the existence of such a point: $j=0$, $n=2$, and the ring-shaped mark means $L>M$. To have the simplest representative, let us put

$$M=0, \quad \lambda=0, \tag{10.1}$$

which leads to

$$\begin{gathered}F=\frac{L}{6}r^4\cos 2\theta=\frac{L}{6}(x^4-y^4),\\ \sigma_r=0, \quad \sigma_\theta=2Lr^2\cos 2\theta, \quad \tau_{r\theta}=Lr^2\sin 2\theta,\\ \sigma_x=-2Ly^2, \quad \sigma_y=2Lx^2, \quad \tau_{xy}=0,\\ \sigma_1=\sigma_y, \quad \sigma_2=\sigma_x, \quad \sigma_1-\sigma_2=2Lr^2, \quad \phi=0.\end{gathered} \tag{10.2}$$

The result $\phi=0$ reveals the most surprising thing, namely that the stress trajectories are *rectilinear* lines $x=$ const. and lines $y=$ const. The only interruption suffered is at (0, 0) at the isotropic point. Except for this, there is no further structural disturbance, and as shown in Fig. 3 we obtain a regular network of stress trajectories. In Fig. 3, as well as in all other figures which show stress trajectories (Figs. 4–6), we use a continuous line for the *first* stress trajectories and a dotted (interrupted) pattern for the *second* stress trajectories.

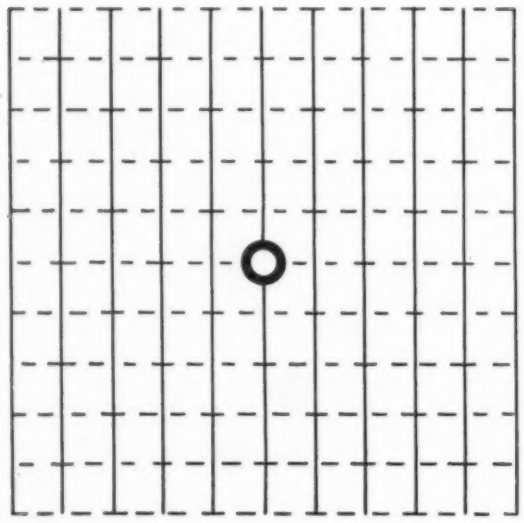

FIG. 3. $N=8$.

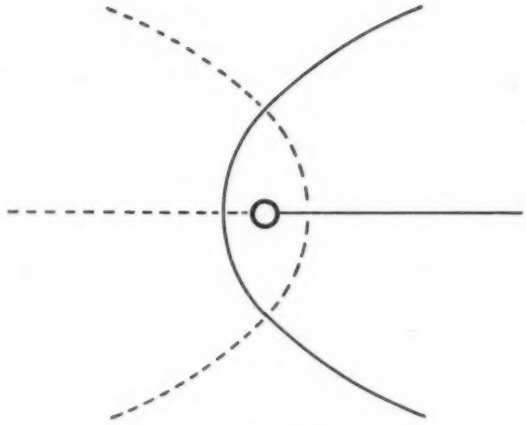

FIG. 4. $N=4$.

Isotropic points of the above kind have been actually observed on photoelastic photographs. Their fundamental "photographical" characteristic is that (1), they are dark spots, cannot be removed by any rotation of the plane of polarization of light, and (2), they *do not* produce a knot of the isoclinic system—an exception (*the only one*) from the general rule saying that an isotropic point is a knot of the isoclinic system. The stress trajectories are to be drawn straight through as if there were no isotropic point.

11. The Number R of Stress Rays

In the vicinity of an isotropic point the system of stress trajectories is so shaped that some stress trajectories pass *through* that point. As stress trajectories usually have multiple points (angular points) at an isotropic point and appear broken and ramified, let us denote by R the number of rays (semi-lines) which are stress trajectories emanating from an isotropic point. For an ordinary, non-isotropic point the two orthogonal stress trajectories through it would give $R=4$ rays. Omitting all of the mathematical analysis, we now state the resulting relative to R: the order n of an isotropic point being given, R may

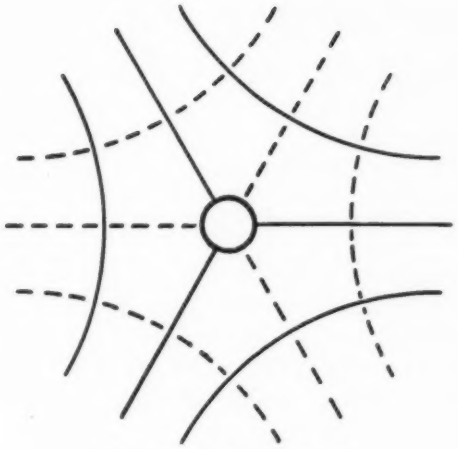

FIG. 5. $N=1$ and $N=12$.

have just one of the following three values:

$$2n, \quad \text{or} \quad 2n+2, \quad \text{or} \quad 2n+4. \tag{11.1}$$

Particulars depend on the comparative sizes of L, M and n in (9.1), namely:

$$\left.\begin{array}{l}(1),\quad R=2n+4 \text{ if } L-M<0;\\ (2),\quad R=2n \text{ if } (L-M)/(L+M)\\ \qquad\qquad \geqslant 1/(n+1);\\ (3),\quad \text{any one of the three values (11.1)}\\ \quad \text{actually possible if}\\ \quad 0<(L-M)/(L+M)<1/(n+1).\end{array}\right\} \tag{11.2}$$

12. The Catalog Number N of an Isotropic Point

For the sake of an orderly exposition of special isotropic points, let us introduce a catalog number N for each isotropic point as defined by

$$N=\tfrac{1}{2}(11n+j-R-2). \tag{12.1}$$

The above formula is arranged in such a way that the catalog numbers proceed in order of the natural sequence

$$N=1, 2, 3, 4, \cdots \tag{12.2}$$

without repetition and without omission. Any two isotropic points which differ either in n, or in j, or in R, will get two *different* catalog numbers by (12.1). The following table gives an exposition of the characteristics of isotropic points Nos. 1–16:

$N=$	1	2	3	4	5	6	7	8	9	10	11	12	13	14	15	16
$n=$	1	1	1	1	2	2	2	2	3	3	3	3	4	4	4	4
$j=$	−1	1	1	1	−2	0	0	0	−3	−1	−1	−1	−4	−2	−2	−2
$R=$	6	6	4	2	8	8	6	4	10	10	8	6	12	12	10	8

(12.3)

13. Examples

Isotropic points Nos. 1, 4, 5, 8, 12 and 16 are those most frequently observed in experimental photoelasticity. The figures as given below show the stress trajectories for those points. Some pairs of isotropic points, differing in order only, have identical stress trajectories. The difference in order would show up in the photograph of the isochromatics as the density of the fringe distribution depends on n. Point No. 8 was shown in Fig. 3. It might be of interest to have a complete catalog up to, say, $N=16$. This work could be done by means of the formulas given in the present paper. For a more detailed account, containing some auxiliary formulas, see author's paper in Russian.[1]

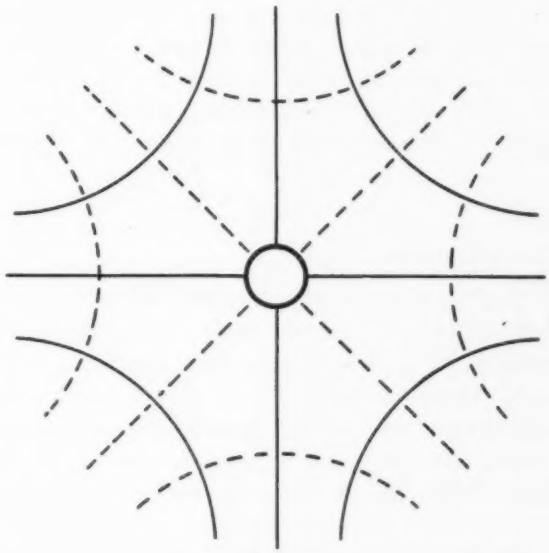

FIG. 6. $N=5$ and $N=16$.

[1] Experimentalnie Methodi Opredelenia Naprajenii i Deformazii v Uprugoi i Plasticheskoi Zonakh" (ONTI NKTP, Moscow, U. S. S. R., 1935), pp. 88–115.

Three-Dimensional Photoelasticity Using Scattered Light

BY R. WELLER

Department of Mechanical Engineering, The State College of Washington, Pullman, Washington

(Received February 8, 1941)

It is possible to use the polarization caused by the scattering of light within a photoelastic model in place of the usual analyzer in a photoelastic polariscope. This enables one, in effect, to use an analyzer which lies within the interior of the model, and so make analyses of three-dimensional stress systems very conveniently. This is accomplished in practice by projecting into the model a beam of polarized light which has been collimated and passed through a slit, thus confining the beam to a thin sheet of light. Such a sheet will illuminate any desired plane section of the model, and in this section will appear interference fringes from which the stresses in the section may be determined. By successive examination of plane sections one may completely investigate the model. In this method the spacing of the fringes is the significant feature, rather than their order, as in previous methods. It is possible, in many cases, to determine the directions of the principal stresses at interior points as well as the maximum shear at such points. Boundary stresses are evaluated both as to direction and magnitude. Equipment for this method differs in constructional details from that employed in plane stress studies in that a source of light of higher intensity must be provided and a slit is used to restrict the beam.

Introduction

UNTIL recently the photoelastic method for stress analysis has been limited to plane stress systems. There now exist, however, two truly three-dimensional methods which are theoretically capable of determining the stress system in any shape whatever. These are, in order of their discovery, the fixation method[1] and the scattered light method.[2] This paper considers the latter.

The Stress-Optic Law

The methods of photoelasticity are based on the fact that suitable transparent materials which possess optical isotropy when unstressed become birefringent under load. The development of this birefringence obeys the following relationships which are known together as the stress-optic law:

1. Light passing through the stressed material divides into two components polarized at right angles to each other. These vibrate along the directions of the "effective principal stresses."[3] That is, if the stress ellipsoid at a point is centrally intersected by the plane of the wave

[1] The first mention of the possibility of this method occurs in J. C. Maxwell, "On the equilibrium of elastic solids," Trans. Roy. Soc. Edinburgh **20**, Part 1, 87 (1849–50). The model material used by Maxwell was apparently a gelatin obtained from the sturgeon. See also A. G. Solakian, "A new photoelastic material," Mech. Eng. **57**, 767, *et seq.* (1935). In German, see G. Oppel, "Polarisationoptische Untersuchung raumlicher Spannungs- und Dehnungzustande," Forsch. Geb. Ingenieur. **7**, 240 *et seq.* (1936). (An English translation is available as Technical Memorandum No. 824 of the National Advisory Committee for Aeronautics entitled "The photoelastic investigation of three-dimensional stress and strain conditions," April, 1937.) R. Hiltscher, "Polarizationoptische Untersuchung des raumlischen Spannungszustande im konvergenten Licht," Forsch. Geb. Ingenieur. **9**, 91, *et seq.* (1938) and A. Kuske, "Das Kunstharz Phenolformaldehyd in der Spannungsoptik," Forsch. Geb. Ingenieur. **9**, 139, *et seq.* (1938). In the United States, Hetenyi has discussed this method, e.g., "The fundamentals of three-dimensional photoelasticity," J. App. Mech. **5**, 149, *et seq.* (1938).

[2] R. Weller, "A new method for photoelasticity in three dimensions," J. App. Phys. **10**, 266 (1939).

[3] D. C. Drucker and R. D. Mindlin ("Stress analysis by three-dimensional photoelastic methods," J. App. Phys. **11**, 724, *et seq.* (1940)) have used the term "secondary principal stresses." Since secondary stresses have, ordinarily, a rather different meaning, it seems desirable to refer to them as "effective principal stresses."

front, the section cut out will be an ellipse. The principal semi-axes of this ellipse are called the effective principal stresses in the plane of the wave front.

2. The relative velocity of the two light components as they pass through such a point is proportional to the difference between the effective principal stresses.

The relative velocity in (2) is a measure of the rate at which the phase shift between the two components increases along the light path. If we express this shift in wave-lengths (assuming monochromatic light) we may write:

$$CdR/ds = S_a - S_b, \qquad (1)$$

where dR/ds is the rate of growth of the phase shift in wave-lengths per unit path length, S_a and S_b are the effective principal stresses, and C is a constant representing the stress-optical sensitivity of the model material. In the event that the direction of the original light beam happens to coincide with one of the three principal stresses at a point, then S_a and S_b will be the other two principal stresses; but in general this is not the case.

Analysis by Scattering

It is convenient to consider the scattering of light from the point of view of the absorption and re-emission of light by vibrating particles. The following are results of the simple theory:

1. A beam of plane polarized light falling on a material particle in an isotropic medium will polarize it and cause it to vibrate in a direction parallel to the electric vector of the light, that is, in a direction normal to the "plane of polarization" and lying in the plane of the wave front.

2. The intensity of light scattered by a vibrator in a given direction is proportional to the square of its apparent amplitude when viewed from that direction. By "apparent amplitude" is meant the component of amplitude normal to the line of sight.

Now consider that a beam of initially plane polarized light passing through a stressed model is continuously analyzed by the scattering process. It will be convenient to assume that the beam has been collimated and passed through a slit so that a plane section of the model is illuminated. At a given point within the piece, the induced motion of a scattering particle will be the result of the combined action of the two light components. This will generally result in the execution of an elliptical orbit in the plane of the wave front. Suppose, however, that the two components arrive exactly in phase. The ellipse then degenerates to a straight line at 45° to the two components and parallel to the direction of the electric vector of the initial polarization. If this point be observed from a point outside the model and along a line of sight parallel to this vibration, no scattered light will be observed. If, however, the two components arrive at this point exactly opposite in phase, the ellipse will degenerate into a straight line at right angles to the previous one and this will now be normal to the same line of sight. A maximum of intensity of scattered light will then be seen. Obviously if one should choose a direction of observation at right angles to the previous one, but still in the plane of the wave front, these effects will be reversed, the region which exhibited no scattering before will now provide a maximum and vice versa.

Accordingly, as the light progresses through the loaded model and the two components progressively get in and out of step with each other there will appear variations in the intensity of scattered light along certain observation directions. These will constitute interference fringes very similar to those observed in the conventional plane photoelastic effect. An exception to the above will be observed in the event that the observation takes place along the direction of vibration of one of the components, that is, along the direction of one of the effective principal stresses. In this case any scattered light will be the result of vibration due to but one of the light components, and quite naturally this cannot result in interference effects. Along any other direction the fringes will be observed, but with varying degrees of distinctness, the best directions being those mentioned first. In fact the disappearance of the fringes when viewed along a direction of effective principal stress affords a convenient means for determining these stress directions.

The spacing of the observed interference fringes will decrease with an increase in stress

intensity and a corresponding increase in the rate of growth of the phase shift. In Eq. (1) if the value of dR is taken as one wave-length, then the value of ds will be the path length along which one cycle of interference takes place; that is, it will be the spacing between two consecutive interference fringes *in the direction of the original light beam*. We may then write

$$C/d = S_a - S_b, \tag{2}$$

where d is the fringe spacing. This gives the average value of the effective stress difference between the two fringes. Unless the stress variation is behaving badly this may be taken as the value at the midpoint. This is the more nearly true as the stress is increased and the fringe spacing decreases, the fringe spacing acting as the gage length over which the stress measurement is made.

Drucker and Mindlin[3] have pointed out that a correction must be made to Eq. (2) since a rotation of the axes of effective principal stress about the wave normal will cause a further crowding of the fringes and lead to values of stress which are too high. If this rotation is small compared to the rate of relative retardation, the correction may be neglected in practice.

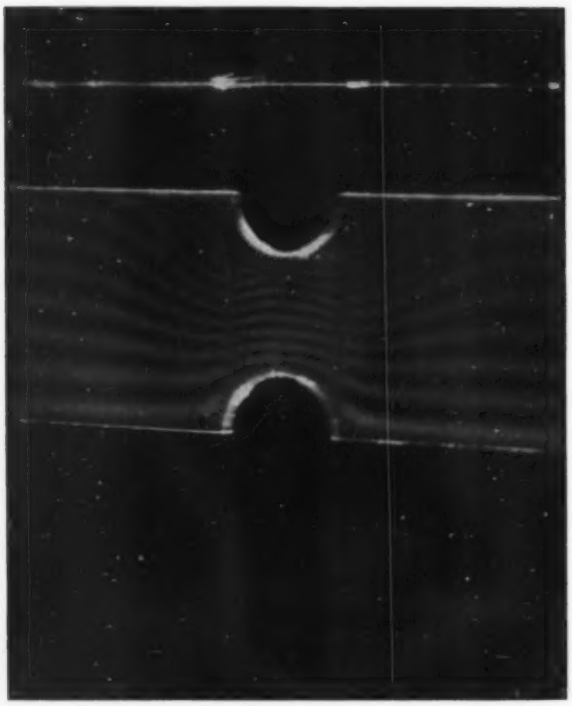

FIG. 1. Fringe pattern of notched tension model. Uniform tension in the shank is indicated by uniform fringe spacing. In the notch the fringes are more closely spaced at the boundaries indicating higher stress than in the center of the section.

FIG. 2. Microphotometric trace of notched section of tension model. In practice, the size of this trace is about ten to twenty times that of the negative. Measurements of fringe spacing may be easily made with a steel scale.

Examples

It will be convenient at this point to consider some examples of the above phenomena. The first of these is that of tension. Figure 1 shows the fringe pattern observed in a tension member of circular cross section having a semicircular notch. Here the direction of the initial light beam was normal to the side of the model and at right angles to the tension. The direction of polarization made an angle of 45° to the direction of the tension in order that the light beam should be split into two equal components. Here $S_a - S_b$ will be the actual tensile stress. The model was photographed from a direction lying in a plane

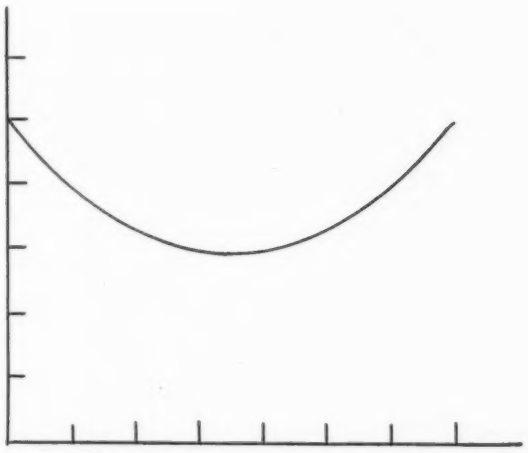

FIG. 3. Stress distribution across notched section of tension model. Values of spacing are obtained from Fig. 2 and inserted in Eq. (2) to obtain stress values at midpoints between fringes.

parallel to the wave front of the light and making an angle of 45° to the direction of the tension. This direction of observation is, of course, either parallel or perpendicular to the direction of the original polarization. In the event that it is parallel, the center of a dark fringe will lie at the point of entrance, and vice versa. This corresponds to the use of either crossed or parallel polarizers in the conventional plane-stress photoelastic procedure.

Uniformity of tension in the shank of the model is evidenced by the fact that the interference fringes are equally spaced, indicating a constant rate of phase shift between the two components of the light beam as they progress through the piece. The use of a uniform tension specimen affords a convenient method for calibrating the model material. It is found, of course, that the value of C in Eq. (1) is simply the fringe value for a unit thickness in the conventional photoelastic method. For photoelastic Bakelite BT-61-893 this is approximately 86 lb. per sq.in. per fringe for direct stress, or half of this in terms of shear.

The stress distribution across the notch is not uniform, as evidenced by the variations in the spacing of the fringes. In order to measure conveniently the spacing of the fringes in such a case one may photograph the pattern and examine the negative with a microphotometer. Figure 2 shows such a record of the fringe spacing in the notch of Fig. 2. Measurement of this microphotometric trace provides data for plotting the curve of Fig. 3, indicating the stress variation across the reduced section.

A second example of the procedure is shown in Figs. 5 and 6. The model is a shaft subjected to torsion and having in it a Woodruff key slot. Figure 4 shows the pattern as viewed along the shaft axis, whereas Fig. 5 shows the view from the side. In each of these cases the illuminated section is normal to the direction of observation. The direction of polarization for Fig. 4 is at right angles to the shaft axis and in Fig. 5 it is parallel to the axis. This results in having the center of a light fringe lie in each case at the point of entrance of the light. The two sets of fringes are therefore actually different aspects

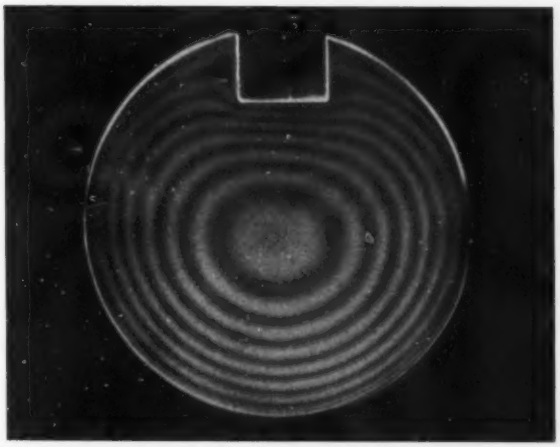

FIG. 4. Fringe pattern due to torsion in shaft with keyway. This pattern is observed when the direction of observation lies along the shaft axis.

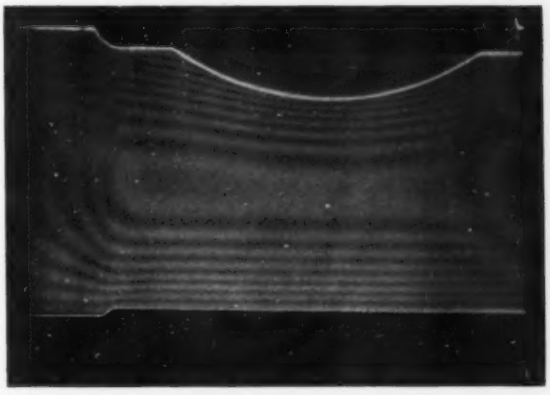

FIG. 5. Fringe pattern due to torsion in shaft with keyway. This is the shaft of Fig. 4 viewed from the side. The direction of polarization of the initial beam has also been rotated through ninety degrees.

of the same set. This is shown by Fig. 6, which gives the shape of the microphotometric traces for the two patterns. It will be observed that for all practical purposes the traces are identical.

It is of interest to recall that the case of torsion was mentioned by Solakian in 1935[1] but received little attention since the existence of a fringe pattern in the chosen section was not easily explained. It should be pointed out that his pattern is actually correct if one considers the excessive deformation to which the model was subjected in this particular instance. It is ordinarily considered that the principal stress directions in such a case are the radii of the shaft and a set of 45° spiral helices winding about the shaft axis. In the case of large strains this is no longer true.[4]

Another example of the utility of the scattering procedure lies in the fact that it may be applied to two-dimensional stress systems in such a way that the entire stress determination may be carried out optically. This has been treated by Drucker and Mindlin.[3]

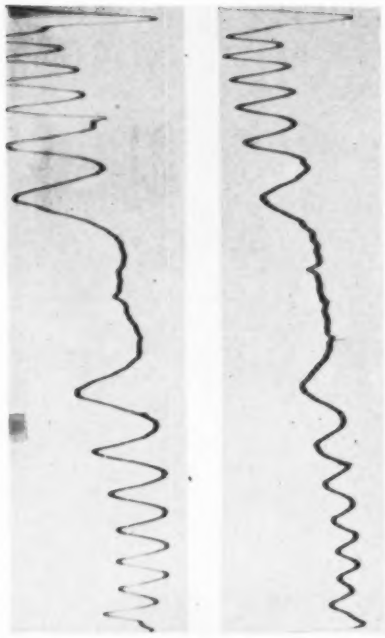

FIG. 6. Microphotometric traces of torsion patterns. The right trace is obtained from Fig. 4, the left from Fig. 5. It will be observed that these are practically identical.

Boundary Stresses

In most applications of the photoelastic method one is interested chiefly in boundary stresses. Here the scattering method enables one to obtain complete information. At a free boundary one of the principal stresses lies normal to the boundary and is of zero magnitude. The other two lie tangent to the boundary. If one projects the light beam into the model at right angles to the surface, the resulting fringe spacing will give the difference between the two tangent stresses. If the model is observed from various directions in a plane tangent to the boundary, there will be found two directions along which the fringes will vanish. These will be the directions of the tangent stresses. If the direction of one of these is known, the light may then be projected parallel to it. The fringe spacing under these conditions will give the difference between the other tangent stress and the (vanishing) normal stress, this difference being equal to the tangent stress itself. The second tangent principal stress may be determined similarly, or one may use the original difference obtained when the beam was projected normal to the boundary.

The General Case

If one desires to evaluate the stresses at an interior point he may proceed as follows. When light is projected through such a point at random the spacing of the fringes straddling the point will give the effective principal stress difference as defined previously. The minimum spacing will

[4] See B. R. Seth, "Finite strain in elastic problems," Phil. Trans. Roy. Soc. **A234**, 231, *et seq.* (1935). Here it is shown that the angle departs from 45° by an amount $\theta a/8$ where θ is the angular strain and a the radius of the shaft. For θ of unity and a of 0.5 this gives 3.6° to be subtracted from 45°. The writer has been troubled by this phenomenon. If the direction of polarization of light entering a circular shaft in which stresses are fixed, but which is examined by scattering, is parallel to a principal stress spiral at the point of entry, it remains so up to the centroid of the section. No fringes are therefore observed in the lower half of the shaft. As soon as the light passes the central plane, however, the direction of polarization is such as to give rise to fringes which are now parallel to the central plane and the effect is exactly as if the lower half of the model were cut away and light projected directly into the central plane. In fact, this cutting away was performed and the effect observed to be identical. The parallel fringes coincide with those observed from a direction lateral to the shaft in the usual scattering procedure. Where the model is loaded in the usual way the strain is small and the effect mentioned above is hardly discernible. Traces of distortion may be observed in the upper half of torsion models, however, and these may never be completely removed by any adjustment of the apparatus. But rotation of the polarizer to near coincidence with the stress directions will enhance the effect, even in cold loading.

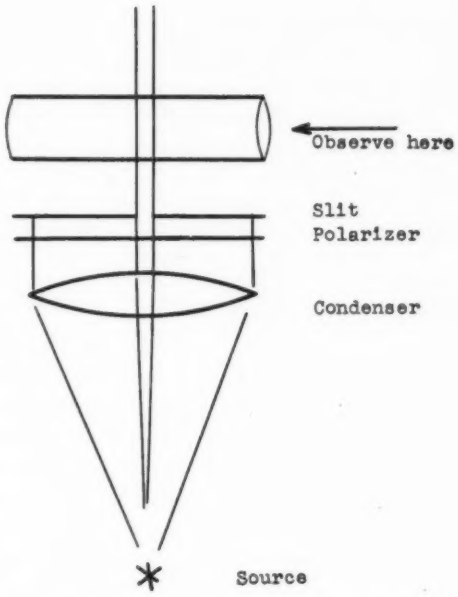

FIG. 7(a). Schematic layout of polariscope for observation by scattered light.

be obtained, however, when the light travels along the direction of the intermediate principal stress. The spacing will then be due to the difference between the maximum and the minimum principal stress, that is, to the maximum shear. This may be obtained by a rotation of the model until the fringe spacing is a minimum, that is, by systematically searching for this position. When one has obtained the maximum shear and the direction of the intermediate principal stress in this way, the other two principal stress directions may be found by locating the two directions of observation along which the fringe system vanishes. Drucker and Mindlin[3] have suggested an alternative procedure in which one measures the fringe spacing from several directions and solves for the stress system by a consideration of these spacings and the angles of light projection. So far as the writer is aware neither of these suggestions has been put into practice.

Apparatus

The type of polariscope employed for plane stress investigations is not particularly suited to the scattering procedure. Equipment more satisfactory for this work is shown in Fig. 7. It is somewhat more compact than the two-dimensional apparatus and, in general, less expensive to construct. Several features of difference are as follows. The light beam is projected vertically upward in order to permit of observation always in a horizontal direction. The light source must be much more intense due to the inefficiency of the scattering process. No analyzing unit is required, but an immersion tank and fluid are necessary to eliminate boundary refraction. A slit must be provided to permit examination of single plane sections.

The light source used has been the Type H-6 high-intensity, water-cooled, 1000-watt mercury arc lamp, supplied by either the General Electric Company or the Westinghouse Company. Smaller lamps may be used but they make a dark room necessary and lengthen photographic exposure inconveniently.

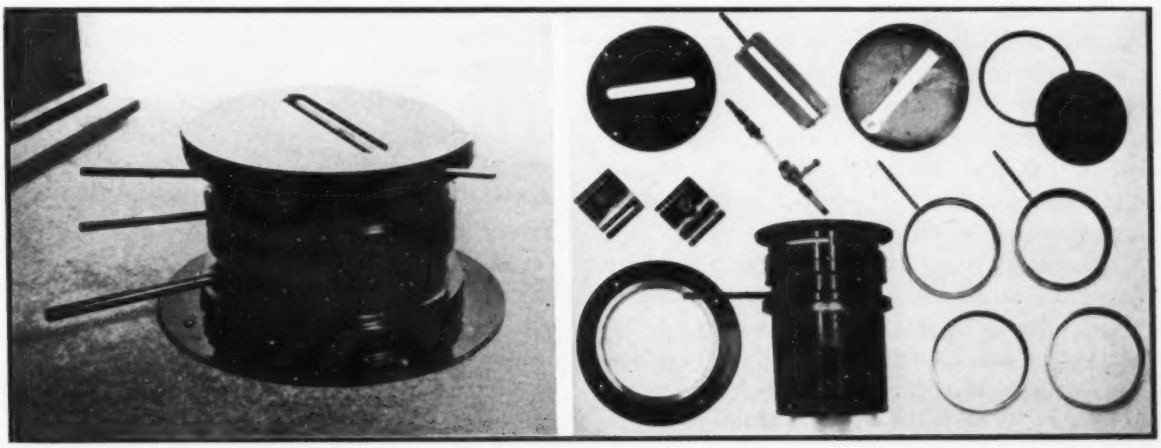

FIG. 7(b). Polariscope for observation by scattered light. The photograph on the left shows the instrument as constructed. The view at the right shows the parts before assembly.

Light from this lamp is collimated by a pair of condensing lenses, each 6.5 inches in diameter and having a focal length of 13 inches. The lamp is arranged so that it may be moved vertically and thus brought to the focal position of the lens combination.

The light then passes through a Polaroid disk of diameter equal to that of the lenses. Provision is also made for the installation of a quarter-wave plate should this become desirable. Both Polaroid and quarter-wave plate may be rotated independently within the housing, each being provided with a graduated scale.

The light then passes through a slit six inches long and of controllable width, the latter varying from about $\frac{1}{2}$ inch to the closed position. The entire housing is arranged to rotate on its support, the slit always remaining parallel to the lamp burner for maximum light efficiency. The slit is of the two-jaw variety, both jaws moving simultaneously so that the center of the observed section does not alter with slit adjustment.

The model to be observed is placed over the slit and light projected into it. Since the face of the model through which the light must enter is not, in general, plane and normal to the beam, the model must be immersed in a liquid having a refractive index equal to that of the model. One therefore requires a tank with transparent bottom and sides. Various liquids are possible in this connection. Best results have been obtained by the writer with "Halowax Immersion Fluid" which is water-white, of low viscosity, and comparatively inexpensive.

It does not seem possible to design a loading frame which will be suitable for any large variety of three-dimensional problems. Rather it has seemed advisable to build small loading fixtures for each investigation. Since the loading device must be partially or completely immersed, the use of fixtures of any size means a large tank and a large quantity of fluid.

Photography may be accomplished without difficulty. During the writer's first experiments he used a 100-watt mercury arc and found that exposures of several hours were necessary. The use of the 1000-watt lamp reduced the time to a few minutes. With a slit width of 0.1 inch, a lens having a speed of $f/6.3$, a film of Weston (daylight) speed of 50, and a Corning No. 5 mercury green filter, the time required is about 5 minutes. Using a Wratten No. 77 filter the exposure is about 1 minute. Without the filters the exposure is approximately 10 seconds but the fringes are not so distinct.

Conclusions

Theoretically, there now exist two methods by which one may completely determine the stress system in any shape. The extent to which this will be true in practice depends on the development of the required laboratory techniques. It is the writer's opinion that the accuracy obtainable from the scattered light method will be approximately equal to that expected from the two-dimensional procedure. It is possible that the investigation of thin sections will require the use of a Babinet compensator, since there may be only one fringe or a fraction of a fringe visible.

The scattering method seems to have the following advantages over the fixation procedure: the gage length is reduced since, in most cases, the fringe spacing is less than the thickness of slices which might be cut out; the deformations are normal in amount, whereas in the fixation method they are about 25 times as great; the model is not destroyed and may be observed under progressive loading and unloading; parasitic optical effects such as initial anisotropy may be observed easily. The last of these deserves special mention since it is not possible in three-dimensional work to subtract the stress due to initial conditions from those observed under load since the stress tensor may rotate during loading.

On the debit side the scattering procedure requires a new form of apparatus for convenient work; the technique of making measurements is new and needs development; it is difficult, for example, to make measurements close to a boundary; the fringes are less distinct and become progressively more so as very thick sections are encountered.

It is probable that the fixation and scattered light methods may, at times, be profitably used in combination, the model having the stresses "fixed" within it by heat treatment and being scanned with a scattering polariscope thereafter, or perhaps before being sliced.

A Photoelastic Study in Vibrations*

BY W. M. MURRAY

Massachusetts Institute of Technology, Cambridge, Massachusetts

UNDER the heading "Dynamic Stress Problems" one includes all those cases in which the stresses vary with time as compared with static stresses which are independent of time, or almost so, if we neglect the effect of creep. In brief, the group of dynamic problems can be divided into two parts; first, those dealing with transient conditions of stress which die down in a short time, as in the case of impact, and secondly, those of a cyclical nature which repeat themselves at regular intervals of time as in the cases of sustained vibration or repeated loading.

To all these problems the photoelastic analysis is not applicable since, like other methods used for determining stresses, it possesses certain limitations. However, provided that these limitations are understood, the application of polarized light to the solution of dynamic problems is a powerful tool for the engineer. Until recently the photoelastic analysis has been applicable only to problems involving plane stress or to those three-dimensional problems which could be simplified to two dimensions, but means have now been developed for making photoelastic analyses of three-dimensional static stress problems. It is very doubtful whether these methods can be applied to dynamic conditions, so that the study of this kind of problem is still limited to two dimensions. Even so, a wide field is open to the investigator.

The development in photoelastic technique which has likely been of most importance in the study of dynamic problems was the introduction of highly sensitive materials (the synthetic resins) which facilitate the use of monochromatic light and photographic recording, thereby eliminating the tedious and uncertain observations made by matching colors with a compensator. Certain work[1] yielding satisfactory results has been carried out on rotating disks with the use of white light, a celluloid model and a compensator, but the labor involved must have been very great even for this special study which was considerably reduced in complexity. This problem of the rotating disk is on the border line between static and dynamic problems since it involves motion but no fluctuation in stress provided that the speed of rotation remains constant.[2] A similar problem but one which belongs truly in the realm of dynamic stresses is that of rotating gears which have been investigated.[3] This latter problem represents a case of cyclical or repeated stressing and as such lends itself to somewhat simpler type of analysis than the problems of transient stress. In this latter field notable work has been done in this country by Frocht,[4] and in Japan by Tuzi[5] and Sekiguti[6] who have investigated stress conditions set up by impact.

Because of the rapidity with which these transient stress waves travel, the apparatus required to photograph and study them is somewhat complicated and for this reason the writer has confined his attention, for the present, to the study of cyclical stress fluctuation which can be examined with very much simpler equipment. Although the equipment and methods used can be applied to a vast number of problems the writer has investigated in particular the stress condition set up in a cantilever beam under resonant vibration, since the available apparatus was readily suited to the problem.

As is the case with most investigations, several arrangements of apparatus are usually tried out before the most satisfactory results can be obtained, and for this study the existing photoelasticity apparatus was adapted by removing the testing machine and replacing it with the vibrator and synchronized shutter. The model, a bar of transparent Bakelite with a rectangular cross section 0.4″ in depth and 0.37″ wide, was clamped firmly (allowing some clearance) to a length of 3″ Duralumin I section

* Paper presented at the Eleventh Semi-Annual Eastern Photoelasticity Conference, May 24–25, 1940 at the Carnegie Institute of Technology, Pittsburgh, Pennsylvania.

on the bottom of which was mounted an electromagnet. By passing a 60-cycle alternating current through the coils of the magnet the whole system could be vibrated including the Bakelite bar, which, if its length were adjusted properly, would vibrate in resonance with an amplitude up to about ½". The 60-cycle vibration was much too rapid to be followed by eye, so a synchronized shutter consisting of a rotating paper disk with a slot operated by a synchronous motor taking power from the same source was introduced. This set-up proved moderately satisfactory since by rotating the frame of the synchronous motor one was able to change the phase relation between the shutter and the vibrating beam and all positions of the cycle could be examined. The main disadvantages with this arrangement were its crudeness and the great length of time required to make a single picture and the fact that of three necessary variables, phase, frequency and amplitude, only the phase relationship of the shutter and the magnitude of the vibration could be controlled, the latter by regulating the power input to the electromagnet.

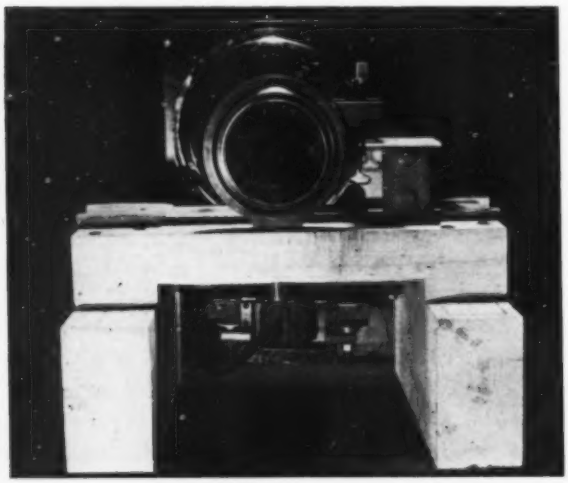

FIG. 1. The electrical vibrator with Polaroid disks.

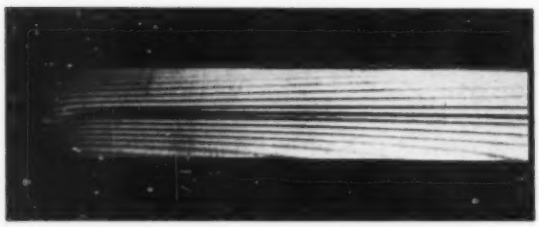

FIG. 2. Fringe pattern obtained with the electrical vibrator.

It was recognized immediately that certain refinements would be necessary in order to make this apparatus more convenient with the result that a smaller length of the Duralumin I was selected, and upon this the magnet was mounted on the lower flange and on the upper flange a suitable clamp for the Bakelite beam was placed. To eliminate all the lenses of the previous photoelasticity apparatus the Duralumin beam with the electromagnet and Bakelite model was mounted on rubber pads in the wooden frame as shown in Fig. 1 and Polaroid disks were set up in front and behind the model. This arrangement was very simple and compact and could be adapted to any light source for either visual observation or photographic recording of the fringe pattern. As the light source a General Radio Strobotac or Strobolux was mounted behind the model. For visual observation this arrangement was excellent, since by suitable adjustment of the frequency of the flashing light source it was possible to make the photoelastic stress pattern appear to be motionless (Fig. 2) or to give the beam the appearance of very slow motion so that all positions of the cycle could be observed. For any visual examination the results were excellent. The apparatus, however, still lacked the desirable feature of a variable frequency which is necessary since the natural frequency of all the models cannot be conveniently arranged for 60 cycles per second. With the two requirements for more nearly monochromatic light and a variable frequency of vibration it was decided to go back to the regular apparatus which possessed a monochromatic light source and to develop a suitable vibrator and light source to go with it.

For the vibrator, then, the necessary requirements were that the frequency, phase and amplitude should all be variable and independent of one another. A miniature mechanical type of vibrator was chosen. This consists of two equal masses which can be rotated around parallel shafts in opposite directions and arranged in such a manner that their centers of gravity always occupy corresponding positions as indi-

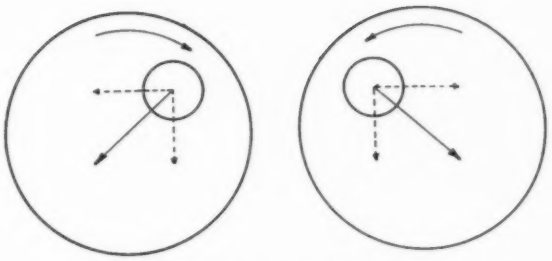

FIG. 3.

cated in the slide (Fig. 3). Because of the fact that the mass and eccentricity for each weight are the same, the centrifugal forces will also be the same. With the correct relative orientation of the centers of gravity the components of force in one direction will balance each other out and the components in the direction at right angles will add up to produce a single force with a sinusoidal variation. This force is used to produce the vibration in the photoelastic model. Regulation of the fluctuating force must then be accomplished by controlling its magnitude and frequency. The former is adjusted by moving the centers of gravity of the weights nearer to or farther from their respective axes of rotation. Means have been provided whereby this may be done while the vibrator is in operation so that one may increase or decrease the amplitude of vibration at will. In tests this feature has been found very useful and highly desirable. Figure 4 shows the vibrator set up in place with the model suspended below it; the rotating weights can be seen at the top but the variable speed motor which controls the frequency is not shown. The holder for the model is arranged so that it can be turned through 90 degrees which facilitates use in different types of polariscopes.

Originally a mechanical shutter was used in which the phase could be regulated relative to the model but this was not satisfactory because of the slack in the driving mechanism. Although some photographs were made with this equipment, it was discarded in favor of a flashing light source or mercury stroboscope of the Edgerton type.

Figure 5 shows a fringe photograph taken with this light source (and a Wratten No. 62 filter) which was mounted in the apparatus. The isochromatic lines are clear and well defined. In this case the model represents a cantilever beam 8″ long with a depth of 0.322″ and a breadth of 0.268″. The end held by the vibrator is enlarged to a depth of approximately $1\frac{1}{8}$″ and the change of section is accomplished with a fillet radius of $\frac{1}{2}$″ to avoid any objectionable concentration of stress at this point. The frequency of the vibration was 3300 cycles per minute and the amplitude at the free end was 0.56″ although the photograph itself was taken when the displacement of the free end was only 0.44″. Although the result has been satisfactory in this case, one feels that it would have been better to photograph the conditions for maximum displacement because at that instant the model is stopped instantaneously and there is less likelihood of blurring the picture because of the movement of the model. With a high speed light source this is not so important because

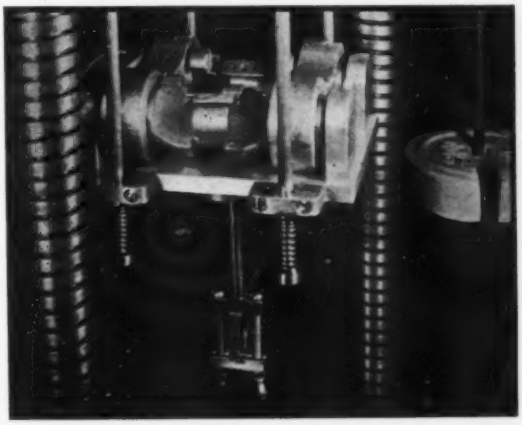

FIG. 4. Mechanical vibrator in the testing machine.

FIG. 5. Fringe photograph obtained with the mechanical vibrator.

the duration of the flash may be just a few ten thousandths of a second. Compared with the electric stroboscope the mechanical one is relatively slow and permits longer time of exposure.

Since a good deal of time has been given to the discussion of the apparatus and its development, let us now turn to the consideration of the results which can be obtained and how they correspond with theoretical computations. The following equation is given by Timoshenko,[7] for the lateral displacement of a prismatical bar subjected to this type of vibration:

$$y=\sum_{i=1}^{i=\infty} X_i(A_i \cos p_i t+B_i \sin p_i t) \qquad (1)$$

where y=the lateral displacement from the mean position.

As the equation stands it represents the general expression for the displacement due to lateral vibration and takes into account all possible normal vibrations. For the case at hand the bar is vibrating in the first mode only so that Eq. (1) may be written in the very much simpler form

$$y=X_1(A_1 \cos p_1 t+B_1 \sin p_1 t). \qquad (2)$$

Hereafter, the subscripts 1 will be omitted as only the first mode is to be considered. The symbols on the right-hand side of Eq. (2) have the following significance:—

$$X=C_1(\cos kx+\cosh kx)+C_2(\cos kx-\cosh kx)+C_3(\sin kx+\sinh kx)+C_4(\sin kx-\sinh kx).$$

A, B, C_1, C_2, C_3, and C_4 are constants to be found.

p=a proportionality factor depending upon the frequency,
$=2\pi\times$frequency.
$k^4=p^2D\rho/EIg$.
D=area of cross section of the bar.
ρ=weight per unit volume of the material.
E=modulus of elasticity.
I=moment of inertia of the cross section.
g=gravitational constant.
L=length of the bar.
x=distance measured along the bar.

Equation (2) contains seven constants which must now be evaluated according to the particular conditions of the problem at hand. For the cantilever beam let $x=0$ at the fixed end and $x=L$ at the free end. Then, one has the following conditions to fulfill:

(a) At $x=0$ $y=0$ hence $(X)_{x=0}=0$
(b) At $x=0$ slope $=0$ hence $(dX/dx)_{x=0}=0$
(c) At $x=L$ bending moment $=0$ hence $(d^2X/dx^2)_{x=L}=0$
(d) At $x=L$ shear $=0$ hence $(d^3X/dx^3)_{x=L}=0$.

From conditions (a) and (b) $C_1=C_3=0$.

From conditions (c) and (d) $\cos kL \cosh kL=-1$ which has for its first root $kL=1.875$ so that the numerical value of C_4 can be expressed in terms of C_2 since

$$C_4=-C_2\frac{\cos kL+\cosh kL}{\sin kL+\sinh kL}=-0.734\ C_2.$$

Therefore

$$y=C_2\{(\cos kx-\cosh kx)-0.734(\sin kx-\sinh kx)\}\times(A\cos pt+B\sin pt). \qquad (3)$$

If one measures the time t from the mean position of the bar, then, when $t=0$, $y=0$, so that $A=0$ and one may write the equation for the displacement as

$$y=BC_2\{(\cos kx-\cosh kx)-0.734(\sin kx-\sinh kx)\}\sin pt. \qquad (4)$$

The combined constant (BC_2) of Eq. (4) can readily be found if one knows the displacement (other than 0) of some point along the beam and the corresponding value of pt.

Equation (4) is now in form suitable for application to the specific problem of the model under test. However, before making any stress computations it will be well to find the effective length and to compare this with the actual length.

From the previous equations

$$k^2=(1.875/Le)^2=p(D\rho/EIg)^{\frac{1}{2}}$$

so that

$$\text{effective length}=Le=\left[\frac{3.515}{p}\left(\frac{EIg}{D\rho}\right)^{\frac{1}{2}}\right]^{\frac{1}{2}}. \qquad (5)$$

The measured values for the beam are:

$$L = \text{length} = 8''$$
$$h = \text{depth} = 0.332''$$
$$b = \text{breadth} = 0.268''$$
$$\text{frequency} = 3300 \text{ cycles per min.}$$
$$E = 620{,}000 \text{ lb./sq. in.}$$
$$\rho = 0.050 \text{ lb./cu. in.}$$
$$g = 32.2 \text{ ft./sec./sec.}$$

Substitution of the numerical values in Eq. (5) gives for the effective length

$$Le = 8.21''.$$

The measured amplitude of vibration at the free end of the beam was 0.56" (this corresponds to $pt = \pi/2$); therefore by substitution in Eq. (4)

$$0.56 = (BC_2)\{[\cos 1.875 - \cosh 1.875] - 0.734[\sin 1.875 - \sinh 1.875]\},$$

from which

$$(BC_2) = -0.280.$$

$$y = -0.280\{(\cos kx - \cosh kx) - 0.734(\sin kx - \sinh kx)\}\sin pt. \quad (6)$$

When the fringe pattern was photographed, the displacement of the free end of the beam was 0.44" so that

$$\sin pt = 0.44/0.56;$$

therefore corresponding to the photograph

$$y = -0.220\{(\cos kx - \cosh kx) - 0.734(\sin kx - \sinh kx)\}. \quad (6a)$$

Differentiating twice with respect to x gives

$$-\frac{M}{EI} = \frac{d^2y}{dx^2} = +0.220\,k^2\{(\cos kx + \cosh kx) - 0.734(\sin kx + \sinh kx)\} \quad (7)$$

where M = the bending moment and, since the stress at the extreme fiber is given by the equation

$$f = \pm Mh/2I, \quad (8)$$

$$f = \pm 0.110k^2Eh\{(\cos kx + \cosh kx) - 0.734(\sin kx + \sinh kx)\}. \quad (9)$$

The stress values along the edges of the beam have been computed from Eq. (9) and are shown plotted in Fig. 6. Two curves are given for the theoretical values; one is based on the actual length (8") of the beam and the other is based on the effective length (8.21"). The third curve shows the photoelastic values obtained from the fringe patters (average of both sides) using a fringe constant at 87.7 lb. per in. per order.

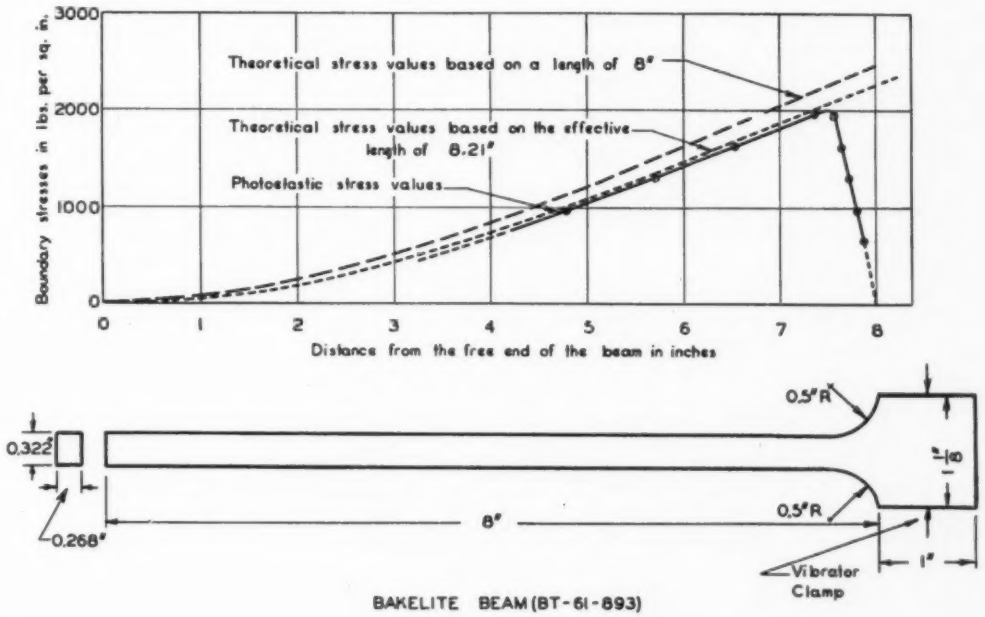

FIG. 6.

The agreement between the actual length and the effective length of the beam is very good (within 3 percent). As one would expect, the effective length is slightly greater than actual length because of imperfect restraint at the fixed end and the fact that the vibrator was clamped on a little more than 8″ from the free end.

Since there is no question about the position of the free end of the beam, all quantities have been plotted with reference to it. The theoretical results are slightly higher than the photoelastic values but the agreement between the latter and the theoretical values computed using the effective length are very good indeed. It may be mentioned that the theoretical equations take no account of shear deflection nor of rotary inertia. However, since these quantities together will produce less than two percent difference in a beam of these proportions, it is reasonable to neglect them.

In conclusion one may say that the photoelastic analysis definitely substantiates the theory and establishes its validity under the test conditions. These are similar to those of certain types of magnetic fatigue testing machines as shown in Fig. 7. For anyone contemplating research of a similar nature the author would suggest the use of some photographic method of recording the displacement of the beam and a high powered stroboscopic light source similar to that advocated by Dr. Sinclair.[8]

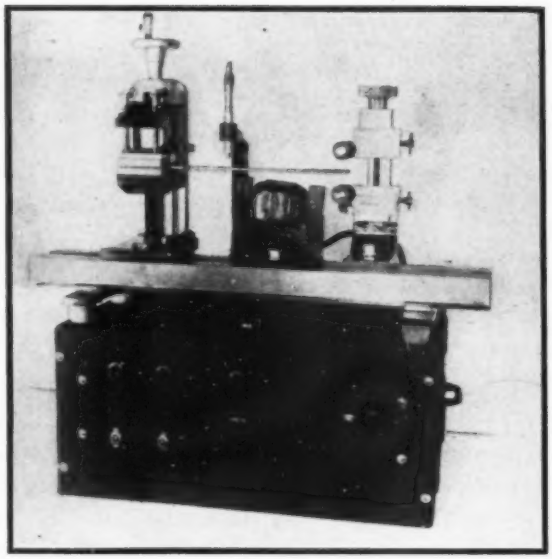

FIG. 7.
(Courtesy of A. V. de Forest, Massachusetts Institute of Technology.)

References

1. T. H. Frost and K. F. Whitcomb, "The stresses in rotating disks," Trans. A. S. M. E. **52** (1930) APM–53–1.

2. M. Hetényi, "The application of hardening resins in three-dimensional photoelastic studies," J. App. Phys. **10**, 295 (1939).

3. W. Dietz, "Photoelastic investigation of dynamic stresses in gears," M. I. T. Thesis, 1924.

4. M. M. Frocht, "Kinematography in photoelasticity," Trans. A. S. M. E. **54** (1932) APM–54–9.

5. Z. Tuzi and M. Nisida, "Photoelastic study of stresses due to impact," Sci. Pap. Inst. Phys. Chem. Research Japan, **26**, No. 566 (1935).

6. J. Obata, "The ultramicrometer, a new instrument for measuring very small displacement of motion and its various applications," Proc. World Eng. Congress, Tokyo **5**, 79 (1925), paper No. 184.

7. S. Timoshenko, *Vibration Problems in Engineering*, second edition (D. Van Nostrand Co., Inc., New York) p. 333.

8. D. Sinclair, "A small high intensity stroboscopic source," Rev. Sci. Inst. **11**, 109 (1940).

9. W. N. Findley, "The fundamentals of photoelastic stress analysis applied to dynamic stresses," Proc. Ninth Semi-Annual Eastern Photoelasticity Conference, Cornell University, May, 1939.

10. H. Meyer, "Spannungsoptische Untersuchung ebener Schwingungsvorgänge," Ingenieur-Archiv **7**, 273–293 (1936).

Abstracts

THE following abstracts are from the Eleventh Eastern Photoelasticity Conference held at the Carnegie Institute of Technology, Pittsburgh, Pennsylvania, in May, 1940. Complete manuscripts for these papers were not available at the time of publication.

A Photoelastic Investigation of the Stresses in the Foundation of the Sardis Dam Spillway. R. R. PHILIPPE,* *U. S. Soils Laboratory,* AND M. M. FROCHT,† *Carnegie Institute of Technology, Pittsburgh, Pennsylvania.—Introduction.* Great progress has been made in recent years in the general field of stress analysis. Nevertheless, the structural engineer is still in search of a suitable method for the analysis of stresses in foundations. The theory of elasticity has yielded valuable results in a limited number of simple cases. However, where the boundaries become irregular and complicated, the theory becomes cumbersome and unwieldy. In these cases the photoelastic method of stress analysis has proved itself to be of special value to the structural engineer. Although some of the assumptions upon which the application of this method to soil mechanics rests may be open to debate, the practical value of the results as a first and useful approximation can hardly be doubted. *The problem:* A recent application of the photoelastic method to the determination of boundary stresses in the foundation for the retaining walls in the Sardis Dam spillway is described. These walls are of the inverted, cantilever "T" type which form the sides of the spillway and retain the overburden through which the spillway was excavated. Two typical sections of these walls were studied: one 41.0 ft.×30 ft. upstream of the control weir, and the other 48 ft.×44 ft. below the control weir. The purpose of this study was to evaluate the magnitude and distribution of normal and shearing stresses caused by combinations of overburden and hydrostatic loads judged to be most severe for these walls. An idea of the size and shape and loading of one of these walls can be obtained from Fig. 1. *The method of analysis:* Models were constructed of the walls, the foundations of which were of gelatin. The isoclinics and isochromatics were observed and recorded by sketches. Two methods were used for calculating the stresses: the "Filon Graphical Method"[1,2] along stress trajectories and the "Shear-Difference Method"[3] along straight lines. The Filon graphical method became of questionable accuracy, due primarily to the difficulty of measuring the variables required by the method. On the other hand, the shear-difference method proved comparatively simple to handle and gave results which were well within engineering accuracy. The final distribution and magnitude of the normal and shear stresses are shown in Fig. 1. A discussion of the results is beyond the scope of this abstract. *Gelatin models:* The introduction of gelatin as a photoelastic material presents certain new problems in technique and calibration. The technique of the preparation of the model was discussed and three methods for the determination of the fringe value were given. The results from a uniformly distributed load over a finite region on the edge of a semi-infinite region were compared with those from a concentrated load on the same plate as well as with the linearly distributed body compressions in a rectangular block of uniform cross section.[4] Attention was called to the necessity for rigid temperature control of the gelatin model. The model for the Sardis Dam foundation was prepared and kept at about 65°F throughout the investigation. The effect of the body forces upon the stress pattern was also discussed.

* Engineer, U. S. Soils Laboratory, Pittsburgh, Pennsylvania.
† Associate Professor of Mechanics, Carnegie Institute of Technology, Pittsburgh, Pennsylvania.
[1] See Max M. Frocht, *Photoelasticity* (John Wiley and Sons, Inc., New York, 1941) Vol. I, Chapter 9.
[2] See E. G. Coker and L. N. G. Filon, *Treatise on Photoelasticity* (Cambridge Press, 1930).
[3] See Chapter 8 of reference 1.
[4] See Figs. 10.16 and 10.17 of reference 1.

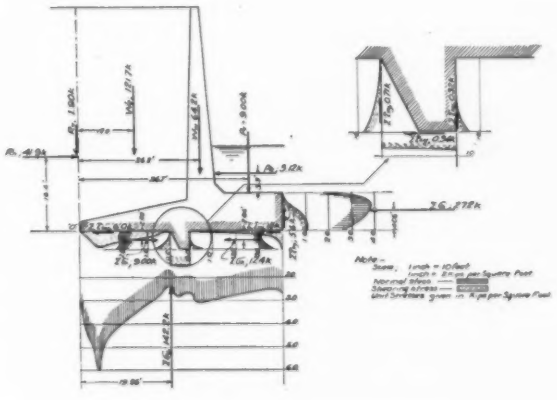

FIG. 1.

The Annealing of Photoelastic Bakelite and the Resulting Effect on Its Physical and Optical Properties. G. H. LEE* AND M. GOLDSTEIN, *Cornell University, Ithaca, New York.*—In recent tests conducted in the Cornell University laboratory on annealed photoelastic Bakelite, certain inconsistencies in the properties of the material were noted. In an effort to determine the cause of these variations, an investigation was instituted to determine the effect of annealing on the properties of Bakelite, i.e., physical and optical creep, Poisson's ratio, Young's modulus and the stress and strain optical coefficients. The study of the annealing methods was made with the aid of a specially constructed annealing oven and a straining frame with a constant temperature testing chamber. The former was so designed as to permit photo-

elastic observation of a Bakelite sample by means of appropriate window construction in the top and bottom of the oven, as its annealing progressed. Care was taken to test all samples at the same temperature in order to eliminate any effect that may arise due to variation in temperature. The sample was fitted with a longitudinal and a lateral extensometer, and the photoelastic effect was observed with the aid of a Soleil-Babinet compensator. The procedure was to choose several unannealed, ground and polished plates of Bakelite (BT–61–893) and to cut them into a number of samples of equal size. Groups were then formed, each consisting of one sample from each plate. The samples from each group were then tested after having been subjected to the same annealing procedure. The results of the given annealing were then taken as the average of the results of the tests on each group. Several groups having been formed, each was subjected to a different annealing procedure and the results compared. One group was tested in the unannealed condition for purposes of comparison with annealed specimens. The results of the study are shown by the accompanying tables. Note that two series of tests were made; one to determine the effect on properties if the samples were left in the oven for a time only sufficient to remove completely the initial stress, and a second to study the effect on properties due to varied time of annealing. It is desirable that the material used in photoelastic investigation have the following properties:—(a) low stress optical coefficient, (b) low creep (physical and optical). With this in mind, if Tables I and II be studied, it will be seen that the best

TABLE I. *Time of annealing just sufficient to remove initial stress.*

ANNEALING TEMPERATURE (°F)	YOUNG'S MODULUS OF ELASTICITY (LB./IN.²)	STRESS-OPTICAL COEFFICIENT (LB./IN.FR.)	STRAIN-OPTICAL COEFFICIENT (FR.IN./IN.)	UNIT CREEP (23 HR.) (IN./IN.)	OPTICAL CREEP (23 HR.) (FR.)
Unannealed	618,000	87.8	1980	0.00083	1.11
184	632,000	88.8	2040	0.00104	1.41
225	612,000	86.2	2050	0.00105	1.49
242	602,000	85.3	2010	0.00103	1.49
276	601,000	85.9	2020	0.00143	1.90

TABLE II. *Effect of time of annealing on the properties of Bakelite temperature of oven 242°F.*

ANNEALING TIME (HR.)	YOUNG'S MODULUS OF ELASTICITY (LB./IN.²)	STRESS-OPTICAL COEFFICIENT (LB./IN.FR.)	STRAIN-OPTICAL COEFFICIENT (FR.IN./IN.)	UNIT CREEP (23 HR.) (IN./IN.)	OPTICAL CREEP (23 HR.) (FR.)
0.44	602,000	85.3	2010	0.00103	1.49
5.0	602,000	86.3	2088	0.00131	1.88
12.0	618,000	89.1	2070	0.00146	1.80

compromise in these properties is obtained for the case of annealing temperatures between 240°F and 250°F, and for a length of time just sufficient completely to remove all initial stress. Accordingly, as the final result of this study on the effect of annealing procedure on photoelastic Bakelite, the following annealing procedure (for specimens of usual thickness) is recommended by the authors:—(1) Preheat oven to 240–250°F, (2) place sample in oven for one hour, (3) oven cool the sample at a rate of approximately 15°F per hour.

* Now at Carnegie Institute of Technology, Pittsburgh, Pennsylvania.

Some Examples of Failure Due to Stress Concentration. R. E. PETERSON, *Westinghouse Electric and Manufacturing Company, East Pittsburgh, Pennsylvania.*—The results of photoelastic investigations are used in industry to a greater extent than is generally realized. Stress concentration factors usually appear in engineering department design manuals years before becoming available in books on machine design. A considerable number of machine manufacturing companies have photoelastic equipment, ranging from simple set-ups to complete laboratories. The reason for all of this is that failures due to actual breaking of parts can in some cases be very dangerous and expensive, and therefore a considerable expenditure can be justified to improve design proportions. The chairman of the committee for this meeting asked that some examples of failure be described so that those engaged in photoelasticity at universities might better appreciate potential applications of their work. In this abstract only a few typical examples will be given. Figure 1 shows fatigue cracks at the base of gear teeth, located exactly where photoelastic tests would show that the cracks should occur. The paper by Professor Dolan[1] deals with this question in more detail. Figure 2 shows fatigue cracks started at the end of a keyway in an overhung street-car motor drive shaft. The variable stress was primarily bending. A similar case where the variable stress was primarily torsion is shown in Fig. 3. This failure was due to a resonance condition occurring in a large motor-generator set. Some work has been done on the general keyway problem using three-dimensional photoelasticity. The general field of fastenings should prove fruitful to the photoelastician. In Fig. 4 is shown a failure through the cheek of a large Diesel engine crankshaft due to variable bending. A similar case due to torsion is shown in Fig. 5. The problem of optimum crankshaft design is one in which photoelasticity can be of considerable assistance, although, of course, other important factors must be kept in mind. Figure 6 shows a failure of the flanged shaft of a Diesel driven generator. A number of helical cracks (usually associated with variable torsion) have joined to produce the saw tooth appearance. If the fillet were larger in proportion to the shaft diameter, one large helical crack would form. If the fillet is very small compared to the shaft diameter (as in Fig. 5) the crack apparently is confined to the fillet proper. The rational design of filleted members calls for considerable aid from photoelasticity. Some twenty examples similar to the above were described in the presentation. Speaking for the industrial laboratories, we are very much interested in the photoelastic work being done at the universities and are particularly hopeful that the newer techniques will be given major attention.

[1] T. J. Dolan, J. App. Phys. **12**, 584 (1941) (this issue).

FIG. 1.

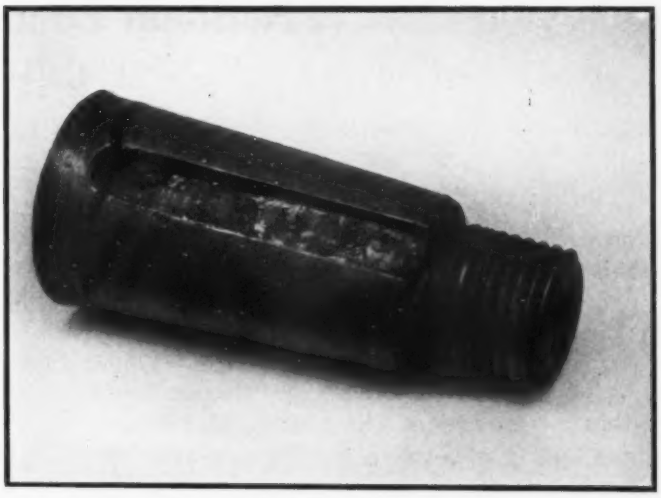

FIG. 2.

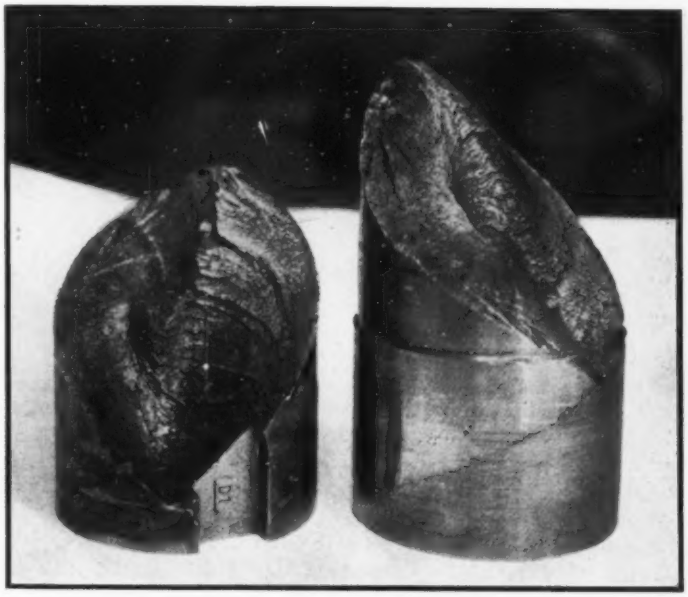

FIG. 3.

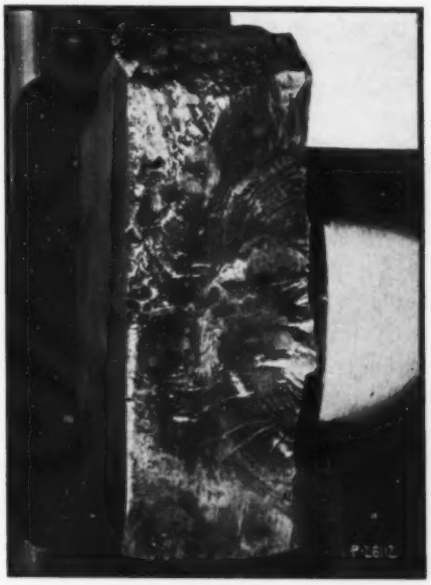

FIG. 4.

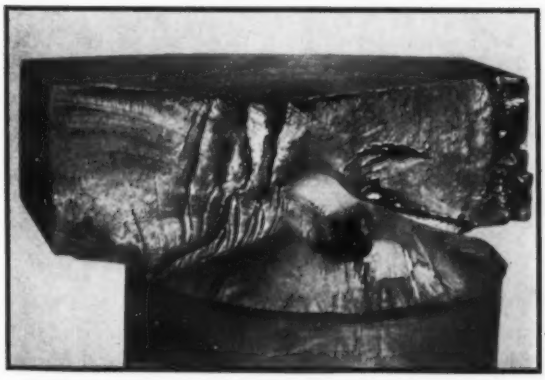

FIG. 5.

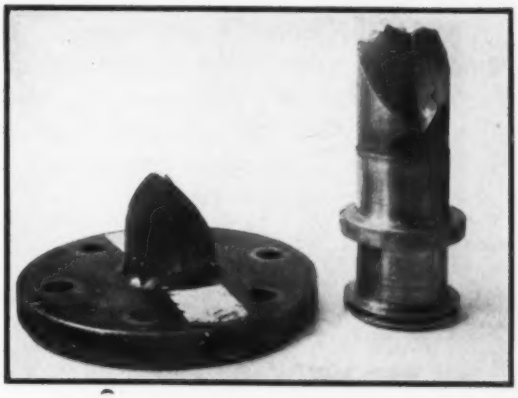

FIG. 6.

Frictional Phenomena. II

A. Gases

BY ANDREW GEMANT
The Detroit Edison Company, Detroit, Michigan

Chapter II. Theory and Experimental Facts on Gaseous Viscosity

ON the basis of the kinetic theory, an explanation is given both of the viscous forces within a gas and of those external frictional forces operative between a gas and a wall. The extent to which the theory is able to reproduce the existing experimental data on the viscosity of different gases, and the variation of viscosity with pressure and temperature are shown.

8. Kinetic Theory

Turning our attention first to the viscosity of gases, it is instructive to review the experimental facts together with the corresponding theoretical considerations. The theory of gaseous viscosity is comparatively simple, and was developed along with the experimental research, whereas with liquids the theory still lags behind the experiments. The reason for this is the relatively simple structure of gases which led to the establishment of the kinetic theory.

The kinetic theory allows certain equations to be deduced connecting the viscosity constant η (Section 4) with other characteristic quantities of the gas. These equations were tested on the experimental material available. The agreement was found to be only partially satisfactory, and this led, in the course of developments, to continual improvements of the theoretical formulae. A short review of this situation is now presented.

We refer to Eq. (6), according to which the frictional force X_y acting on the x-z plane in the direction of the x axis is given by

$$X_y = -\eta du/dy,$$

if the flow u depends only on y (see Fig. 3(a)). This type of flow is called a parallel flow, since all velocities are parallel to one direction (the x axis).

In gases molecules are so far apart from each other that the motion of the molecules is of primary importance, and their mutual attraction, which becomes essential in liquids and solids, is only of secondary, though not negligible, interest. The mechanism of the frictional forces, too, is based on the movement of the molecules.

The mechanical explanation of the viscous force will be understandable if we recall one of the elementary laws of mechanics. The momentum, M, of a mass m_0 with velocity v is defined as $m_0 v$. If a force f acts upon the body, we have the relation

$$f = m_0 dv/dt$$

or

$$f = dM/dt. \tag{14}$$

In other words: The force acting upon a body is given by the increase of its momentum per second.

This law can be used directly in this case. The viscous drag acting upon the x-z plane is due to the gas molecules impinging upon that surface, and trying, so to speak, to carry it along with them. The magnitude of the force is, according to (14), equal to the momentum transported through that surface in the unit of time. The amount of this momentum can easily be computed.

Let the number of molecules per unit volume be n and the mass of each molecule be m. As to the velocity factor in M, the thermal components can be disregarded, since they are equal at both sides of the surface, and a finite transport of momentum is not possible. The speed component that has to enter in M is the flow velocity

$$u = u_0 + y du/dy,$$

and here again only the second term is of importance. If the y component of the thermal motion of individual molecules is now denoted by v, and the number of molecules in the volume

unit having such a velocity component is denoted by n_v, then the number of such molecules hitting the surface unit of the x-z plane in the time unit is $n_v v$, and we have

$$\frac{dM}{dt}=\sum_v n_v v\left(m\frac{du}{dy}y\right), \tag{15}$$

summing over all the different v values. Here y is determined by the location of the molecule at its last collision before passing the plane x-z, since it had acquired the velocity u during that collision. Suppose a molecule hitting the x-z plane at O (Fig. 5) has had its last collision at O', with a path r and a y component $-y$ between the two points. We then have

$$v/c=-y/r,$$

where c is its thermal velocity. In reality c is distributed according to Maxwell's law, but we operate here with its average value. Placing y into (15), we have

$$f=-\frac{1}{c}\frac{du}{dy}\sum_v n_v m v^2 r.$$

The average of r is called mean free path in the kinetic theory of gases, and is denoted by λ. Thus, we write

$$f=-\frac{\lambda}{c}\frac{du}{dy}\sum_v n_v m v^2.$$

The sum $\sum_v n_v m v^2$ is shown in the theory to be the pressure p of the gas, thus

$$f=-(\lambda p/c)du/dy.$$

Comparing the last equation with Eq. (6), we have

$$\eta=\lambda p/c. \tag{16}$$

Using the relation, as supplied by the theory, for p:

$$p=nmc^2/3,$$

we also have for η the alternative equation:

$$\eta=nm\lambda c/3=0.33\rho\lambda c, \tag{16a}$$

where $\rho=nm$=density of the gas.

The physical reason for η being proportional to $\rho\lambda c$ is this: Both the density (ρ) and the temperature (c) favor an increase in the number of molecules which effect a transportation of momentum. Because of a finite gradient du/dy, the transported momentum per molecule is larger the farther away from the surface the last collision has occurred, that is, the larger the mean free path.

Equations (16) and (16a) refer the viscosity constant η to other known molecular constants of the gas. It is a theoretical relation of remarkable simplicity which allows a check in the light of experimental facts.

The factor $\frac{1}{3}$ in (16a) is only an approximation, since a constant velocity was used instead of taking account of a Maxwell distribution. Several later calculations, especially by Chapman[1] have shown that the factor 0.33 has to be increased. Accordingly, we write

$$\eta=0.49\rho\lambda c. \tag{16b}$$

Equation (16b) can be used to compute values of the mean free path λ from measurements of the viscosity. The density of the gas is known, and the average velocity c is computed by means of the relation

$$mc^2=(8/\pi)kT, \tag{17}$$

(k=Boltzmann constant=1.37×10^{-16} c.g.s. and T=absolute temperature).

After λ has been computed, it is possible to make use of a further relationship to calculate the diameter σ of the molecules, a quantity that enters the kinetic theory when we picture the molecules as rigid elastic spheres from the

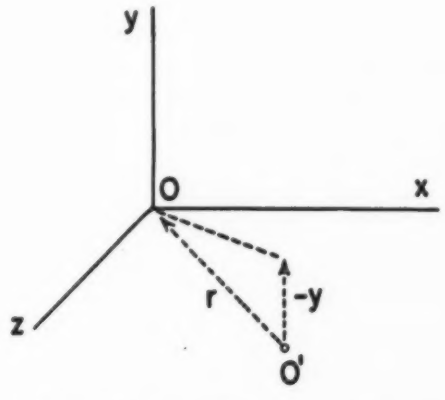

FIG. 5. Diagram of molecule transferring momentum.

standpoint of collision. The theory then gives

$$\lambda = 1/\sqrt{2}\pi n\sigma^2, \qquad (18)$$

which allows σ to be calculated from λ, and thus from viscosity data. The calculated values of λ and σ are in fair agreement with values of the mean free path and molecular diameter as computed from entirely different experimental data.

The following table gives the results of some computations, compiled by Kennard,[2] based on the data of several authors, chiefly Trautz[3] and co-workers. The c.g.s. unit of the viscosity is called 1 poise.

TABLE I. *Mean free path and molecular diameter of gases computed from viscosity data ($p=1$ atmos., temperature $=15°C$).*

GAS	η (10^{-6} POISE)	λ (10^{-6} CM)	σ (10^{-8} CM)
Ammonia	97	4.5	4.4
Carbon dioxide	145	4.2	4.6
Ethylene	100	3.6	4.9
Helium	194	18.6	2.2
Hydrogen	87	11.8	2.7
Mercury vapor 219°C	470	8.3	4.3
Neon	309	13.2	2.6
Nitrogen	173	6.3	3.7
Oxygen	200	6.8	3.6
Water vapor	93	4.2	4.6
Xenon	224	3.8	4.8

9. *Experimental Facts*

We now turn to certain fundamental experimental facts and compare them with the above theory.

Substituting (18) into (16b) it can be seen that the density cancels out, since n is proportional to ρ. It follows that the viscosity is independent of the density, as well as of the pressure, if the temperature is constant. This independence is a consequence of η being proportional to the product $(\rho\lambda)$. It seems strange, perhaps, but it is confirmed, at least approximately, by the experiment. The viscosity of gases increases only slowly at high densities. The increase of the viscosity of air at 30°C up to 320 atmospherics[4] is shown in Fig. 6. The viscosity of gases appears to decrease at very low densities; a discussion of this effect will be given below.

This independence of the pressure has also a practical importance. In certain cases—for instance, in the measurement of internal damping of solids by means of vibrations—it is desired to eliminate the losses due to the viscosity of the air.

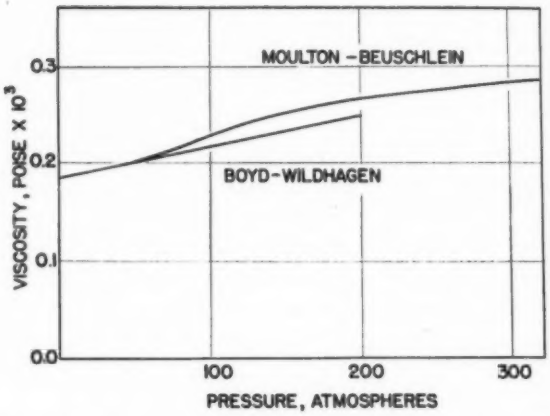

FIG. 6. Viscosity of air at 30°C up to 320 atmospherics according to Moulton-Beuschlein.

The specimen is therefore placed in a container with reduced pressure. It has to be borne in mind that the losses due to a viscous flow of the air will *not* be reduced by such procedure. In case there is a turbulent flow (a nonstationary process as compared with the viscous flow), losses might be reduced if the pressure decreases. At high frequencies losses due to sound radiation will be reduced also; but this has nothing to do with the viscosity of the medium.

The effect of temperature upon viscosity can be seen from (16b) in combination with (17). Accordingly, η ought to be proportional to $\sqrt{T}$. Figure 7 shows, according to Kennard, the viscosity of some gases as a function of the absolute temperature. It can be seen that the increase is decidedly stronger than according to the $\frac{1}{2}$ power, especially at higher temperatures where the slopes are nearly constant.

Sutherland has developed a theory that accounts for this deviation. He introduces attraction forces with a potential $U(r)$ between the molecules. The effect of such forces is illustrated in Fig. 8. Molecule A, if no such forces are present, will pass by molecule B without collision (path 1). If the potential U is finite, A will either be deflected (path 2), or even driven against molecule B, causing a collision (path 3). For a given U, it will depend on the velocity of the molecule whether it will follow a path like 2 or 3, slower velocities favoring stronger deflections.

In carrying out this idea quantitatively, Sutherland arrives at an effective cross section

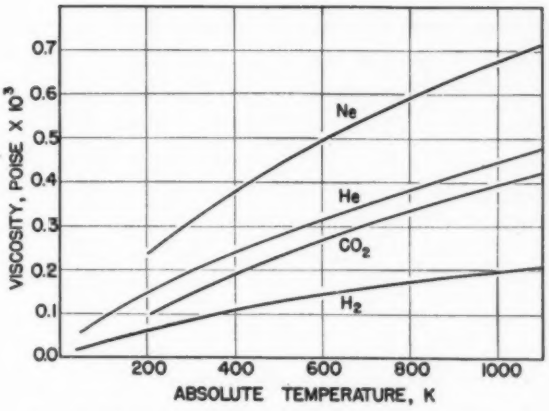

FIG. 7. Viscosity of different gases as a function of temperature.

S_{eff}, given by an equation:

$$S_{\text{eff}} = S_0(1 - 4U(\sigma)/mc^2), \qquad (19)$$

indicating an increase as compared with S_0, the real cross section, since U is negative. Substituting Eq. (19) into (18) and (16), it is easy to see that the viscosity will take the form

$$\eta = aT^{\frac{1}{2}}/(1 + C/T). \qquad (20)$$

This formula indicates an increase with temperature stronger than with the $\frac{1}{2}$ power. The reason for this behavior is an increase of the mean free path with increasing temperature (path 2 preferred to path 3).

As a quantitative check indicates, even the Sutherland formula fails to account completely for the $\eta(T)$ curves. The Sutherland constant C in Eq. (20) was determined by Ribaud and Vasilesco[5] for air, N_2, A and CO_2. It increases slightly in the temperature range 0 to 1600°C. Some recent papers by Massey and Mohr[6] introduce a quantum-mechanical concept for the collision with fairly good success in computing viscosity values. Hellund and Uehling[7] also developed a general theory of transport in gases, using quantum-mechanical conceptions of the collision process. The equations for viscosity show the same dependence on temperature and pressure as the classical formulae, except that the coefficients contain the quantum-mechanical data.

Itterbeek and Paemel[8] measured the viscosity of argon at low temperatures, but could not reproduce the results by means of a theoretical equation. Keesom and Keesom[9] find a linear increase of viscosity of hydrogen with temperature in the range of 20 absolute.

As to the viscosity of chemically different gases, Eqs. (16) and (18) indicate a proportionality to $m^{\frac{1}{2}}/\sigma^2$. Since the cross section increases with mass, a large variation of η will not be expected. Still, the variation of m is larger than that of σ, and, therefore, the viscosity is expected to increase with the molecular weight. Both these conclusions are confirmed by the data as shown in Table I.

Itterbeek and Claes[10] found the viscosity ratio deuterium/hydrogen very near $\sqrt{2}$, in agreement with the theory. With decreasing temperature the ratio decreased.

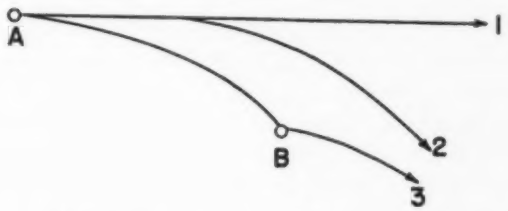

FIG. 8. Collision of molecules under forces of attraction.

Much research has been done on the viscosity of gaseous mixtures. Adzumi[11] measured the viscosities of mixtures of low molecular weight hydrocarbons between 20 and 100°C, and determined the constants in Eq. (20). Frequently maxima and minima in the curves referring the viscosity to the concentration ratio of the mixtures were observed. Schröer[12] criticizes the work of Adzumi whose results do not agree with the theoretical formula of Schröer.

The viscosity, as well as the thermal conductivity, decreases if a magnetic field is applied. Results of Senftleben and Gladisch[13] refer to oxygen and nitrogen monoxide, and can be formulated by a few simple relations.

10. Theory of Slip

Up to this point, theory and experimental data on the viscosity constant η of gases were discussed, without reference to the technique of measurements. Although this latter aspect will not be treated in detail, the principle of such tests has to be mentioned for a better discussion of slip. More details on measurements will be

given in connection with liquids (see Chapter IV) and solids.

One of the most frequently used methods is that utilizing the flow in narrow circular tubes. With a given flow the pressure difference at both ends is measured, and these data allow the constant η to be computed. A simple apparatus of moderate accuracy on this basis has been recently described by Weber.[14] Another typical method is that of two concentric cylinders, the outer being rotated at a constant speed, the inner elastically suspended. The torque of the inner cylinder, corresponding to a given speed of the outer, is a measure of the viscosity of the gas between the cylinders. Bearden[15] made use of this method for a precision determination of the viscosity of air at 20.00°C. It is 1819.20 $\pm 0.06 \times 10^{-7}$ poise, calculated after Inglis[16] had computed the effect of a minute eccentricity of the two cylinders.

In both cases there will be a certain interaction between the gas and the solid walls, and this interaction is likely to affect the data. If such interaction could be avoided entirely, then η could be measured without interference on the part of the walls. Such method is supplied by the determination of damping of freely propagating acoustic waves (see Chapter III). The two principles mentioned above are, however, more practicable, and, therefore, generally used. For this reason it will be necessary to consider the interaction between gases and walls; in other words, to consider the *external* viscosity of gases, as compared with the internal viscosity η. We shall see that the practical consequences of such considerations become important, especially at low gas pressures.

Whereas η, the internal viscous force was defined, according to Eq. (6), as proportional to the velocity gradient, an external viscous force between a gas and a wall must evidently be proportional to the velocity difference between the two, and, in case the wall is stationary, simply to the velocity u of the gas. The viscous force per surface unit acting between the gas and the solid is then given by eu, where e is the constant of external viscosity.

Let us consider the layer of the gas nearest the wall. There will be two opposite forces acting upon it: The solid wall pulls it backwards by a force eu, and the next gaseous layer pulls it forward with an intensity $\eta du/dz$ (z = perpendicular to the wall). Thus in equilibrium

$$eu = \eta du/dz. \tag{21}$$

Introducing the so-called coefficient of slip ζ by means of the definition

$$\zeta = \eta/e, \tag{22}$$

we have

$$u = \zeta du/dz. \tag{23}$$

Equation (23) is then to be used as the boundary condition in any mathematical treatment of a gaseous flow.

An expression for ζ (or e) on the basis of the kinetic theory can be given in the following way.[17] Again considering the layer next to the wall, it transfers momentum from the bulk of the gas to the wall, and the two evidently must be equal. As shown above (Eq. (14)), the viscous drag $\eta du/dz$ is equal to the transfer of momentum per second. Since this transfer in the bulk occurs in both directions, and in equal amounts, the transfer in one direction from the bulk to the boundary layer is

$$\tfrac{1}{2}\eta du/dz.$$

Now as to the transfer from the layer to the wall. The theory shows that $\frac{1}{4}(nc)$ molecules strike the surface unit per second. The total momentum striking the wall is $\frac{1}{4}ncmu$. The specific assumption should now be added that the total momentum is absorbed by the wall, none being reflected. This happens if the wall is rough, and the molecules are severally reflected to and fro before their final escape, thus losing their velocity component u completely. Equalling the two momentums, we have

$$\tfrac{1}{2}\eta du/dz = \tfrac{1}{4}ncmu$$

and, comparing with Eq. (23):

$$\zeta = 2\eta/ncm.$$

Substituting Eq. (16b) into the expression for ζ, and writing 1.0 instead of 0.98, we have

$$\zeta = \lambda. \tag{24}$$

Since λ is inversely proportional to the pressure, (24) can be given the form

$$\zeta = \zeta_0/p, \tag{24a}$$

where ζ_0 is a constant independent of the pressure. It can be seen that the slip coefficient increases with decreasing pressure.

It can be shown that its value at atmospheric pressure is too low to be of much importance. Consider Eq. (23) and write orders of magnitude, instead of actual figures. For du/dz, then, we write u_g/z_a where $u_g \sim$velocity of the gas and $z_a \sim$dimension of the apparatus (radius of tube, for instance). We have, then, with Eq. (24) and $u_w =$velocity of gas at the wall:

$$u_w/u_g \sim \lambda/z_a. \tag{25}$$

λ at atmospheric pressure is $\sim 10^{-5}$ cm; hence $u_w/u_g \ll 1$, in other words, slip is negligible. The boundary condition is $u_w = 0$ with a fair degree of approximation.

With decreasing pressure the mean free path increases, and the slip velocity cannot be neglected. This will result in a relatively increased flow, the same as if the viscosity constant were to decrease. Finally, when $\lambda > z_a$, the character of the flow changes entirely and is controlled by the external friction e, which is proportional to the pressure. This is the key for the understanding of the so-called "molecular air pump," as shown in Section 11.

For an illustration of the significance of a finite slip let us consider the flow, discussed in Section 7, which has been treated with the assumption that there is no slip at the boundaries. Let us now generalize the case and use Eq. (23) for a boundary condition. Whereas (11) remains unchanged, we have for u

$$u = (p/2\eta)(h^2 - z^2) + \zeta ph/\eta. \tag{11a'}$$

Thus we see that to the parabolic component of u is being added another term, constant over the whole cross section. For the total flow V we have:

$$V = 2ph^3/3\eta + 2\zeta ph^2/\eta. \tag{11b'}$$

In utilizing Eq. (12), we get for the total heat developed W,

$$W = 2p^2h^3/3\eta + 2\zeta p^2h^2/\eta. \tag{11d'}$$

However, if we compute the heat developed within the liquid, using (11c) as before, we arrive at (11d) which is only the first term in (11d'). This seeming contradiction is explained by interpreting the second term in (11d') as the heat developed in the external friction process. That this conclusion is correct can be shown directly. Applying our general equation $A_f = -uf$, from Section 2, the viscous drag at the wall is $-eu_w$; thus, the heat developed is eu^2_w, for both walls together $2eu^2_w$. Substituting u_w from Eq. (11a'):

$$u_w = \zeta ph/\eta,$$

we obtain exactly the second term in Eq. (11d').

11. Experiments on Slip

Before discussing some experimental facts, related to the slip coefficient, a brief derivation of the flow formula for circular tubes should be given. The formula also will be used extensively throughout this whole monograph.

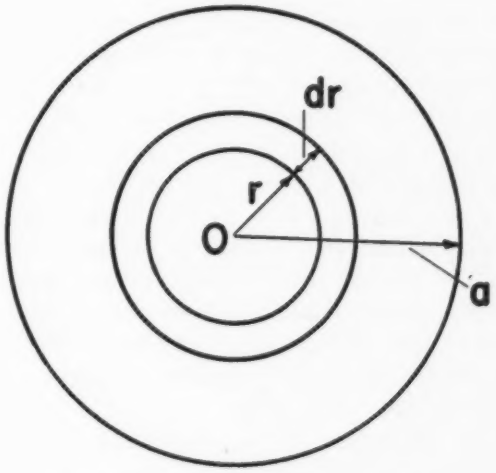

FIG. 9. Cross section of cylindrical tube.

Figure 9 is a cross section of a cylindrical tube of radius a and length l, at the ends of which the gas pressure is p_1 and p_2, respectively. A steady stream of gas will flow through the cylinder, with a volume output of V per second. The gas velocity u in axial direction will be a function of the radius r, as shown below. Considering a cylindrical volume of radius r, thickness dx (x=axis), and applying Eq. (8) for the x component of the forces, we have

$$\pi r^2 dp + 2\pi r dx \eta du/dr = 0,$$

and, integrating over the whole length:

$$\frac{du}{dr}=-\frac{r}{2\eta}\frac{p_1-p_2}{l}.$$

Integrating over r with the boundary condition (23), we have

$$u=\frac{1}{4\pi}(a^2-r^2+2\zeta a)\frac{p_1-p_2}{l}. \qquad (26)$$

In carrying out the integration $2\pi\int_0^r rudr$ over the cross section, the volume V is obtained:

$$V=\frac{\pi a^4}{8\eta}\left(1+\frac{4\zeta}{a}\right)\frac{p_1-p_2}{l}. \qquad (27)$$

With $\zeta=0$, this equation reduces to the well-known Poiseuille formula. In the second term ζ has to be replaced by ζ_0/p according to Eq. (24c), in order to have V as an explicit function of the pressure. Eq. (27) is only valid if (p_1-p_2) is small as compared with p; otherwise in the integration of the second term we should have taken into account that ζ is a function of the pressure. In the second term of the exact equation the expression $\ln(p_1/p_2)$ should stand instead of $(p_1-p_2)/p$.

Eq. (27) clearly shows, as pointed out in the previous section, that for normal pressures, when $\lambda/a\ll 1$, slip can be neglected. In reducing the pressure, the output increases, even if $\Delta p=p_1-p_2$ remains constant. For very low pressures the flow becomes inversely proportional to the pressure (for given Δp).

These predictions of the theory were verified experimentally by Stacy[18] and van Dyke.[19] It should be recalled that in deducing (24) the absorption coefficient of the wall (f) has been taken as unity. If the value of f is left open, one has for ζ instead of (24)

$$\zeta=(2-f)\lambda/f. \qquad (24b)$$

Millikan has calculated f from the measurements just mentioned, utilizing the rotating cylinder apparatus and using an equation in principle analogous to (27). The value of f was in certain cases 1.0, in others around 0.9, thus justifying the use of Eq. (24).

Adzumi[20] found that the slip coefficient for a gas in metal capillaries varies with the nature of the metal. He considers the gas molecules as being adsorbed at the wall, and derives expressions for the slip coefficient on this basis.

Important research in this field has been done by Knudsen[21] and Gaede.[22] Let us consider Eq. (27) and see how the flow depends on the pressure, if the pressure difference is a given fraction of the total pressure, or $(p_1-p_2)/p=\text{constant}$. The first term is then proportional to p, the second becomes independent of p. If not the volume, but the total amount of the gas (volume times pressure) is asked for, then the first term becomes proportional to p^2, the second to p. Thus, in plotting pV as a function of p (Fig. 10), the quadratic curve 1 would be obtained if Poiseuille's equation should hold for the whole pressure range. But, since for lower pressures the function must be linear, curve 2 should be expected. In actual experiments curve 2 was

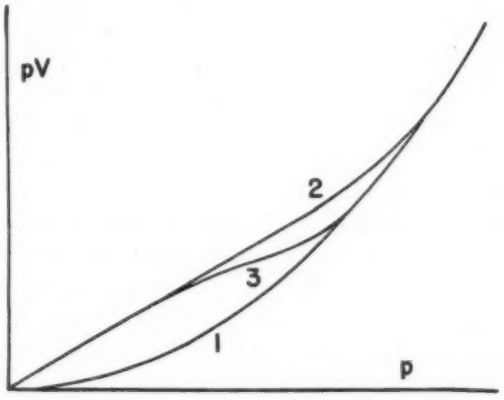

FIG. 10. Output of flow as a function of pressure in the Poiseuille and free-molecular range.

verified in the lowest range, the transition, however, occurring, via curve 3, for reasons not quite clarified.

The lowest range is of particular interest. It occurs when $\lambda\gg a$; thus, the first term in (27) can be neglected entirely. This type of flow is sometimes called the free-molecular flow, since intermolecular collisions do not occur at all. The only interaction is that between individual molecules and the wall. Gaede has utilized the flow in this range in his so-called molecular pump using rotating cylinders. One can see from curve 1 of Fig. 10 that for a given fraction of pressure

difference (say 10 percent of the existing pressure), the output of a pump would be extremely low on the basis of Poiseuille's law. But, on the basis of 3, which actually takes place, the output of a pump can still be appreciable, even when the absolute value of the pressure drops to a very low value. This is just the mechanism of the molecular pump. One cylinder rotates against another and, when the pressure has dropped to a low value, carries off the remainder of the gas by means of the external friction, operative in this range.

An interesting application of slip at atmospheric pressure is Carson's determination[23] of the pore size in papers by using Eq. (27). He argues that a in papers is so small that the second term cannot be neglected. In carrying out flow measurements across paper at 1 and 0.9 atmospheric the average pore radius is computed. The values vary from 0.2 to 1.2μ.

Bibliography for Chapter II

1. S. Chapman, Phil. Trans. Roy. Soc. **217A**, 115 (1918).
2. E. H. Kennard, *Kinetic Theory of Gases* (McGraw-Hill Book Company, Inc., New York, 1938).
3. M. Trautz and R. Heberling, Ann. d. Physik **20**, 118 (1934).
4. R. W. Moulton and W. L. Beuschlein, Trans. Am. Inst. Chem. Eng. **36**, 113 (1940).
5. G. Ribaud and V. Vasilesco, Comptes rendus **208**, 1884 (1939).
6. H. S. W. Massey and C. B. O. Mohr, Proc. Roy. Soc. **144**, 188 (1934).
7. E. J. Hellund and E. A. Uehling, Phys. Rev. **56**, 818 (1939).
8. A. v. Itterbeek and O. v. Paemel, Physica **5**, 1009 (1938).
9. W. H. Keesom and P. H. Keesom, Physica **7**, 29 (1940).
10. A. v. Itterbeek and A. Claes, Physica **5**, 938 (1938).
11. H. Adzumi, Bull. Chem. Soc. Japan **12**, 199 (1937).
12. E. Schröer, Zeits. f. physik. Chemie **B43**, 103 (1939).
13. H. Senftleben and H. Gladisch, Ann. d. Physik **33**, 471 (1938).
14. R. L. Weber, Am. Phys. T. **7**, 163 (1939).
15. J. A. Bearden, Phys. Rev. **56**, 1032 (1939).
16. D. R. Inglis, Phys. Rev. **56**, 1041 (1939).
17. R. A. Millikan, Phys. Rev. **21**, 217 (1923).
18. L. J. Stacy, Phys. Rev. **21**, 239 (1923).
19. K. S. van Dyke, Phys. Rev. **21**, 250 (1923).
20. H. Adzumi, Bull. Chem. Soc. Japan **14**, 343 (1939).
21. M. Knudsen, Ann. d. Physik **35**, 389 (1911).
22. W. Gaede, Ann. d. Physik **41**, 289 (1913).
23. F. T. Carson, J. Research Nat. Bur. Stand. **24**, 435 (1940).

Velocity Measurement of Transient Mechanical Motions

S. KEILIEN
Pass and Seymour, Inc., Syracuse, New York
(Received December 5, 1940)

Measurements of velocity of rapid non-recurrent mechanical motions by means of an oscillograph are described. Two methods of measurement are given: One by modifying the optical system of the oscillograph, and the other by employing a slotted disk mounted on mechanism under test. These methods offer practical means of time-distance relation measurements of small devices, such as spring-actuated levers, cam mechanisms, triggers, etc., whose performance would be affected due to the additional load required to operate auxiliary measuring instruments.

THERE are many transient non-recurrent mechanical motions, whose time-distance relationship (velocity, acceleration) is difficult to measure unless elaborate apparatus is employed. Velocity of such devices as spring-actuated levers, cam mechanisms, triggers, over-center mechanisms and other "snap" mechanical movements, which occur in a very short interval of time and whose traveled distance is relatively small, may be easily measured by means of an oscillograph, which may be found in many electrical laboratories.

An oscillograph is usually associated with the measurement of electrical phenomena, such as current, voltage, power and their phase relationship. Or it is widely used in the investigations of minute mechanical motions producing changes in the sensitively-tuned electrical circuits, such as measurement or recording of sound or of mechanical vibrations in terms of electrical oscillations, by means of a microphone.

Mechanical movements may also be studied directly, without having their motion relayed through the medium of an electrical device (contacts, microphone, photoelectric cell, etc.). In many cases this is of paramount importance, since the coupling of the mechanism under study to a device that operates the oscillograph vibrator involves absorption of some energy otherwise available for the operation of the device proper, or it creates the possibility of unaccountable delay in the time element recording, with consequent erroneous results.

Take, for example, a small current-interrupting mechanism, whose contacts, when tripped, open with a quick motion, essential for successful arc rupturing. The velocity and the acceleration of contacts separation are very important elements in the determination of the device's performance.

To measure the average velocity of the device's travel is a relatively easy task, for the time (T) required to complete the travel could be measured with two oscillograph galvanometers, or by other simple means, the traveled distance (S) may be easily calculated, and the average velocity (V) may then be computed from the basic formula

$$V=S/T. \tag{1}$$

However, it is well known that a mechanism, when started from rest, cannot reach its maximum velocity instantaneously due to inertia of parts, and in order to determine the true character of the motion, it is necessary to know the instantaneous values of velocity during any interval of time of movement's travel.

If a point is moving along any path, the instantaneous velocity (v) is the average velocity over indefinitely small period of time, including the instant, or,

$$v=ds/dt, \tag{2}$$

where ds is the distance traveled during the indefinitely small interval of time dt. Consequently, if the instantaneous positions of the mechanism could be recorded simultaneously with the elapsed time, the rate change in travel may be calculated and represented graphically.

The problem, therefore, is to record the relative positions of the mechanism from start to end of its travel, either at regular and known distance intervals, or continuously, in relation to a known time scale. Thus, if a trace of the mechanical

motion could be produced simultaneously with a record of a timing wave (alternating current of known frequency) the instantaneous values of velocity may be calculated.

If the oscillatory mechanical motion is small, of an order of 1 to 5 degrees, an oscillograph vibrator mirror may be fastened to the shaft of the moving element. The mirror, being very small will not materially affect the inertia of the mechanism under consideration. The mechanism is then mounted within the oscillograph case in place of a vibrator, and so adjusted that the movement of the mirror causes the reflected light beam to trace a record on the moving oscillograph film, thus recording the mechanism's position at any instant of its travel.

In case the mechanical motion is relatively large (about 60°) then the above method could not be used, inasmuch as the light beam would be thrown beyond the width of the oscillograph film. To diminish the scale of the beam throw the optical system of the oscillograph has to be modified by the use of a prism, located in the light beam path.

By referring to Fig. 1, it will be observed that the prism, which is attached to the shaft of the oscillating mechanism under investigation, is placed in the path of the light beam reflected from a galvanometer mirror. This galvanometer is not connected electrically, and thus the beam its mirror reflects is stationary. When the prism oscillates, the refracted beam produces a straight-line trace on the oscillograph film, which when set in motion at right angles to the beam travel, will produce a curve in right-angle coordinates.

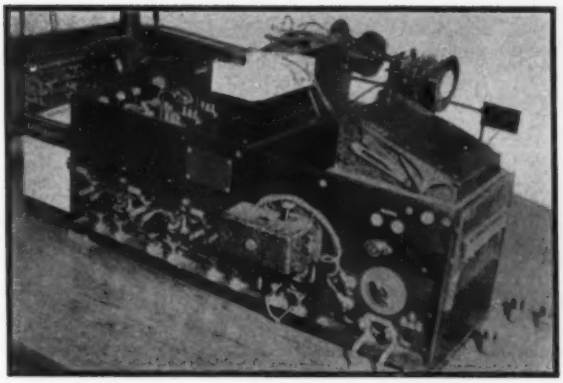

FIG. 2. Oscillograph and auxiliary apparatus showing the prism attached to the mechanism and located in the path of the reflected light from the stationary galvanometer mirror (prism method).

Actual apparatus set-up is shown in Fig. 2. A small prism is mounted on a shaft rotating in fixed bearings. This assembly is placed within the oscillograph case so that the prism lies in the light beam path reflected from a stationary galvanometer mirror. The shaft carrying the prism is attached to the shaft of the oscillating mechanism under investigation. The mechanism may be mounted outside of the oscillograph light-tight enclosure. Since the prism is rigidly connected to the mechanism, its movement must necessarily correspond to that of the mechanism. Consequently, the beam deflection, as recorded

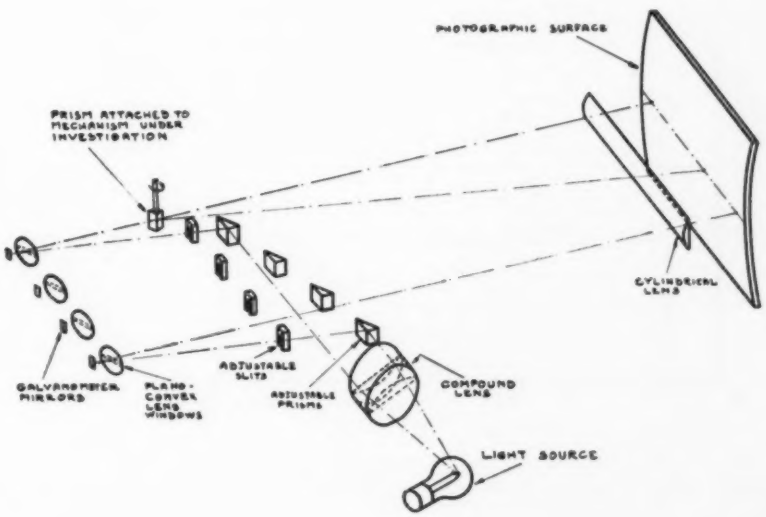

FIG. 1. Schematic diagram of oscillograph elements showing the position of prism attached to the mechanism under investigation for prism method.

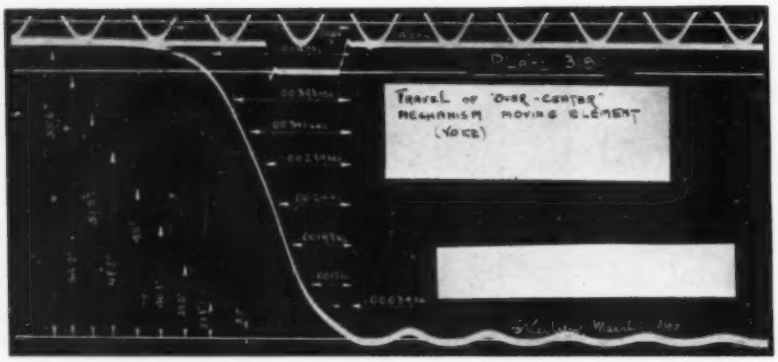

FIG. 3. Oscillogram showing a record produced by motion of the prism which was attached to the moving element (yoke of an "over-center" mechanism). Simultaneous record of time scale is made to permit calculation of mechanism velocity (prism method).

on the film, will be proportional to the movement of the mechanism.

To determine the position of the mechanism during any instant, the prism travel has to be calibrated. This is accomplished with a pointer attached to the prism shaft and a graduated dial. Curve plotted with beam deflection as abscissae and angular travel of prism as ordinates, makes it possible to determine the instantaneous angular positions of the mechanism from the trace on the film.

An alternating current wave of known frequency recorded simultaneously with the phenomenon on the same film furnishes the timing scale for determination of the elapsed time between various points of mechanism travel. From these data, the values of ds and dt may be obtained and substituted in Eq. (2) to calculate velocity (v) at any instant of the mechanism travel.

An oscillogram of such measurement is reproduced on Fig. 3. It represents a curve produced

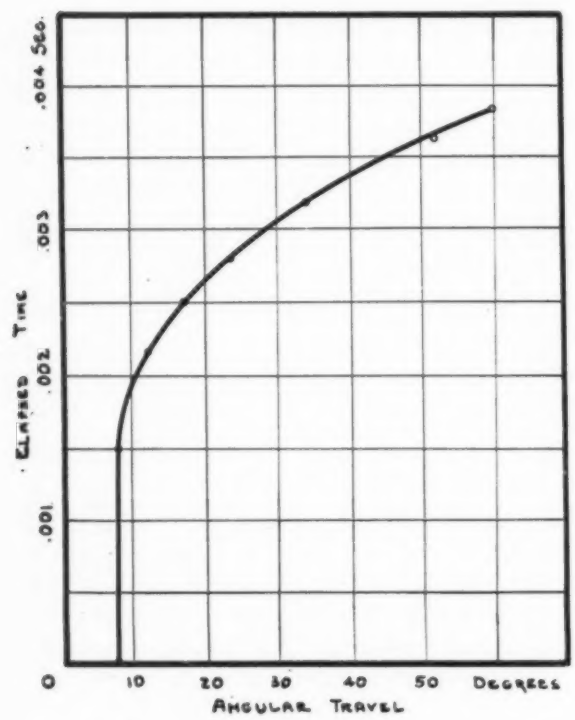

FIG. 4. Curve showing the relation between the angular travel and the elapsed time of a moving element (yoke of an "over-center" mechanism).

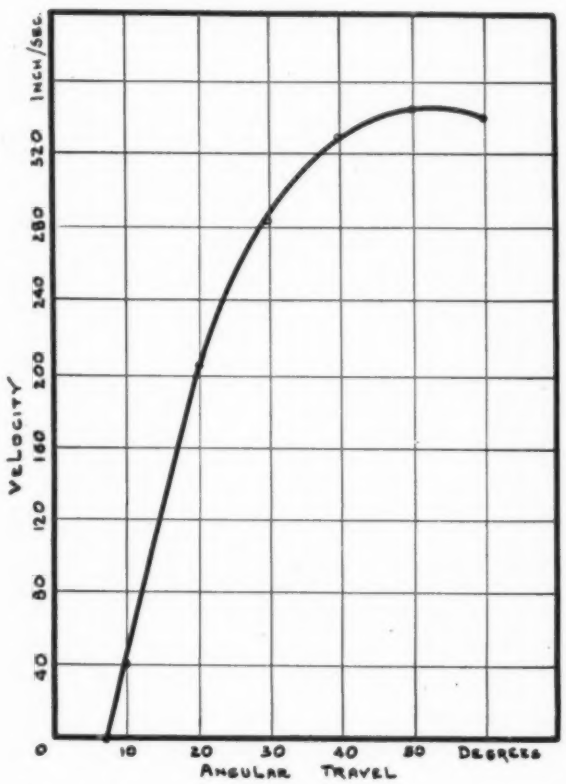

FIG. 5. Curve showing relation between the angular travel and the velocity of the moving element (yoke of an "over-center" mechanism).

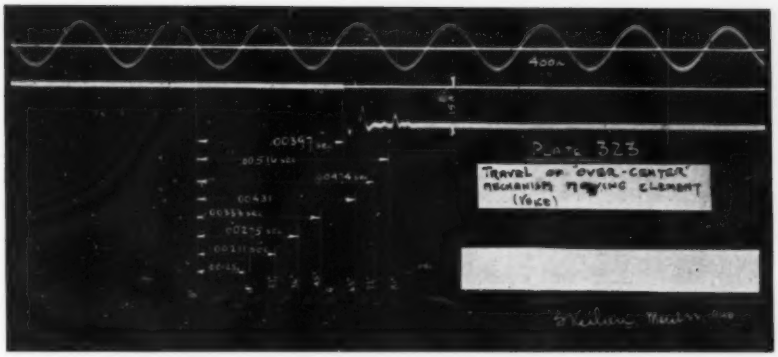

FIG. 6. Oscillogram showing the record of the angular travel of the moving element (yoke) of an "over-center" movement. The record of an interrupted beam was produced by a slotted disk which was placed in the path of a light beam reflected from a stationary galvanometer mirror. Current (0.15 amp.) was carried by contacts attached to the yoke (slotted disk method).

by an "over-center' mechanism, in which a spring, when loaded, releases a yoke which swings through an angle of 60°. A space-time curve, Fig. 4 shows graphically the time rate of mechanism motion. From the data of this curve the relation between velocity and mechanism travel was determined and plotted, on Fig. 5.

Velocity of mechanisms which do not lend themselves readily to practical means of fastening of prisms to their moving elements may be determined by a slotted-disk method. A light weight disk, with slots pierced radially and spaced at known angular intervals, is mounted on the spring-driven intermittently moving shaft of the mechanism under investigation. The mechanism is mounted within the oscillograph case so that the slots permit the light reflected from a stationary galvanometer mirror to fall upon the moving film during the disk's rotation. This produces an interrupted trace on the film. As in the previous method, the timing wave is simultaneously recorded on the film, to provide the time scale for calculation of the velocity. An oscillogram obtained by this method is reproduced on Fig. 6. It is quite apparent that since the angular travel and the time elapsed may be measured, the velocity may be readily calculated as described above. The apparatus arrangement is shown on Fig. 7.

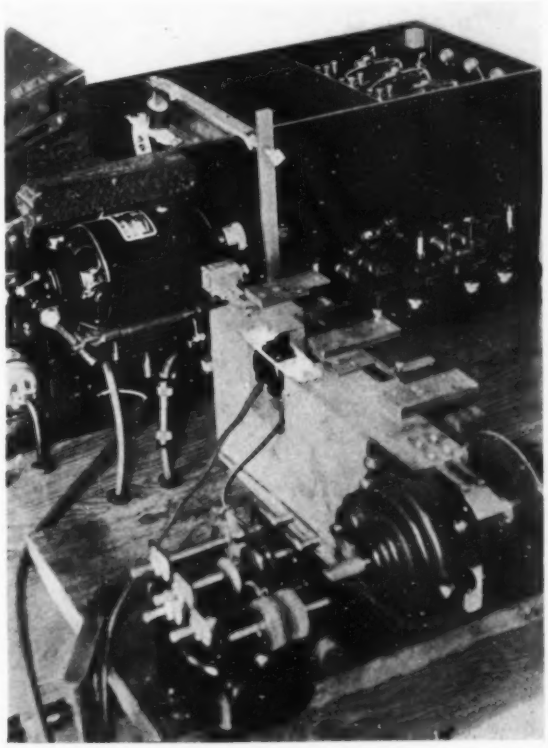

FIG. 7. Apparatus showing the oscillograph and the mechanism under investigation, carrying a slotted disk, and mounted within the oscillograph case. The motor in foreground operated the mechanism through gear reducing means (slotted disk method).

It must be borne in mind that for measurements described above it is desirable to have an oscillograph with accessories permitting recording at relatively high film speeds (up to 35 feet per second).[1] If the transient is of very short duration (0.001 second) such equipment is essential.

It has been found that these methods of measuring the velocity of transient mechanical movements offer results of relatively high degree of accuracy with the apparatus usually found in electrical laboratory, and are applicable to small mechanisms, whose performance would be affected by the additional load required to operate the auxiliary velocity recording or measuring instruments.

[1] S. Keilien, "Oscillograph—versatile tool in studying transient phenomena," Elec. J. **35**, 61 (1938); S. Keilien, "Improving products through research and test for quality," Product Engineering **10**, 24 (1939).

A Simple and Rigorous Method for the Determination of the Heat Requirements of Simple Intermittently Heated Exterior Walls

ELMER G. SMITH
Agricultural and Mechanical College of Texas, College Station, Texas
(Received December 17, 1940)

Buildings such as churches and auditoriums that are not continuously heated need larger heating plants than continuously heated buildings because of the large transient heat currents that must be supplied to the cold walls while the temperature of the building is being raised. The present unsatisfactory practice is to estimate the magnitude of these currents by various unreliable empirical methods. The purpose of this paper is twofold. First, for simple exterior walls, an equation is derived by means of which tables can be computed that will make rapid and reliable determinations possible. Second, the equation is put into such a form that the actual calculation of the tables can be carried out by N. Y. A. boys whose services can be obtained without cost. The unidirectional heat flow equation is solved for the boundary conditions that the outdoor temperature remains constant, the temperature of the wall is constant previous to time $t=0$, and after that time a constant heat current is applied to the wall. The solution is obtained in a form simple enough for the boys to handle by putting part of it in dimensionless form which makes it possible to plot a family of curves, which in turn make it possible to obtain numerical solutions without resorting to the very tedious "cut and try" process.

IN a building such as a church or an auditorium that is heated occasionally and allowed to cool when not in use, the required capacity of the heating plant is determined, in part, by the magnitude of the transient heat currents into the walls and furniture during the time in which the temperature of the interior of the building is being raised. To date, no method for determining the magnitude of these heat currents has been devised that is both simple enough and accurate enough to permit the rapid and reliable calculations that those engaged in this particular industry need to be able to make. It is the purpose of this paper to derive a rigorous equation for a simple exterior wall and put it in a usable form.

Since the heating plant is usually run at a rather high and constant rate while the temperature of the building is being raised, the assumption that heat is being delivered to the walls at a constant rate during the transient period is probably reasonably accurate.

Choose the origin and signs as indicated in Fig. 1. Choose the temperature scale arbitrarily in such a manner that its zero corresponds with the initial temperature of the building and its contents. Let

$\Theta \equiv$ temperature on the arbitrary scale.
$x \equiv$ distance from the indoor surface of the wall.
$L \equiv$ the thickness of the wall.
$i \equiv$ the heat current per unit area at any point in the wall.
$r \equiv$ the thermal resistivity of the wall.
$c \equiv$ the thermal capacitance per unit volume of the wall.
$t \equiv$ time.

The differential equations for the wall then are

$$-(\partial\theta/\partial x)dx = ridx$$
$$-(\partial i/\partial x)dx = cdx(\partial\Theta/\partial t).$$

The solution of the above equations is

$$\Theta = A_1 \exp[-(rcp)^{\frac{1}{2}}x] + A_2 \exp[+(rcp)^{\frac{1}{2}}x]$$
$$i = (cp/r)^{\frac{1}{2}}A_1 \exp[-(rcp)^{\frac{1}{2}}x] - (cp/r)^{\frac{1}{2}}A_2 \exp[+(rcp)^{\frac{1}{2}}x],$$

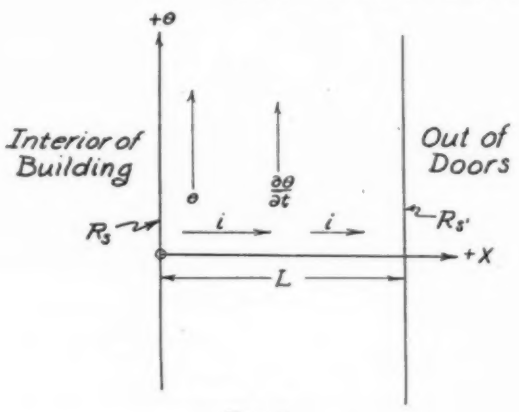

FIG. 1.

where A_1 and A_2 are independent of x and $p \equiv (\partial/\partial t)$.

The boundary conditions are:

$$i = i_s 1 \quad \text{when } x = 0$$
$$\Theta = R_{s'} i_L \quad \text{when } x = L,$$

where

$i_s \equiv$ the constant heat current per unit area that is assumed to enter the indoor surface of the wall continuously after $t = 0$.

$1 \equiv$ Heaviside's unit function.

$R_{s'} \equiv$ the surface resistance per unit area of the outdoor surface of the wall.

$i_L \equiv$ the heat current per unit area through the outdoor surface of the wall.

It should be noticed that although i_s is a constant, i_L is a function of time and must be eliminated before A_1 and A_2 can be determined.

After A_1 and A_2 have been determined, the equation for the temperature at any point in the wall may be written:

$$\Theta = \frac{\begin{array}{l} \cdot R_{s'}[\exp[+(rcp)^{\frac{1}{2}}(L-x)] + \exp[-(rcp)^{\frac{1}{2}}(L-x)]] \\ \qquad + (r/cp)^{\frac{1}{2}}[\exp[+(rcp)^{\frac{1}{2}}(L-x)] - \exp[-(rcp)^{\frac{1}{2}}(L-x)]] \end{array}}{R_{s'}(cp/r)^{\frac{1}{2}}[\exp[+(rcp)^{\frac{1}{2}}L] - \exp[-(rcp)^{\frac{1}{2}}L]] + [\exp[+(rcp)^{\frac{1}{2}}L] + \exp[-(rcp)^{\frac{1}{2}}L]]}.$$

Application of the Bromwich integral to the above equation gives

$$\Theta = \frac{i_s}{2\pi j} \oint \frac{\begin{array}{l} R_{s'}[\exp[+(rc\lambda)^{\frac{1}{2}}(L-x)] + \exp[-(rc\lambda)^{\frac{1}{2}}(L-x)]] \\ \qquad + (r/c)^{\frac{1}{2}}[\exp[+(rc\lambda)^{\frac{1}{2}}(L-x)] - \exp[-(rc\lambda)^{\frac{1}{2}}(L-x)]] \end{array}}{\{R_{s'}(c\lambda/r)^{\frac{1}{2}}[\exp[+(rc\lambda)^{\frac{1}{2}}L] - \exp[-(rc\lambda)^{\frac{1}{2}}L]] + [\exp[+(rc\lambda)^{\frac{1}{2}}L] + \exp[-(rc\lambda)^{\frac{1}{2}}L]]\}\lambda} e^{\lambda t} d\lambda,$$

where $j \equiv (-1)^{\frac{1}{2}}$. To get rid of the radicals let $\lambda \equiv -(u^2/rc)$.

When the above substitution has been made and account taken of the fact that λ goes around its contour twice when u goes around its contour once, the result, after simplification and reduction to trigonometric form, is

$$\Theta = \frac{ri_s}{2\pi j} \oint \frac{\exp(-u^2 t/rc)[R_{s'} u \cos\langle (L-x)u\rangle + r \sin\langle (L-x)u\rangle]}{u^2(-R_{s'} u \sin\langle Lu\rangle + r \cos\langle Lu\rangle)} du. \tag{1}$$

In Eq. (1) and throughout the paper the broken line bracket $\langle\ \rangle$ encloses an angle. It is evident that a double pole occurs at

$$u = 0$$

and simple poles occur where

$$R_{s'} u \sin\langle Lu\rangle - r \cos\langle Lu\rangle = 0. \tag{2}$$

The residue at the double pole can easily be found to be

$$[R_{s'} + r(L-x)]/r. \tag{3}$$

Before the final results of this investigation can be expressed as a formula, as they must be if they are to be useful, some easy way to solve Eq. (2) must be found. The method adopted can, however, be limited in range to those values of $R_{s'}$, L, and r, that occur in the walls of buildings. For the present, it will be assumed that such a method has been found. Let

$\phi \equiv$ any solution of Eq. (2).

The Laurent expansion about any of the points ϕ can now be found by the following process. Find the Taylor's series about the point ϕ for each of the following quantities.

$$1/u^2, \tag{4}$$

$$\exp(-u^2 t/rc), \tag{5}$$

$$R_{s'} u \cos\langle (L-x)u\rangle + r \sin\langle (L-x)u\rangle, \tag{6}$$

$$-R_{s'} u \sin\langle Lu\rangle + r \cos\langle Lu\rangle. \tag{7}$$

Multiply the expansions of (4), (5), and (6), together. In the expansion of (7) delete every term that contains

$$R_{s'} \phi \sin\langle L\phi\rangle - r \cos\langle L\phi\rangle$$

as a factor because by the definition of ϕ as a solution of Eq. (2) all such terms are zero for any possible value of ϕ. Finally, divide the product of the expansions of (4), (5), and (6) by the remaining terms of the expansion of (7).

When this has been done the residue for any of the simple poles can be seen to be

$$\frac{\exp(-\phi^2 t/rc)[(R_{s'}\phi\cos\langle\phi(L-x)\rangle+r\sin\langle\phi(L-x)\rangle]}{\phi^2[-R_{s'}(L\phi\cos\langle L\phi\rangle+\sin\langle L\phi\rangle)-rL\sin\langle L\phi\rangle]}. \tag{8}$$

Since the solution is the sum of the residues (3) and (8) multiplied by ri_s, the final result is

$$\theta=i_s\left\{R_{s'}+r(L-x)-r\sum_{-\infty}^{+\infty}\frac{\exp(-\phi^2 t/rc)[R_{s'}\phi\cos\langle\phi(L-x)\rangle+r\sin\langle\phi(L-x)\rangle]}{\phi^2[R_{s'}(L\phi\cos\langle L\phi\rangle+\sin\langle L\phi\rangle)+rL\sin\langle L\phi\rangle]}\right\}, \tag{9}$$

where ϕ takes on all the real values given by the following equation:

$$R_{s'}\phi\sin\langle L\phi\rangle-r\cos\langle L\phi\rangle=0. \tag{10}$$

The quantity to the right of the summation sign in Eq. (9) can be simplified to some extent. If the quantities $\cos\langle\phi(L-x)\rangle$ and $\sin\langle\phi(L-x)\rangle$ are expanded in terms of the sines and cosines of $\langle L\phi\rangle$ and $\langle\phi x\rangle$, it will be noticed that the coefficients of $\sin\langle\phi x\rangle$ add up to zero because of Eq. (10). Also, from Eq. (10) $\cos\langle L\phi\rangle=(R_{s'}/r)\phi\sin\langle L\phi\rangle$. When this substitution has been made and the result simplified, Eq. (9) may be written

$$\theta=i_s\left\{R_{s'}+r(L-x)-r\sum_{-\infty}^{+\infty}\frac{\exp(-\phi^2 t/rc)(R_{s'}^2\phi^2+r^2)\cos\langle\phi x\rangle}{\phi^2(LR_{s'}^2\phi^2+rR_{s'}+Lr^2)}\right\}. \tag{11}$$

By setting $x=0$ in Eq. (11), the expression for the temperature of the interior surface of the wall is obtained. If, in addition, the arbitrary temperature scale is replaced by the ordinary Fahrenheit or centigrade scale, the result may be written

$$\theta_s-\theta_i=i_s\left\{R_{s'}+rL-r\sum_{0}^{+\infty}\frac{\exp(-\phi^2 t/rc)2(R_{s'}^2\phi^2+r^2)}{\phi^2(LR_{s'}^2\phi^2+rR_{s'}+Lr^2)}\right\}, \tag{12}$$

where

$\theta_i \equiv$ the initial temperature of the building and its contents.

$\theta_s \equiv$ the instantaneous temperature of the interior surface of the wall.

In Eq. (12), the lower limit of the summation has been changed from $-\infty$ to 0, and compensated by introducing a factor of 2. This is possible because ϕ occurs only as ϕ^2 and according to Eq. (10), for every possible positive value of ϕ there is a negative value of equal absolute magnitude and vice versa. In order to put Eq. (12) in terms of the instantaneous temperature of the air inside the building, apply Ohm's law to the interior surface of the wall, which gives

$$R_s i_s=\theta_a-\theta_s, \tag{13}$$

where

$R_s \equiv$ the surface resistance per unit area of the indoor surface of the wall.

$\theta_a \equiv$ the instantaneous temperature of the air inside the building.

Substitution of the value of θ_s from Eq. (13) into Eq. (12) and the solution of the resulting equation for i_s gives

$$i_s=\frac{\theta_a-\theta_i}{R_s+R_{s'}+rL-r\sum_{0}^{+\infty}\frac{\exp(-\phi^2 t/rc)2(R_{s'}^2\phi^2+r^2)}{\phi^2(LR_{s'}^2\phi^2+rR_{s'}+Lr^2)}}. \tag{14}$$

It is necessary to make the use of Eq. (14) less laborious. The first step in this direction is to write Eq. (10) in dimensionless form as follows

$$(rL/R_{s'})=L\phi\tan\langle L\phi\rangle.$$

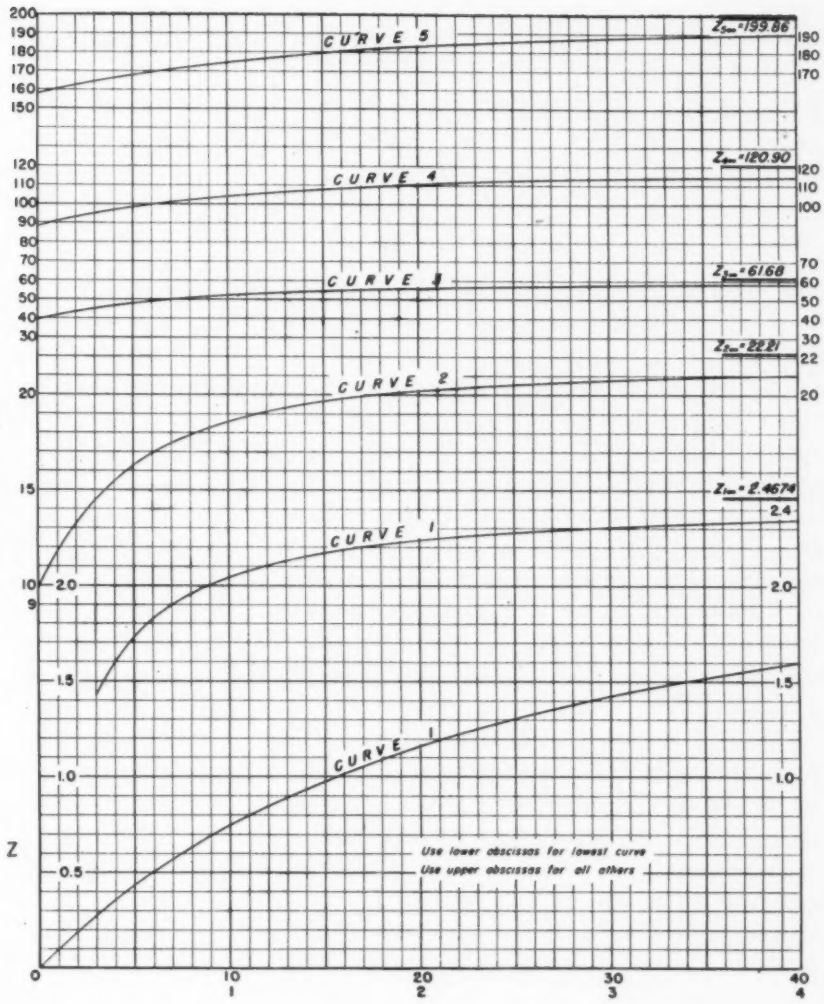

FIG. 2. Values of z for exterior wall absorbance equation.

$$\frac{R}{R_{s'}} = \frac{\text{Total resistance of wall exclusive of both surface resistances}}{\text{Surface resistance of outdoor side of wall}}$$

In the above equation let the dimensionless quantity

$$L\phi \equiv \sqrt{z}$$

and also let

$$rL \equiv R,$$

where

$R \equiv$ the total thermal resistance per unit area of either exterior or interior surface of the wall, exclusive of both surface resistances.

The equation can now be written

$$(R/R_{s'}) = \sqrt{z} \tan \sqrt{z}. \qquad (15)$$

In order to make it possible to use Eq. (15), Eq. (14) must be written in terms of z and R. In addition, let

$$cL \equiv C \qquad t = T$$
$$\Theta_a - \Theta_i = 1 \qquad i_s = a,$$

where

$C \equiv$ the total thermal capacitance of the wall per unit area of either interior or exterior surface.

$T \equiv$ the time in which the temperature of the air in the building must be raised from its initial temperature Θ_i to a comfortable temperature Θ_a.

$a \equiv$ the heat current that must be supplied per unit area of interior wall surface for each degree that it is desired to raise the temperature of the air.

When all the above changes have been made, Eq. (14) becomes

$$a=\frac{1}{R_s+R_s'+R-\sum_{0}^{+\infty}\frac{2RR_{s'}^{2}+(2R^3/z)}{(zR_{s'}^2+RR_{s'}+R^2)\exp(+zT/RC)}}. \tag{16}$$

The determination of z can be made very easy by plotting a family of curves having z as ordinates and $R/R_{s'}$ as abscissas. In order to provide ample accuracy, the chart actually used is 18 inches by 24 inches divided into 1-millimeter squares. A simplified reproduction of it is given in Fig. 2. For some walls one term of the summation is sufficient and five are always ample. The quantity represented by the symbol "a" should have a name for the sake of convenience and, since it is to be used in much the same manner as conductance, it will hereafter be referred to as the "absorbance" of the wall in question.

Equation (16) is in a sufficiently simple form so that the calculation of tables of absorbances can be safely left to groups of undergraduate students provided those who are reasonably careful are selected. Once tables of absorbances have been prepared, the heat requirements of an exterior wall can be found very quickly. For instance, if the outdoor temperature is 0°F, the indoor temperature 40°F, and it is desired to raise the indoor temperature to 70°F, it is only necessary to multiply the conductance of the wall by 40, then multiply its absorbance by 30, add the two results together and multiply by the area of the wall.

As soon as it can be prepared a paper will be published describing a method by which the absorbances of more complicated walls such as plastered hollow tile with brick veneer can be determined with sufficient accuracy to be entirely satisfactory for use in connection with the determination of required heating plant capacities. Another paper will be devoted to the absorbances of interior walls and furniture.

This paper is an abbreviation of a portion of the material presented as a doctor's thesis at the University of Texas. Especial thanks are due to Dr. S. L. Brown for his kindness in agreeing to supervise this thesis under very difficult circumstances and to Dr. E. G. Keller, who is primarily responsible for what knowledge the writer has of the kind of mathematics used in this paper.

The Heat Requirements of Simple Intermittently Heated Interior Walls and Furniture

ELMER G. SMITH
Agricultural and Mechanical College of Texas, College Station, Texas
(Received December 17, 1940)

This paper does for simple interior walls and furniture what the previous paper did for simple exterior walls. Unidirectional heat flow is assumed and the boundary conditions are simpler than for the simple exterior wall so that the solution is easily expressed in the form of a formula. The treatment of the interior surface resistance as a constant quantity is justified.

IN the previous paper, the writer derived an equation by which it is possible to compute tables that engineers can use to calculate quickly the heat requirements of simple intermittently heated exterior walls. It is the purpose of the present paper to do the same thing for simple interior walls and simple furniture such as church pews, theater seats, and table tops.

Consider a simple interior wall that is initially at a uniform temperature throughout, and arbitrarily choose the temperature scale so as to make that temperature zero. Also choose the

space coordinate so that $x=0$ at the surface of the wall. Thus, as indicated by Fig. 1, the origin of temperature is at the initial temperature of the interior of the building and the origin of space is at the surface of the wall. Also with reference to Fig. 1, let:

$L \equiv$ half the thickness of the wall.
$x \equiv$ distance from the surface of the wall (x is to be positive inward toward the mid-plane of the wall as indicated in the figure).
$i \equiv$ the heat current per unit area at any point in the wall.
$\Theta \equiv$ the temperature, on the arbitrary scale, at any point in the wall.
$r \equiv$ the thermal resistivity of the wall.
$c \equiv$ the thermal capacitance per unit volume of the wall.
$t \equiv$ time that has elapsed since appreciable heat began to enter the room or auditorium.

As in the case of the simple exterior wall, the differential equations are

$$-(\partial\Theta/\partial x)dx=(rdx)i$$
$$-(\partial i/\partial x)dx=(cdx)\partial\Theta/\partial t$$

and the solutions are

$$\Theta=A_1\exp[-(rcp)^{\frac{1}{2}}x]+A_2\exp[+(rcp)^{\frac{1}{2}}x]$$
$$i=(cp/r)^{\frac{1}{2}}A_1\exp[-(rcp)^{\frac{1}{2}}x]-(cp/r)^{\frac{1}{2}}A_2\exp[-(rcp)^{\frac{1}{2}}x],$$

where $p\equiv\partial/\partial t$.

A_1 and $A_2 \equiv$ quantities independent of x.

As indicated in Fig. 1, the boundary conditions are

$$i=0 \quad \text{when} \quad x=L,$$
$$i=i_s 1 \quad \text{when} \quad x=0,$$

where $1 \equiv$ Heaviside's unit function.

$i_s \equiv$ the constant heat current that begins to enter the wall at time $t=0$ and continues thereafter.

The solution of the equations subject to the above boundary conditions gives for the temperature at any point in the wall

$$\Theta=ri_s\left[\frac{t}{rcL}+\frac{(L-x)^2}{2L}-\frac{L}{6}\right]-\frac{2ri_sL}{\pi^2}\sum_{n=+1}^{n=+\infty}\frac{(-1)^n}{n^2}\exp(-n^2\pi^2t/rcL^2)\times\cos\langle(L-x/L)n\pi\rangle. \quad (1)$$

Since our immediate objective is to obtain an expression for the temperature of the wall surface when the air in the building first reaches a comfortable temperature we shall let

$T \equiv$ the time that elapses between the instant when appreciable heat first begins to enter the room and the instant when the air first reaches a comfortable temperature,

$x=0$,
$\Theta=\Theta_s-\Theta_i$,

where

$\Theta_s \equiv$ the temperature of the wall surface on the ordinary centigrade or Fahrenheit scale when the air in the building first reaches the desired temperature.
$\Theta_i \equiv$ the initial temperature of the building and contents also expressed in C° or F°.

Then Eq. (1) becomes

$$\Theta_s-\Theta_i=ri_s\left[\frac{T}{rcL}+\frac{L}{3}\right]-\frac{2ri_sL}{\pi^2}\sum_{n=+}^{n=+\infty}\frac{\exp(-n^2\pi^2T/rcL^2)}{n^2}. \quad (2)$$

As in the case of the exterior wall our ultimate object is to find an expression for i_s in terms of T,

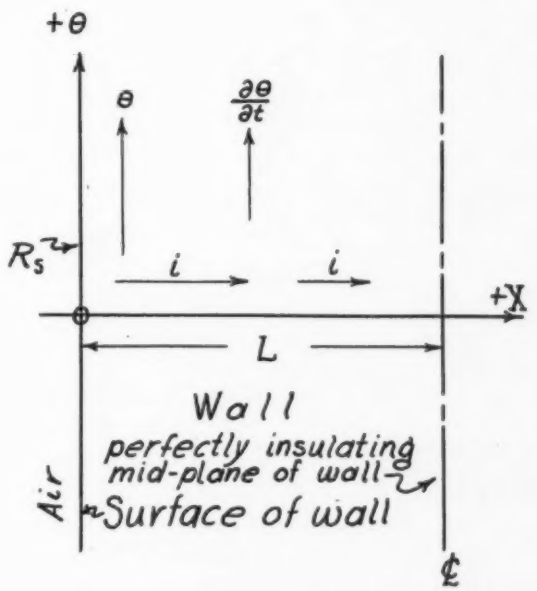

FIG. 1.

the constants of the wall, Θ_i and Θ_a where

$\Theta_a \equiv$ the desired air temperature.

In order to eliminate Θ_s, the temperature of the wall surface, we may apply Ohm's law to the interface between the air and the wall at the instant when the air first becomes comfortable which gives

$$\Theta_a - \Theta_s = i_s R_s, \qquad (3)$$

where

$R_s \equiv$ the surface resistance of the wall.

As will be explained later, the treating of the wall air interface as a pure resistance does not mean that there is any intention to neglect the effect of radiation.

The substitution of the value of Θ_s from Eq. (3) into Eq. (2) and the solution of the resulting equation for i_s gives:

$$i_s = \frac{\Theta_a - \Theta_i}{R_s + r\left[\frac{T}{rcL} + \frac{L}{3}\right] - \frac{2rL}{\pi^2}\sum_{n=+1}^{n=+\infty} \frac{\exp\left(-n^2\pi^2 T/rcL^2\right)}{n^2}}. \qquad (4)$$

In compiling a set of tables, convenience to the user should receive careful consideration. In the case of the tables for which this paper lays the foundation, it will probably happen more or less frequently that the exact wall to be heated will not be listed in the tables. In order to make it easy to decide what wall or walls listed are most nearly equivalent to a given wall, it is highly desirable to list the total thermal capacitance per square foot of surface and the total resistance, or conductance, per square foot of surface for each wall. Consequently labor will be saved by putting Eq. (4) in terms of these quantities. Also, as in the case of the previous paper, we must tabulate not i_s but $i_s/\Theta_a - \Theta_i$ which as before will be called the absorbance of the wall. Consequently, Eq. (4) can be written

$$a = \frac{1}{R_s + \frac{R}{3} + \frac{T}{C} - \sum_{n=1}^{n=\infty} \frac{(2R/\pi^2)}{n^2 \exp\left[+(\pi^2/RC)Tn^2\right]}}, \qquad (5)$$

where

$a \equiv$ the absorbance of the wall $\equiv$ the number of heat units that must be supplied to each square foot of the wall for each degree that it is desired to raise the temperature of the air in the room or auditorium.

$R \equiv rL \equiv$ the total resistance of the wall between its mid-plane and its surface per square foot of surface.

$C \equiv cL \equiv$ the total thermal capacitance of the wall between its mid-plane and its surface per square foot of surface.

Equation (5) is written in the form that has been found most convenient for making actual calculations.

It remains to justify the use of the constant R_s to designate the entire resistance of the wall surface to the penetration of heat even including radiation from various sources, the temperatures of which usually vary at different rates. To determine whether R_s could be considered a constant or would have to be treated as a function of T, a considerable number of tests was run on a plastered experimental wall 12 inches thick, both when bare and when acoustically treated. As a result of these experiments and some supplementary calculations it was found that, for ordinary methods of heating where an appreciable part of the heat reaches the walls in the form of radiation, R_s could be taken as 0.63 square foot hour degree F per B.t.u., for any value of T between $\frac{1}{2}$ hour and 8 hours. A more complete summary of these experiments and their results will be found in the thesis mentioned in the first paper.

In conclusion, thanks are again due to Drs. S. L. Brown and E. G. Keller of the University of Texas.

Effects of Heat Treatment on Field Emission from Metals*

J. H. Daniel
George Eastman Research Laboratories, Massachusetts Institute of Technology, Cambridge, Massachusetts
(Received April 25, 1941)

The cylindrical electron projector tube affords a convenient means of investigating the effects of heat treatment on field emission from metals. It is found that large, unstable field currents, designated as "anomalous" field emission, are due to the presence of surface electro-positive impurities. As evidenced by the "blackout" of the twinkling projector tube patterns, these impurities may be removed from tungsten, tantalum, or molybdenum by temperatures of 2200°K or greater, but it was found impossible to remove them from nickel. While the effect of gas adsorption on anomalous field emission is relatively minor, tube pressures even as low as 10^{-7} mm Hg increase the frequency of "breakdown." This phenomenon is probably caused by rearrangement or disruption of impurity layers, or even of the metal itself, due to positive ion bombardment. Making surfaces microscopically smooth greatly decreases the magnitude of anomalous field emission currents, and therefore the likelihood of breakdown, but cannot take the place of sufficiently severe heat treatment in removing the anomalous type of emission completely. In the course of these experiments, calculations were made which make possible the prediction of the tension on the projection tube filament necessary to prevent violent vibration of the filament as high voltages are applied to the tube. Since such cylindrical tube geometry is of common use in experimental work, the results of these calculations are given.

Introduction

FIELD emission of electrons from metals occurs when the application of a strong electrostatic field so lowers and thins the potential barrier at the surface of the metal that electrons escape through the barrier by virtue of wave-mechanical penetration. One of the earliest recognized characteristics of field emission currents was their extreme dependence on the heat conditioning of the emitting surface, particularly during the initial raising to high temperatures.

Millikan and Eyring[1] made extensive measurements of current as a function of voltage for various amounts of heat treatment on thoriated tungsten filaments.[2] They found that a semi-logarithmic plot of current *vs.* voltage for a raw wire with no previous heating showed discontinuities in a decreasing slope as the voltage was raised to a maximum value. As the voltage was reduced, a comparatively smooth curve with greater average slope for the same voltages (or even the same currents) was followed. This smoother curve was in general reversibly reproducible if the first maximum values of current and voltage were not exceeded. After a period of heating, this same type of behavior was again exhibited, but for temperatures above 1100°K, progressively higher voltages were required to produce the same currents.

From tables presented by Millikan and Eyring,[1] it is evident that the voltage necessary to produce a given current, defined as the "critical voltage," increases very markedly for heat treatments at or above about 1900°K. They explain this as being due to removal of surface impurities, plus a rounding off of the surface peaks from which most of the emission took place (due to concentration of the electrostatic field around these peaks, and evidenced by fluorescent spots on the glass walls of the tube) both by the heating and by the more energetic positive ion bombardment at higher voltages. The drastic increase in critical voltage was apparently not permanent, as the critical voltage decreased again with long standing. Several cases in which the current suddenly increased discontinuously by factors of 100 or 1000 were observed.

Observations of this kind, while having no significance to fundamental theory of metals, are of practical importance in determining the kind of metal and "conditioning" process which should be given high voltage tubes to minimize the possibility of breakdown due to field emis-

* Part of a thesis presented for the degree of Doctor of Science, from the Department of Physics, Massachusetts Institute of Technology, October 1940.

[1] R. A. Millikan and H. Eyring, Phys. Rev. **27**, 51 (1926).

[2] No mention is made of any effect which might be expected due to activation of the filaments. If none was observed, the fact would stand in agreement with the experiments of A. J. Ahearn, Phys. Rev. **50**, 238 (1936). A probable explanation is given in reference 15.

sion. Measurements such as Millikan made are extremely time consuming and tedious, but the electron projector tube offers a quicker way for obtaining the desired information.

Experimental Apparatus

The type of projector tube used is shown in Fig. 1. The fluorescent screen is of calcium tungstate and willemite sprayed on the glass wall and covered with a potassium silicate coating (to prevent bombardment of the filament with particles detached from the screen) as described by Martin.[3] The screen potential closely follows the collector potential up to perhaps 10,000 volts by virtue of its secondary emission properties. Emission of electrons from the wire takes place radially due to the geometry of the electrostatic field and its concentration around the filament.[4] Thus the electrons striking the screen give an emission image of the wire surface which is greatly magnified in circumference.[5]

For the high voltages necessary to obtain field emission patterns, it was found that quite often the filament suddenly broke into violent vibration, making observations impossible. Since this tube geometry is of common use in experimental work, and the same difficulty will limit the range of any measurements made with voltages upward of 1000 volts, some time was spent in investigating the phenomenon, and information was obtained which enabled the behavior of a given tube to be predicted.

Experimental facts easily observed were: As the voltage on a particular tube was raised, a reproducible, critical value was reached at which the filament quite abruptly broke into fairly large amplitudes of vibration. The frequency

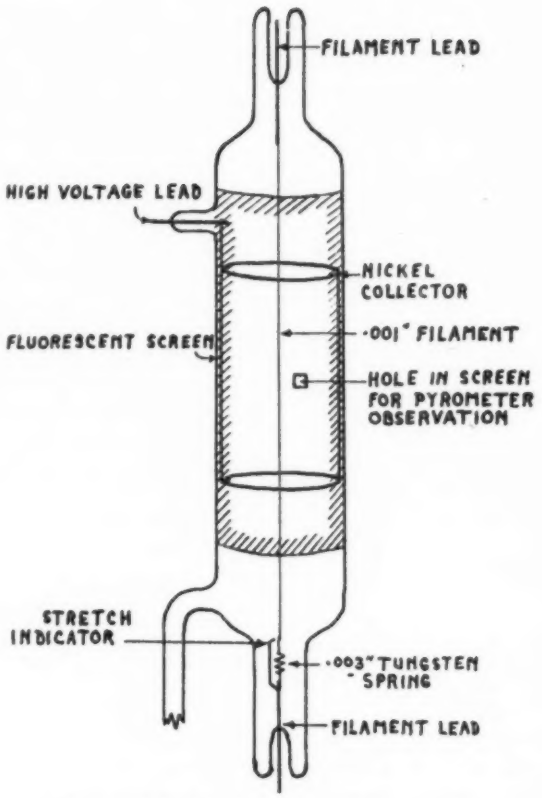

Fig. 1. Cylindrical electron projector tube.

was not necessarily 60 cycles per second nor any multiple thereof; the vibration did not take place in a fixed plane, but in one which rotated in azimuth around the stationary filament axis; almost never was any but the fundamental mode present. Such characteristics seemed to point to a condition of unstable equilibrium being suddenly attained by the stationary wire as the force on it produced by the electrostatic field exceeded a critical value. With this in mind, the forces on the wire were computed,[6] and the following expression obtained for the voltage necessary to initiate vibration:

$$V \geq 6.8 \times 10^4 (T^{\frac{1}{2}}/l) R \log_{10}\left(\frac{R}{r}\right), \qquad (1)$$

where V is the voltage between screen and filament, T the tension in grams on the filament, l the length of the filament in centimeters, R the radius of the screen in centimeters, and r

[3] S. T. Martin, Phys. Rev. **56**, 947 (1939).

[4] As given by the equation

$$F = \frac{V}{(r+x)\ln R/r},$$

where F is the potential gradient or field at distance x measured radially outward from the wire surface, V the potential difference between wire and screen, and r and R the respective radii of the wire and screen.

[5] Distortions at the wire surface (where the field is greatest) of the cylindrical symmetry of the field, due to its local concentration about the small projections from which field emission takes place, account in large measure for the fact that field emission images consist of elongated bright spots rather than very thin lines around the screen circumference. See Fig. 2.

[6] J. H. Daniel, "Studies of field emission," Sc. D. Thesis, Massachusetts Institute of Technology (1940), Appendix I.

the radius of the filament in centimeters. Solving for the tension necessary to prevent vibration:

$$T \geq 2.16 \times 10^{-10} \frac{V^2 l^2}{R^2[\log_{10}(R/r)]^2}. \quad (2)$$

For a wire not accurately centered, the effect[6] on (1) and (2) is small and tends to lessen the tension necessary to prevent vibration.

Using (1) or (2) in conjunction with Blodgett and Langmuir's[7] specifications for design of a helical tungsten spring[8] to give maximum safe tension at temperatures up to 2800°K, where the tension vanishes (due to expansion of the filament), the onset of vibration can be predicted for any temperature. If the filament is not to be heated to 2800°K, greater tension may be applied to hold off vibration to higher voltages. If high voltage is to be applied only when the filament is cold or at low temperatures, a short stiff spring may be used which goes slack at a safe temperature, but exerts a strong tension at lower temperatures. The behavior of all tubes constructed carefully with hydrogen-fired springs[7] according to the above specifications was found to confirm the theory from which (1) and (2) were derived.

To extend the specifications to filament metals other than tungsten, it was found sufficiently good to calculate the allowable stretch of the tungsten spring as the fraction of that required for a tungsten filament represented by the product of the ratio of the melting point of the metal to that of tungsten by the ratio of their respective linear coefficients of expansion. This gives the following approximate stretches: tantalum stretch = 0.83 tungsten stretch, molybdenum stretch = 0.77 tungsten stretch, nickel stretch = 1.06 tungsten stretch.

All filaments used were of 0.001 inch diameter except those of molybdenum, which were of 0.002 inch diameter. Temperatures of the tungsten wires were computed from the diameter (determined by accurate weighing of a measured length) and the current input, using the Jones-Langmuir tables.[9] Temperatures of the tantalum wires were computed similarly using tabulated values of A' in Table I of Malter and Langmuir.[10] Temperatures of wires of other metals were measured with a special micropyrometer constructed for use with filaments of small diameter,[11] and calibrated on a lamp standardized by the National Bureau of Standards. Measurements of temperature, made on the tungsten and tantalum wires with this pyrometer and compared with the calculated values, indicated a probable discrepancy of less than ±20°K for values taken from a graph of individual measurements, and less than ±50°K for the individual measurements themselves. Filaments of about 20 centimeters length were used, so corrections for end losses due to heat conduction through the leads were negligible. For the type of observations now to be described, such temperature measurements were more than accurate enough.

Observations

Figure 2 shows typical field emission patterns obtained from a raw tungsten General Electric 218 wire (No. 1 in Table I) at various stages of heat conditioning. In each case the filament was kept at a fixed temperature, usually for ten minutes, then brought to room temperature. The voltage necessary to produce the pattern was applied immediately, and the pattern photographed. For temperatures up to about 1600°K the pattern was far from being the static representation necessarily shown in a photograph, but consisted of numerous brilliant, twinkling spots which continually appeared, disappeared, and reappeared. This activity was quite intense for a period of several minutes, but if the field remained on, it gradually diminished. The pattern meanwhile became less brilliant, but never became completely stable even after several hours. If the voltage was raised and then lowered, patterns obtained during the decreasing range of voltages were less brilliant and probably somewhat less active

[7] K. B. Blodgett and I. Langmuir, Rev. Sci. Inst. **5**, 321 (1934).

[8] Specifications for molybdenum springs may be found in an article by G. L. Tawney, Rev. Sci. Inst. **10**, 152 (1939).

[9] H. A. Jones and I. Langmuir, Gen. Elec. Rev. **30**, 310, 354, 408 (1927).

[10] L. Malter and D. B. Langmuir, Phys. Rev. **55**, 743 (1939).

[11] M. L. Benson, Master's Thesis, Massachusetts Institute of Technology (1935).

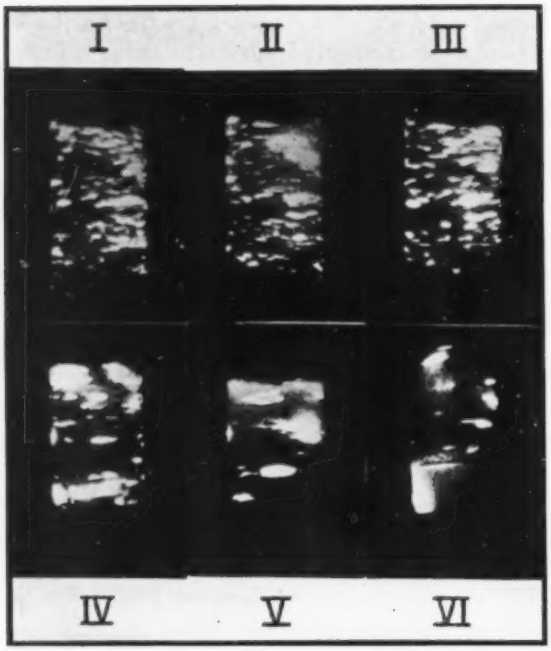

FIG. 2. Electron projection tube patterns produced by anomalous field emission from a 0.001-inch diameter raw polycrystalline General Electric 218 tungsten wire at room temperature.

I. After heat treatment incidental to baking of tube at 800°K (pattern is similar if tube is not baked at all). Fluorescent screen potential = 5000 volts.
II. After 10 minutes at 1200°K. Screen potential = 5000 volts.
III. After 10 minutes at 1500°K. Screen potential = 5000 volts.
IV. After 10 minutes at 1700°K. Screen potential = 7000 volts.
V. After 10 minutes at 1800°K. Screen potential = 9000 volts.
VI. After 10 minutes at 1900°K. Screen potential = 10,000 volts.

(by activity is meant the amount of flickering present) than those for the same voltage values during the initial voltage increase. This corresponds qualitatively to the current-voltage curves obtained by Millikan and Eyring, and the process was called by them "current conditioning."

For temperatures greater than 1600°K, the pattern became progressively less brilliant (or higher voltages were required to produce a pattern), and the emission spots more stable and less numerous. Not infrequently as the voltage was raised, an extremely brilliant spot would suddenly appear, gradually diminish in brilliance for a minute or two, but remain permanently in the pattern. Such spots must have indicated a disruption of the surface, or of the impurity layers on the surface[12]; they were sometimes so violent as to cause a sort of "recoil" of the filament. They correspond to the breakdown phenomena mentioned in the literature.

The most important characteristic of this heat conditioning, however, is the lack of pattern, or complete "blackout" obtained after heating to 2000°K, for voltages several times as large as those previously required to produce a pattern. For the wire of Fig. 2, 20,000 volts[13] were insufficient to produce a single trace of light from the screen. If higher voltages could be applied without vibration setting in, a breakdown usually occurred, which, in most cases, healed up after another ten minutes heating at 2000°K. Heating periods of one minute or less at 2000°K were, in general, insufficient to produce blackout, but if the temperature was elevated to 2300°K or 2400°K, such short periods were sufficient. Periods of several hours below 1900°K did not produce blackout. The emission giving rise to the twinkling patterns existing before the occurrence of blackout will be called "anomolous" field emission, to distinguish it from the steadier, more predictable emission which took place after blackout, but was so small as to be insufficient to cause any visible fluorescence.

Figure 3 shows the heat conditioning history of a 0.002" Callite Type 400 RI molybdenum wire (No. 9). At 1810°K a blackout was obtained, but on raising the temperature further to 1850°K, spots again appeared. These remained until the 2260°K heating period (enough evaporation took place at this temperature to darken the screen slightly), whereupon blackout appeared complete. This early blackout, followed by subsequent reappearance of anomalous field emission, occurred at 1750°K in one (No. 10) of the other two molybdenum wires (No. 5 and No. 10) tested. The other (No. 5) exhibited permanent blackout at 1900°K. The accompanying thermionic pictures (with subscripts A) were taken immediately following the field emission pattern pictures. There was usually a fair correspondence in position of bright bands in thermionic patterns

[12] Such disruptions of the tungsten surface were actually observed with the optical microscope in the case of field emission from sharp points. Positive ion bombardment, concentrated on the small emitting areas by the electrostatic field geometry, could cause such intense local heating as to reduce the tensile strength of the metal below the strong electrostatic forces to which it is subjected.

[13] That the corresponding surface field existed even though the fluorescent screen perhaps did not rise above 10,000 volts was assured by the nickel anode.

to positions of spots in field emission patterns. These bands also disappeared when final blackout occurred for anomalous field emission (they did not disappear for the "premature" blackout which was observed only for molybdenum), and a uniform pattern with longitudinal die marks (which did not appear with wires polished microscopically smooth) as the chief feature remained.

After blackout had been produced, admitting air to the tube containing wire No. 9 and then pumping it down again to a pressure of 10^{-6} or 10^{-7} mm Hg without even baking it failed to remove the blackout. Even after the tube lay around in the laboratory at atmospheric pressure with a cork in the tubulation for a week, no anomalous field emission appeared when it was again evacuated. When it had remained at atmospheric pressure on the vacuum system for another week, the tube showed small spots as in Fig. 3-VI upon evacuation and application of 10,000 volts. An idea of the dimness of these spots may be obtained from the fact that this was a 60-second exposure as compared to the usual one- to ten-second exposures. Heating the filament to only 1200°K removed the spots.

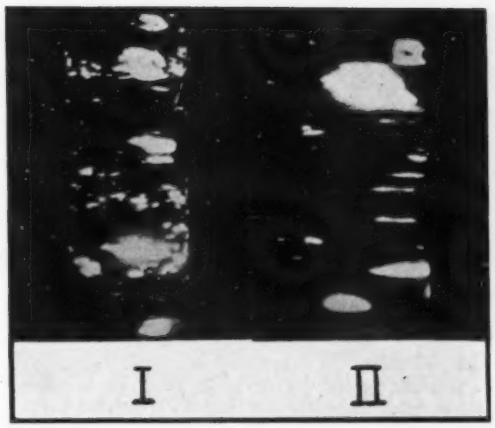

FIG. 4. Electron projector tube patterns produced by anomalous field emission from a 0.001-inch diameter raw polycrystalline Driver-Harris Grade "A" nickel wire at room temperature.

I. No heat treatment. Screen potential = 3000 volts.
II. After 10 minutes at 1530°K. Screen potential = 5000 volts.

After two more weeks at atmospheric pressure on the vacuum system, one spot appeared, but was removed by a temperature of 1100°K. Molybdenum wire No. 10 exhibited the same sort of behavior, as did tungsten wire No. 2, slight thermionic bands accompanying the field

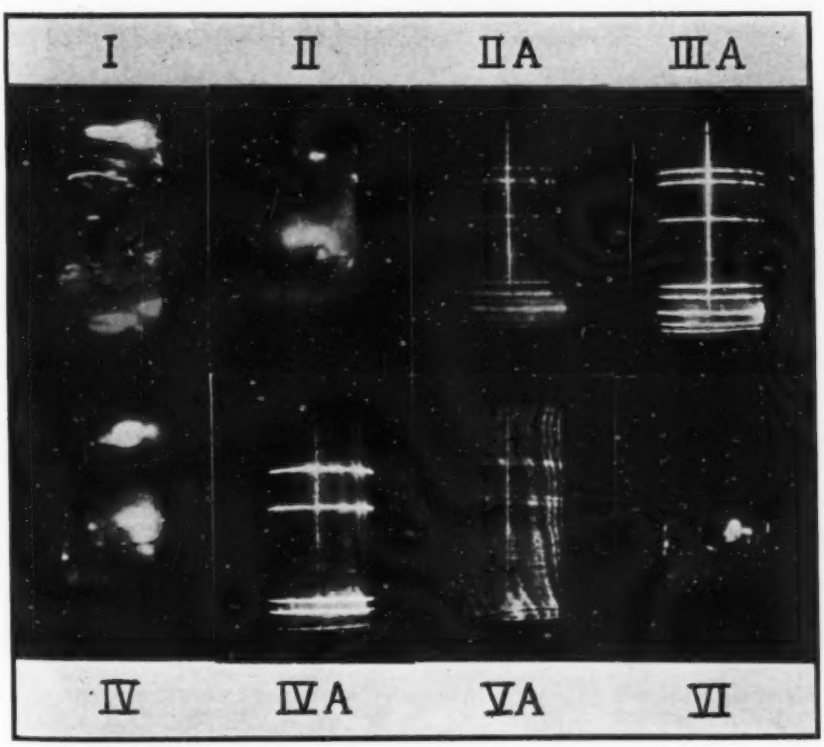

FIG. 3. Electron projector tube patterns produced by anomalous field emission (by thermionic emission in pictures with subscripts *A*) from a 0.002 inch diameter raw polycrystalline Callite type 400 RI molybdenum wire at room temperature.

I. After 10 minutes at 1200°K. Screen potential = 4000 volts.
II. After 10 minutes at 1700°K. Screen potential = 6000 volts.
II-A. Thermionic pattern for same conditions as in Fig. 3-II. Screen potential = 4000 volts. Temperature = 1700°K.
III-A. Thermionic pattern after 10 minutes at 1810°K. Screen potential = 4000 volts. Temperature = 1800°K.
IV. After 10 minutes at 1900°K. Screen potential = 11,000 volts.
IV-A. Thermionic pattern for Fig. 3-IV. Screen potential = 4000 volts. Temperature = 1900°K.
V-A. Thermionic pattern after 10 minutes at 2200°K. Screen potential = 4000 volts. Temperature = 1900°K. Note longitudinal die marks.
VI. After two weeks at atmospheric pressure. Screen potential = 10,000 volts.

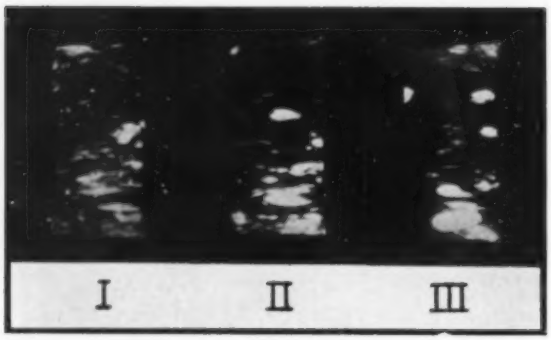

FIG. 5. Electron projector tube patterns produced by anomalous field emission from a 0.001-inch diameter raw polycrystalline Driver-Harris Grade "A" nickel wire at room temperature.

I. No heat treatment. Screen potential = 4000 volts.
II. After 10 minutes at 1200°K. Screen potential = 4000 volts.
III. After two hours at 1600°K. Screen potential = 5000 volts.

emission spots. Wire No. 2 was then removed from the tube and placed in glass tubing. After four days it was remounted, having been handled only with cotton-gloved hands. Upon evacuation it behaved exactly as though undergoing heat treatment for the first time. Two other tungsten wires, one tantalum, and one molybdenum wire behaved in the same manner.

Figures 4-I and 4-II show the patterns of a 0.001" Driver-Harris Grade "A" nickel wire after treatment at room temperature and at 1530°K, respectively. The wire (No. 3) broke while cold under 5000 volts. Figure 5 shows the history of a second nickel wire which broke at 1650°K.

Figure 6 shows the patterns (badly underexposed) obtained from a tungsten wire polished microscopically smooth by a mechanical grinding process described by Nelson.[14] The patterns were very dim, and consisted of only a few spots, but the blackout was quite definite, and occurred at approximately the same temperature (1900°K) as for the unpolished tungsten wires. On the smooth wire the spots were much more stable, and the effects of current conditioning less noticeable.

Figure 7 shows tantalum patterns. With the two tantalum wires (Nos. 8, 11) investigated a blackout also occurred, although at a slightly higher temperature—about 2300°K. However, the blackout was not quite so complete as with tungsten and molybdenum, for spots could be obtained from both wires by applying sufficiently high voltages (from 15,000 to 20,000 volts) even after ten minutes at 2600°K. Both wires broke at 2800°K.

Table I summarizes further the results obtained from tungsten, tantalum, molybdenum, and nickel wires.

CONCLUSIONS

The less spectacular anomalous field emission pattern given by the microscopically smooth tungsten wire, and its disappearance at 1900°K, show that although surface roughness has a great deal to do with the magnitude of anomalous

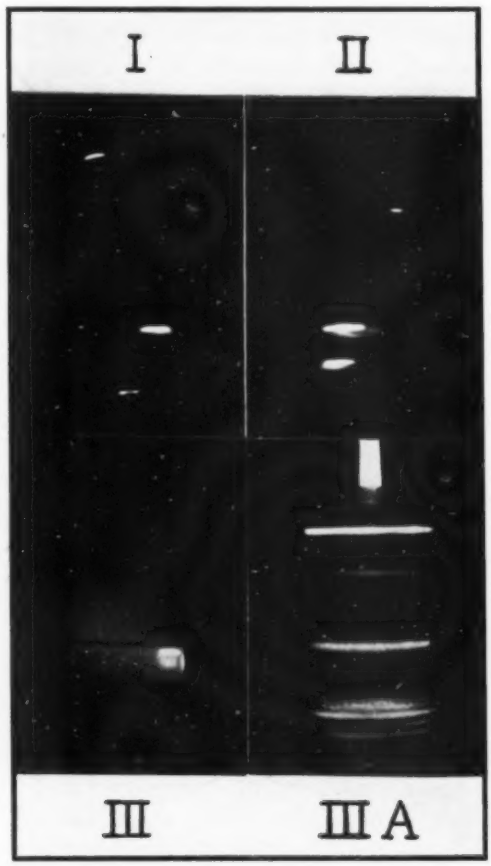

FIG. 6. Electron projector tube patterns produced by anomalous field emission from 0.001-inch diameter G. E. 218 tungsten wire polished microscopically smooth.

I. No heat treatment. Screen potential = 5000 volts.
II. After 10 minutes at 1650°K. Screen potential = 6000 volts.
III. After 10 minutes at 1850°K. Screen potential = 9000 volts.
III-A. Thermionic pattern for Fig. 6-III. Screen potential = 4000 volts. Temperature = 1800°K.

[14] R. B. Nelson, "The grain structure of tungsten filaments," Ph.D. Thesis, Massachusetts Institute of Technology (1938).

TABLE I.

Wire No.	Description	Avg. Pressure During Test	Blackout Temperature	Melting Point	Remarks
1	0.001-inch G. E. 218 tungsten	4×10^{-8}	2000°K for 10 minutes	3640°K	
2	Same as No. 1	3×10^{-8} mm Hg	1870°K for 10 minutes	3640°K	
4	Same as No. 1, but polished microscopically smooth	2×10^{-8}	1900°K for 10 minutes	3640°K	
8	0.0011-inch Fansteel Ta	2×10^{-8}	2400°K for 10 minutes	3120°K	Blackout not so definite nor so complete. Wire broke under tension at 2800°K.
11	Same as No. 8	not measured	2200°K for 10 minutes	3120°K	Same as for No. 8.
5	0.002-inch Callite Type 400 RI Mo	2×10^{-8}	1900°K for 10 minutes	2890°K	
9	Same as No. 5	not measured	2260°K for 10 minutes	2890°K	Premature blackout occurred at 1810°K.
10	Same as No. 5	not measured	2200°K for 10 minutes	2890°K	Premature blackout occurred at 1750°K.
3	0.001-inch Driver-Harris Grade "A" nickel	6×10^{-7}		1725°K	Anomalous field emission still definitely present after 10 min. at 1530°K. Wire broke while cold under 5000 volts.
6	Same as No. 3	2×10^{-8}		1725°K	Anomalous field emission still definitely present after 2 hours at 1600°K. Wire broke while sagging at 1650°K.
7	Same as No. 3	3×10^{-8}		1725°K	Wire broke while cold under 5000 volts (defective weld?).

Note.—Wires were heated at each new temperature (usually 100°K higher) for at least ten minutes—longer if necessary to bring pressure back to former value. Pressures were measured with a tantalum plate ion gauge calibrated on air against a McLeod gauge in the range 10^{-3} to 10^{-6} mm Hg, and checked for Barkhausen oscillations and photoelectric emission from the plate. All observations and measurements were made with the tubes on the vacuum system and liquid nitrogen around the trap.

field emission currents, it is not a factor in determining the blackout temperature. Thus a smooth surface is advantageous in lessening anomalous field currents, but is no more important than sufficiently severe heating of the surface, which alone can remove such currents completely.

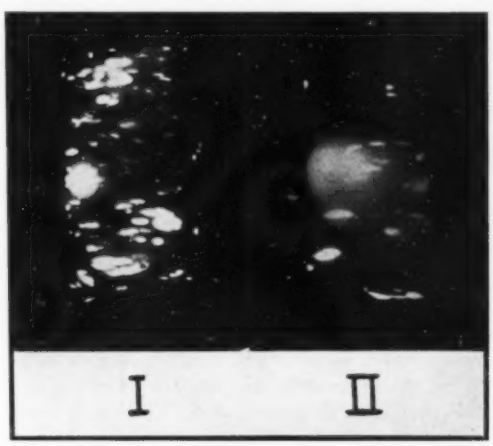

FIG. 7. Electron projector tube patterns produced by anomalous field emission from 0.001-inch diameter Fansteel tantalum wire at room temperature.

I. No heat treatment. Screen potential = 3000 volts.
II. After 10 minutes at 2000°K. Screen potential = 10,000 volts.

The persistence of blackout after air has been admitted to the emitting surface shows that anomalous field emission is not due to adsorbed gases. This is a fact which could not be assumed without such proof since the blackout temperatures are in the neighborhood of those required to remove some of these gases from metallic surfaces. The logical cause is thus narrowed to electro-positive surface impurities such as the alkalis, which tend to lower the work function, and which normally require some time to reach the filament unless it is handled or brought into contact with objects such as other metals or glass (e.g., tungsten wire No. 2). Further investigations of surface conditions using point projector tubes[15] make it apparent that while

[15] J. H. Daniel, Phys. Rev. (to be published).

surface electro-positive material is necessary and sufficient for the production of anomalous field emission, with any but the best surface conditions[16] such material is accompanied by the presence of adsorbed gas.

In contrast to the lack of dependence of blackout (or removal of electro-positive materials) on vacuum conditions, the phenomenon of breakdown certainly occurs more frequently under relatively poor vacuum conditions (pressures of 10^{-7} mm Hg or greater). This can be explained if local disruption of the surface due to violent positive ion bombardment is assumed[12] to be the primary cause of breakdown. The same assumption explains the greater frequency of breakdown observed with surfaces not subjected to heat treatment, since the greater emission from the impurity layers produces more positive ions. That an actual disruption of the surface takes place, and in some instances extreme local heating occurs, has been shown with field emission from points.[15] With such points it was proved also that the production of blackout by heating is not due to smoothing of the surface by surface tension (since this occurs at much higher temperatures)—a fact which is indicated here by the return of anomalous field emission patterns upon contamination after blackout has been produced.

The metals tungsten, tantalum and molybdenum can be rid of anomalous field emission by short heating periods at 2200°K or above. It is impossible to clean nickel sufficiently at any temperature below its melting point to get rid of anomalous field emission.

The author wishes to express his appreciation to Professor W. B. Nottingham for suggesting this problem in field emission. Thanks are also due Mr. L. W. Ryan for aid in glass blowing operations.

[16] It is also demonstrated strikingly that total pressure is not always a significant criterion of surface condition.

Here and There

Summer Course in Photoelasticity

To meet the growing interest in photoelasticity, the Department of Mechanical Engineering of the Massachusetts Institute of Technology, Cambridge, Massachusetts, is sponsoring a short summer course dealing with this method of stress analysis. This course will extend from July 28 to August 8. Its inclusion in the summer session is primarily for the benefit of those engaged in industry or other occupations which prevent attendance at the Institute's regular winter session.

The thirteenth semi-annual meeting of the Eastern Photoelasticity Conference was held at the Massachusetts Institute of Technology, under the auspices of the Department of Mechanical Engineering, on June 12, 13, and 14.

★

Applied Mechanics Courses Offered

A staff of sixteen experts from Europe and America, representing "the best men available in the fields of mathematics, engineering and physics," has been selected to take charge of summer instruction and research in applied mechanics at Brown University, Providence, Rhode Island, according to an announcement made by the University's news bureau. The summer session, which began on June 23 and is to continue through September 13, is designed to help overcome a bottleneck in the supply of men with highly specialized knowledge who are needed in defense industry. Dean Roland G. D. Richardson of Brown's Graduate School is the Director of the program.

★

Chicago University's Fiftieth Anniversary

More than 160 of the nation's leading scientists and scholars, including thirty-two distinguished men and women who will be awarded honorary degrees, will report basic achievements and advances in learning in a five-day series of symposia sponsored by the University of Chicago. The symposia will be held on the Midway Quadrangles in the week climaxing the celebration of the University's Fiftieth Anniversary, beginning September 22, according to a recent announcement. Thirty-nine universities, including six in foreign nations, and fifteen museums, research organizations and government agencies will be represented in the symposia. They will deal with newest fundamental advances in the biological, physical, and social sciences, the humanities, law, business, religion, and social service, in keeping with the theme of the University's celebration, "New Frontiers in Education and Research." Sessions in the biological and physical sciences will be held jointly with the American Association for the Advancement of Science. Dr. Frederic Woodward, vice president emeritus, is Director of the Fiftieth Anniversary. Robert A. Millikan and Ernest O. Lawrence, Nobel prize winners in physics, are among the speakers.

New Society Holds First Meeting

The American Society for X-Ray and Electron Diffraction starts its existence with a charter membership of 124. The officers elected for 1941 are: *President*, M. L. Huggins of the Eastman Kodak Company; *Vice President*, B. E. Warren of the Massachusetts Institute of Technology; *Secretary-Treasurer*, George Tunell of the Geophysical Laboratory, Washington, D. C.

The first meeting of the Society was held at Gibson Island, Maryland, in cooperation with Section C of the American Association for the Advancement of Science. The program scheduled was as follows:

Monday, July 28

10:00 A.M. B. E. WARREN. **Theory and Practice of Particle Size Determination.**

7:30 P.M. M. J. BUERGER. **New Experimental Techniques in Crystal Structure Analysis.**

Tuesday, July 29

10:00 A.M. A. L. PATTERSON. **Fourier Series as Applied to Crystal Structure Determination.**

7:30 P.M. C. S. FULLER. **X-Ray Studies of Linear Polymers of Known Chemical Constitution.**

Wednesday, July 30

9:00 A.M. N.R.C. COMMITTEE ON X-RAY AND ELECTRON DIFFRACTION

10:00 A.M. P. DEBYE AND P. P. DEBYE. **Discussion of Theoretical and Experimental Electron Diffraction Methods.**

2:00 P.M. Business meeting.

7:30 P.M. E. W. HUGHES. **Recent X-Ray and Electron Diffraction Work at the California Institute of Technology.**

Thursday, July 31

10:00 A.M. L. O. BROCKWAY. **Recent Electron Diffraction Work on Gas Molecules.**

2:00 P.M. M. L. FULLER. **Applications of Electron Diffraction to Industrial Problems.**

Friday, August 1

10:00 A.M. E. F. BURTON. **Applications of the Electron Microscope.**

2:00 P.M. V. K. ZWORYKIN, J. HILLIER, AND A. W. VANCE. **Preliminary Report on 300,000-Volt Electron Microscope.**

★

Sloan Fellowship Award

W. Endres Bahls, who is in charge of development and design work in connection with special radio tubes at the Harrison, New Jersey, laboratories of the RCA Manufacturing Company, has been awarded an Alfred P. Sloan Foundation Fellowship for a year of advanced study of industrial problems at the Massachusetts Institute of Technology. One of eleven engineers chosen from all United States industry to receive the honor, Mr. Bahls will spend one year at the Institute attending the Business and Engineering Administration School.

The purpose of the Fellowship is to permit men actively engaged in industry to study such subjects as finance, accounting, labor relations, economics, law, and marketing, stressing the sociological aspects of modern industry.

★

Modern Plastics Competition Announced

Modern Plastics Magazine is now sponsoring its Sixth Annual Modern Plastics Competition. The sponsors of this annual competition invite all plastic-using firms, designers, molders, laminators, fabricators, materials suppliers, machinery and die makers to participate. Any plastic object or product will be deemed eligible if it has been designed or has reached the market since September 1, 1940. The competition and concurrent display of entries will be held in the main headquarters of Modern Plastics, Chanin Building, 122 East 42nd Street, New York. The final deadline for all entries is September 8.

★

Scientific Editor Receives Appointment

Samuel Glasstone has been appointed Scientific Editor of Princeton University Press, it was announced recently by Joseph A. Brandt, Director of the Press. Dr. Glasstone was born in London, England, and was educated in the University of London, where he obtained the degrees of Doctor of Philosophy and Doctor of Science. He taught physical chemistry in the University of London, the University College of the Southwest of England and the University of Sheffield. Since 1939 he has been research associate in chemistry at Princeton University. Dr. Glasstone is internationally known for his researches in physical chemistry and particularly in electrochemistry.

The object of Princeton University Press in appointing Dr. Glasstone as its Scientific Editor is to encourage and facilitate the publication of scientific books, particularly works of a specialized character which may lie outside the purview of the ordinary commercial publishers.

★

Films on Flying Available

The first basic films on flying available to educational institutions, prepared by Erpi Classroom Films, of Long Island, New York, in collaboration with the University of Chicago, were released in June. The films were produced under the direction of Dr. Reginald J. Stephenson, Assistant Professor of Physics at the University of Chicago, and Lieutenant Walter T. Brownell, Director of the University's student pilot training program. The presentation is in two reels, "Theory of Flight" and "Problems of Flight."

★

Calendar of Meetings

August

27–29 American Institute of Electrical Engineers, Yellowstone National Park

September

8–12 American Chemical Society, Atlantic City, New Jersey

8–10 American Astronomical Society, Williams Bay, Wisconsin

22–26 American Association for the Advancement of Science, Chicago, Illinois

25–26 Society of Automotive Engineers, Milwaukee, Wisconsin

October

6–10 National Safety Council, Chicago, Illinois

12–15 American Society of Mechanical Engineers, Louisville, Kentucky

13–16 Society of Motion Picture Engineers, New York, New York

15–17 American Society of Civil Engineers, Chicago, Illinois

20–24 American Society for Metals, Philadelphia, Pennsylvania

20–24 American Welding Society, Philadelphia, Pennsylvania

Letter to the Editor

Deterioration of Photographic Films before Development*

WAYNE T. SPROULL
General Motors Research Laboratories, Detroit, Michigan
May 8, 1941

PHOTOGRAPHIC films and plates are commonly sold with an expiration date stamped on the package which implies a warning that deterioration with time is to be expected before development. Discussion of the nature and causes of this deterioration is meager in the publications on photography. High temperature and high humidity accelerate the deterioration, but there may be other factors involved because film and plates deteriorate slowly even when stored in a cool dry place.

If cosmic rays were one of the principal factors responsible for the deterioration of films and plates, the prospects that photographic manufacturers could ever discover a way to prevent such deterioration would be very poor. Hence the negative character of the results of these experiments is in a sense encouraging because it confirms the generally accepted theory that film and plate deterioration before development is due to humidity and temperature effects which the manufacturers may some day overcome.

Millikan and Cameron[1] have computed from their experimental data that the total energy per square centimeter per second that flows into the top of the earth's atmosphere in the form of cosmic rays is about one-tenth of the total energy coming into the earth's atmosphere in the form of starlight and heat. One would expect film or plates exposed to starlight for a few months to show signs of fogging. Old film when developed behaves in some ways like slightly fogged film. It seems reasonable, then, that cosmic rays might be partly responsible for the pre-development deterioration of photographic films and plates.

Upon this theory, one might expect x-ray films to deteriorate somewhat more rapidly than films intended for exposure to ordinary light, because their thicker double emulsions, designed to make them more sensitive to x-ray exposure might also make them more sensitive to cosmic-ray exposure. In order to test this theory, some Eastman "Verichrome" roll film and some Agfa "Non-screen" x-ray film was purchased in Detroit on February 3, 1939. One-half of each type of film was sent to Mr. Harry S. Donald of the Calumet and Hecla Consolidated Copper Co. and Allied Companies, of Calumet, Michigan. Mr. Donald kindly stored these films on February 27, 1939, 2057 feet vertically beneath the surface of the ground in a shaft just south of the one used by Wilson[2] in his cosmic-ray experiments. Both shafts are in the same type of rock, and Wilson's data indicate that at this depth, the cosmic-ray intensity is only about one twenty-thousandth of that at ground level. Meanwhile, the remaining films were stored at an ordinary place in Detroit.

On March 28, 1941, the films were removed from the mine and on April 2, 1941, some of these mine-stored x-ray films were developed along with some of the x-ray films stored in Detroit, and a piece of new Agfa "Non-screen" film. These films were developed and fixed together. Figure 1 shows a print made from the three films. Both the film stored in the mine and that stored in Detroit appear fogged when compared to the new film, and the fogging is about equal in both old films. The conclusion is obvious that cosmic-ray exposure is not a major factor in the deterioration of x-ray films before development.

An additional test of the x-ray films was made by radiographing some steel strips laid in a criss-cross pattern over all three types of film simultaneously. This radiograph shows that, in addition to the fogging effect of age (causing the very lightly exposed portions of the negative to appear darker), there is a loss of sensitivity with age, shown by the fact that the heavily exposed portions of the old film are not as dark as the equally heavily exposed portions of the new film. One might suspect that cosmic rays could be partly responsible for fogging old film, while the loss of sensitivity might be due to other causes. However, the radiograph shows that the mine-stored film behaves in all respects like old film, which indicates that cosmic rays are not a major factor in causing either phase of the deterioration.

On April 16, 1941, tests were made on the Verichrome roll film. The film was loaded in a camera which was used to photograph a small illuminated sign in an otherwise dark room. The sign served to mark the film permanently so it could be identified as new film or as film stored in the mine or in Detroit. The results were in agreement with those obtained in the x-ray film experiments. It is evident that the mine storage film is inferior to the new film and that it behaves like the film stored in Detroit.

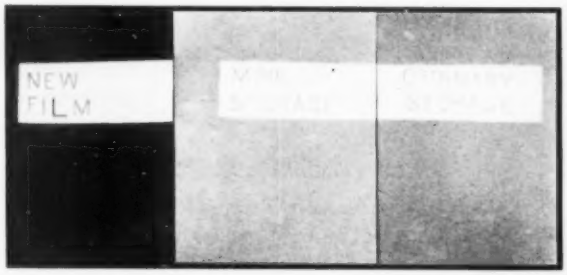

FIG. 1. This print was made from the three different films by a single exposure. The fact that the mine storage film in the center has fogged with age to practically the same degree as the ordinary storage film is evident.

* This work was carried out on the author's own initiative and was not connected with the work of the General Motors Laboratory.

[1] R. A. Millikan and G. H. Cameron, Nature **121**, 26 (1928).

[2] Volney C. Wilson, Phys. Rev. **53**, 337 (1938).